Doctoral Dissertation

Establishment of combinatorial material exploration method based on high-throughput experimentation and genetic algorithm

Ken Takimoto

Supervisor: Toshiaki Taniike

Graduate School of Advanced Science and Technology

Japan Advanced Institute of Science and Technology

Materials Science

March 2023

Abstract

Ken Takimoto (2020025)

Most of the chemical reactions in the world are composed of several elementary reactions. Therefore, even if one element is controlled, other elements will affect it, making it difficult to achieve the desired control. For this reason, it is common practice to add multiple elements for control, and this makes material design multidimensional. However, because the interactions between elements in multidimensional material design are very complex, material development to date has mainly been a trial-and-error approach based on intuition and experience. In this dissertation, combinatorial materials exploration, which combines materials informatics (MI) and high-throughput experimentation (HTE), leads to a new design guideline for materials. The main research results are as follows:

In **Chapter 2**, a high-throughput experimental protocol was established for yellowing inhibition of transparent plastics on the basis of solution film casting on microplates and ultraviolet/visible spectroscopic evaluation using a microplate reader. The combination of this protocol with a genetic algorithm (GA) enabled a large-scale exploration for stabilizer formulations. Furthermore, the obtained data were analyzed and validated based on decision tree classification and force-directed graphs. As a result, we succeeded in deriving a formulation design guideline that it is important to formulate as many mutually complementary and synergistic stabilizers as possible.

In **Chapter 3**, HTE instrument and GA were studied in combination. Catalyst design for low-temperature pyrochemical reforming of methane was investigated. The vast amount of data generated by the high-throughput experiments was subjected to various data science techniques to obtain guidelines for catalyst design and process optimization. Catalyst exploration revealed that the combination of elements belonging to different families, mainly Ni and Pd, has a synergistic effect on catalytic performance. Visualization using force-directed graphs also revealed that it is important to include as many synergistic elements as possible in the design of high-performance catalysts.

In summary, the two verifications achieved a large-scale combinatorial search. In addition, it was found that it is very important to select and coexist elements that establish synergistic effects with each other in the multidimensional material design for chemical reaction control. In conclusion, this study has demonstrated a new methodology for multidisciplinary material design through “Realization of multidimensional exploration”, ”Discovery of new combinations” and “Derivation of design guidelines”.

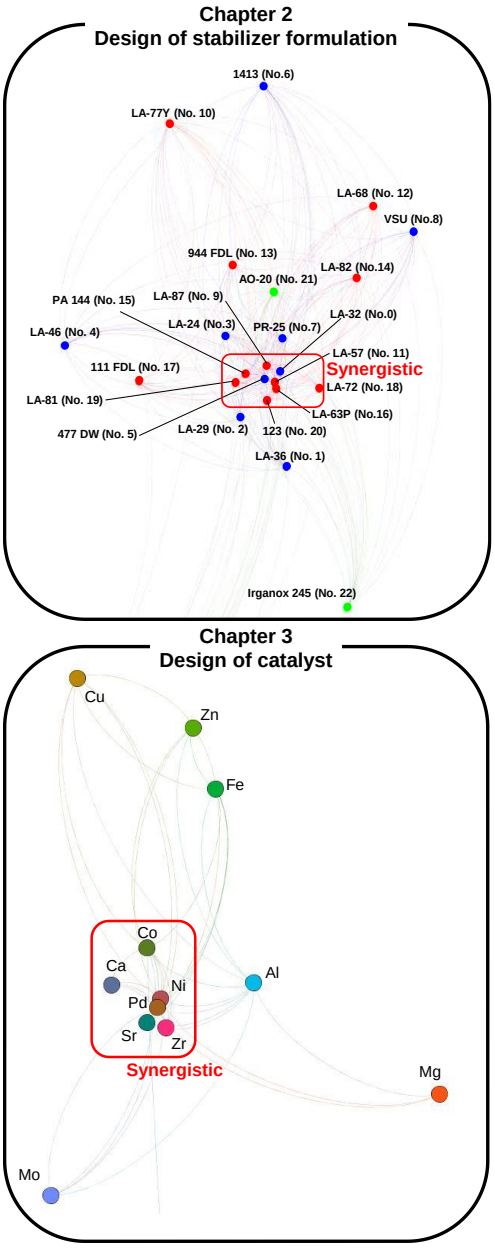

Fig. 1. Materials design guidelines in this dissertation.

Keywords: combinatorial materials exploration, materials informatics, high-throughput experimentation, photo degradation, dry-reforming reaction

Referee-in-chief: Professor Toshiaki Taniike
Japan Advanced Institute of Science and Technology

Referees: Professor Tatsuo Kaneko
Japan Advanced Institute of Science and Technology

Professor Kazuaki Matsumura
Japan Advanced Institute of Science and Technology

Professor Dam Hieu Chi
Japan Advanced Institute of Science and Technology

Associate Professor Keisuke Takahashi
Hokkaido University

Preface

The present thesis is submitted for the Degree of Doctor of Philosophy at Japan Advanced Institute of Science and Technology, Japan. The thesis is consolidation of results of the research work on the topic “Combinatorial materials exploration for controlling chemical reactions” and implemented during April 2020–March 2023 under the supervision of Prof. Dr. Toshiaki Taniike at Graduate School of Advanced Science and Technology, Japan Advanced Institute of Science and Technology.

Chapter 1 provides a general introduction of the research field, and accordingly the objective of this thesis. **Chapter 2** describes the exploration for stabilizer formulations for the control of yellowing of polymeric materials and the design guidelines for formulations obtained from analysis based on data scientific methods. **Chapter 3** The paper describes the exploration for low-temperature dry reforming catalysts for methane and the design guidelines for the catalysts obtained from the analysis based on data scientific methods. Finally, **Chapter 4** describes the general conclusions of this thesis. The work is original, and no part of this thesis has been plagiarized.

Ken Takimoto

Graduate School of Advanced Science and Technology

Japan Advanced Institute of Science and Technology

March 2023

Acknowledgements

I would like to express my sincere gratitude to my advisor, Prof. Toshiaki Taniike of the Japan Advanced Institute of Science and Technology (JAIST), for his enthusiastic guidance, valuable opinions, harsh comments that helped me grow, and heartfelt encouragement, which greatly contributed to the completion of this paper. His patience, encouragement, and professional guidance helped me throughout all of the research and writing of this paper. I would also like to thank Senior Lecturer Patchanee Chammingkwan and Asst. Prof. Toru Wada for many helpful discussions and advice. I would also like to express my sincere gratitude to the members of Taniike Laboratory for their valuable comments, cooperation, and support.

I deeply appreciate Prof. Tatsuo Kaneko (JAIST), Prof. Kazuaki Matsumura (JAIST), Prof. Dam Hieu Chi (JAIST), Associate Prof. Keisuke Takahashi (Hokkaido University) for their review and valuable suggestions. Last but not the least, my gratitude also extends to my family who has been assisting, supporting, and caring for all my life. Special thanks should go to my friends for their utmost care and moral support.

Ken Takimoto

Graduate School of Advanced Science and Technology

Japan Advanced Institute of Science and Technology

March 2023

Table of contents

Chapter 1

General Introduction

Chapter 1

1.1. Materials research and development for controlling chemical reactions

Since most chemical reactions are composed of multiple elementary processes, fully controlling a chemical reaction is synonymous with controlling all the elementary processes in the system. The design of solid catalysts that control chemical reactions tends to be multidimensional in terms of their composition and structure because the elementary processes that can be controlled by a single design parameter are only a part of the chemical reaction, and multiple parameters are needed to achieve the necessary control [1–3]. For example, catalysts for CO oxidation consist of two or more metals supported on a metal oxide to efficiently control elementary processes such as adsorption and activation of O_2 and CO molecules, and the formation and decomposition of carbonates [4–6]. In additive formulations to inhibit the oxidative degradation of polymers, additives such as UV absorbers, excited chromophores stabilizers, and metal deactivators that inhibit the formation of radicals caused by heat, light, and impurities, primary anti-oxidants such as phenolic and hindered amine antioxidants that scavenge the generated radicals, and secondary antioxidants such as phosphorus and sulfur based antioxidants that decompose peroxides are employed in combination [7]. Since the way that a material interacts with chemical reactions is extremely complex, the research and development for the materials that control chemical reactions has

largely relied on a trial-and-error approach based on researchers' intuition and experiences. However, multidimensional material design leads to e an enormous number of potential materials to be tested for a desired purpose.

1.2. Combinatorial approach

To the challenge of materials research and development for controlling chemical reactions, a systematic approach for combinatorial exploration in chemistry, called combinatorial chemistry, has been established since the 1990s. This is an effort to find the combination with the best performance or to discover universal knowledge such as common characteristics (combination rules) of combinations by searching a parametric space consisting of combinations of compounds in library using efficient means such as high-throughput experimentation (HTE). Combinatorial chemistry is a method that has expanded from the field of drug discovery to the field of materials science. In drug and ligand development, combinatorial chemistry can be applied to optimization as well as discovery of new substances. However, in materials science, it is mainly applied to optimization.

1.3. Materials informatics

Efficient control of most chemical reactions requires the control of many factors,

which is usually too complicated to implement solely based on human considerations. Therefore, a trial-and-error approach based on human intuition and experience has continued to the present day.

In recent years, there has been remarkable progress in materials informatics (MI), which is a field that combines materials science and data science to inductively extract correlations and laws between material performance and structure from systematically accumulated data, and to derive new design guidelines for target materials. Thus, in order to realize MI, various elements are required, including a platform for accumulating all kinds of data on materials, data analysis, and machine learning (Fig. 1.1) [8]. Although MI is making rapid progress in terms of methods, the current situation is that it has by no means led to the development of materials that can have an impact on the world. The main reason for this is the lack of sufficient material data with quality and quantity.

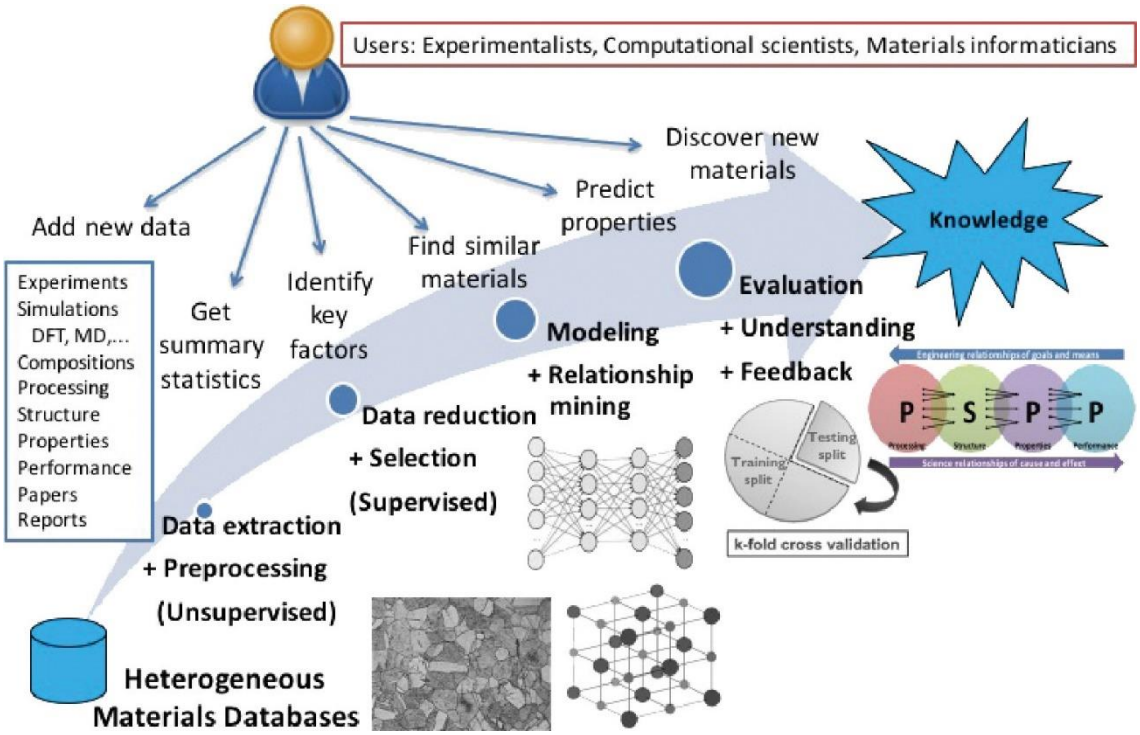

Figure 1.1. The knowledge discovery workflow for materials informatics. The overall goal is to mine heterogenous materials databases and extract actionable processing-structure-property-performance linkages to enable data-driven materials discovery and design. Reproduced from Ref. [8].

1.4. High-throughput screening

With the urgent need to develop new materials to realize a sustainable society, it has become important how to develop highly functional materials efficiently in a short period of time. However, most material development is conducted using methods that rely on trial and error. Using this approach, various materials have been discovered over a long history, making new discoveries increasingly difficult. To overcome this situation, it is

necessary to examine efficient methods of material development and to speed up research.

In recent years, there has been growing interest in high-throughput experiments (HTE), in which the synthesis and evaluation of large quantities of materials are handled by highly automated and parallelized equipment [9,10]. HTE, which has developed in the field of drug discovery, has extended beyond drug discovery into the field of materials science, such as catalysis and polymers. For example, Dai et al. designed a CCD image analysis system and a photocatalytic reactor for UV light, screened a library of catalysts for photocatalysis, and found that TiO_2, ZrO_2, Nb_2O_5, and WO_3 are highly active catalysts [11].

1.5. Genetic algorithm

Evolutionary methods are methods that mimic the evolutionary process of living organisms and aim for optimization by changing and selecting data structures. Based on the idea that living organisms solve specific optimization problems in the process of evolution, genetic algorithms (GA) are a typical example of such methods that aim to realize efficient computational systems. GA is an algorithmic version of Darwin's theory of evolution (Figure 1.2), and its greatest strength is its ability to efficiently conduct systematic searches without prior knowledge. GA is a process in which the best individuals in a population survive and others are eliminated, as shown in Figure 1.2. The population evolves and is eliminated as it repeats crossover, in which genes among

individuals are combined to produce new individuals, and mutation, in which some of the genes of an individual mutate, and approaches an optimal solution [12].

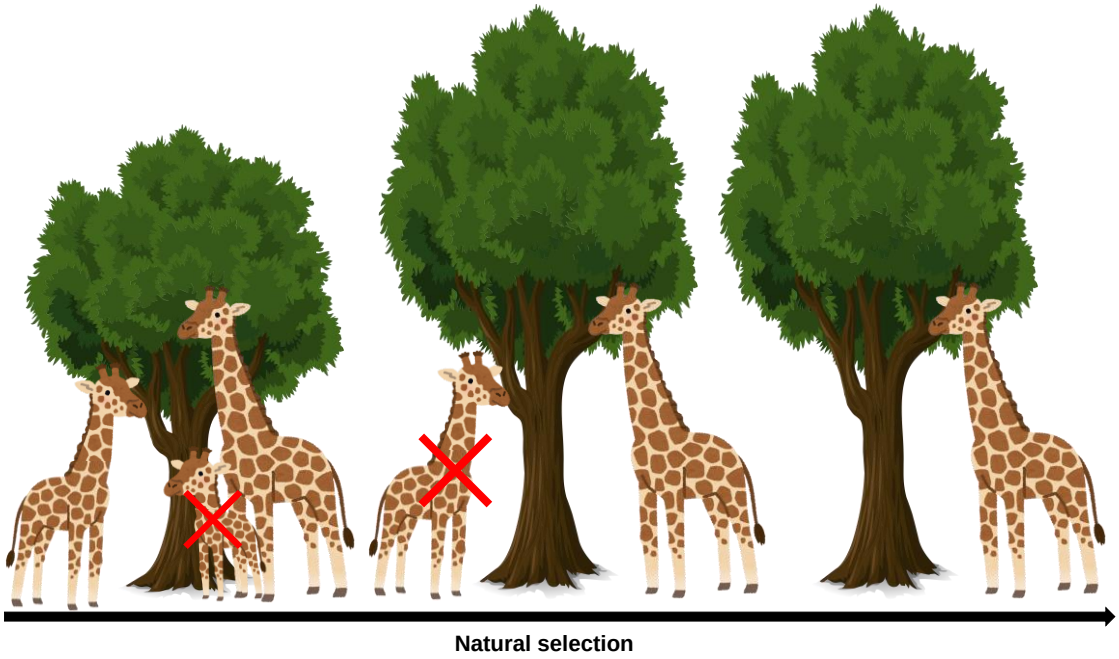

Figure 1.2. Darwin's theory of evolution.

1.6. Degradation of polymeric materials

Degradation that occurs during the molding process and use of polymeric materials gradually changes their physical properties, such as mechanical and optical properties [13,14]. Degradation mechanisms depend on the type of polymer material and the environment in which it is used, but are mostly categorized as thermal oxidative degradation, photo degradation, hydrolysis, or a combination of these factors [15–17]. It is the combined action of these factors that complicates the degradation of polymeric

materials.

1.6.1. Reaction mechanism of photo degradation

The physical properties of polymeric materials are significantly degraded by solar irradiation during outdoor use [18]. In particular, yellowing caused by photo-degradation is a major problem for glass substitute materials such as poly bisphenol A carbonate (PC), polystyrene (PS), and polymethyl methacrylate (PMMA) [19–21]. photo degradation of polymers can be broadly classified into two main categories: singlet oxygen oxidation, which proceeds by direct reaction of singlet oxygen with the substrate, and autoxidative degradation reactions, which involve repeated formation of radicals and their binding to oxygen.

The formation of singlet oxygen results from the quenching of the excited state of the sensitizer. Hydroperoxide is formed and decomposes, leading to chain scission and carbonyl group end formation [22].

As shown in Figure 1.3, autoxidative degradation occurs when oxygen reacts with alkyl radicals generated by heat or light to form peroxy radicals, which scavenge hydrogen from other polymer chains to form hydroperoxides. When this hydroperoxide is decomposed, new alkyl radicals are generated, which accelerate degradation through a chain reaction. Through these mechanisms, polymers undergo a series of chemical reactions, including cleavage of molecular chains, formation of cross-links and carbonyls,

and oxidation by radical species generated by autoxidative degradation, resulting in yellowing and cracking of polymer materials [23].

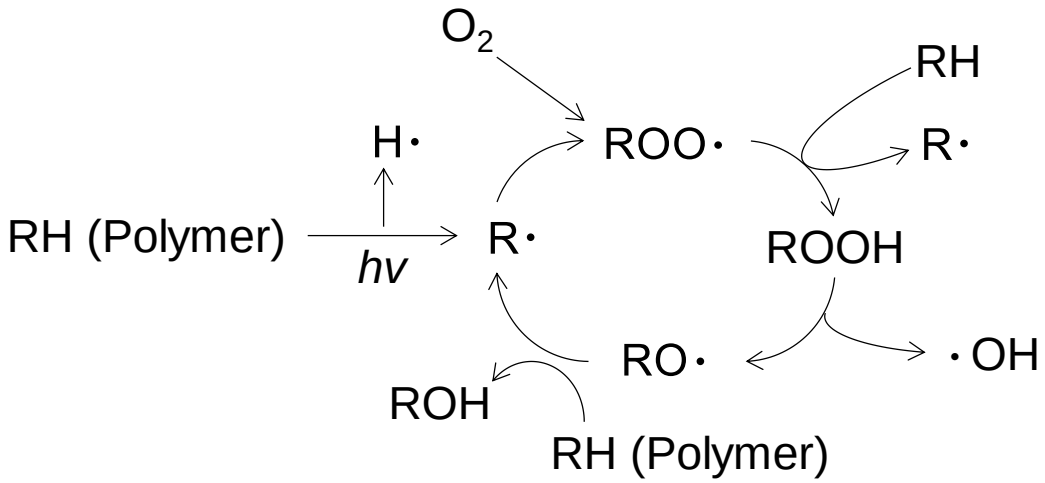

Figure 1.3. Mechanism of autoxidative degradation.

1.6.2. Stabilizers to suppress degradation

In order to control the degradation of polymeric materials, stabilizing agents are generally added to polymeric materials [24–26]. In other words, the durability of the polymeric materials is designed by adding stabilizers selected according to the degradation mechanism. Stabilizers are classified into radical chain initiation inhibitors, radical supplements, and peroxide decomposition agents, depending on the phase in which they act on autoxidative degradation. The radical chain initiation inhibitors prevent the initiation of autoxidative degradation by preventing the formation of radicals in advance, which are the starting point of radical chain reactions (autoxidative degradation).

Major radical chain initiation inhibitors include metal deactivators, UV absorbers, and quenchers [27–29]. The radical supplements play a role in breaking chain reactions by trapping radicals formed in polymeric materials. Phenolic antioxidants and hindered amine light stabilizers (HALS) are major radical supplements [30,31]. Peroxide decomposition agents decompose hydroperoxides generated from peroxyl radicals, preventing them from radical cleavage and initiating chain reactions. Major peroxide decomposers include phosphorus antioxidants and sulfur antioxidants [32,33].

As shown in Figure 1.4, HALS has a basic structure of 2,2,6,6-tetramethylpiperidine and has ae function of scavenging radicals generated from polymers due to photodegradation, with nitroxyl radical compounds as the main active species [34]. However, the detailed mechanism is still under debate due to the complex mechanism of photo-degradation and the small amount of HALS added in a polymer. It is known that HALS having the N-H form cannot perform well in stabilizer formulations that involve acidic substances. For this, N-OR type HALS has been developed, which is less basic and hence, is usable in the presence of acidic substances.

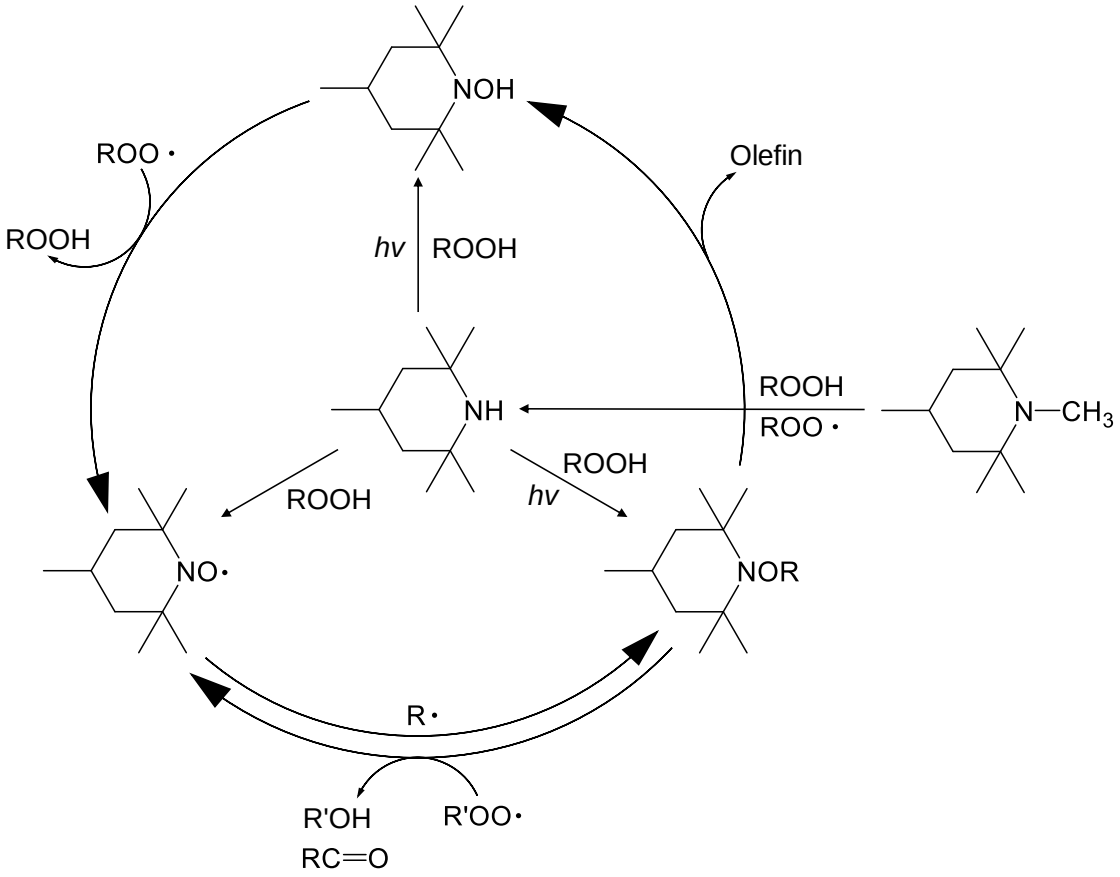

Figure 1.4. Stabilization mechanism by HALS.

UV absorbers have a variety of basic skeletons, and their structures differ in terms of the absorption wavelength and the mechanism of mitigating absorbed light energy. Figure 1.5 shows the generally accepted mechanism for the most widely used benzotriazole UV absorbers, where intramolecular hydrogen bonding is involved [35]. Absorption of UV light results in an excited state S_1, followed by a polarized structure S1' and then returning to the ground state S_0, mainly by the release of thermal energy and subsequent H^+ transfer. Triazine, benzophenone, and salicylate systems also work by similar relaxation mechanisms [36,37]. On the other hand, UV absorbers without

intramolecular hydrogen bonds, such as cyanoacrylates, mitigate light energy to a greater degree by emission [38].

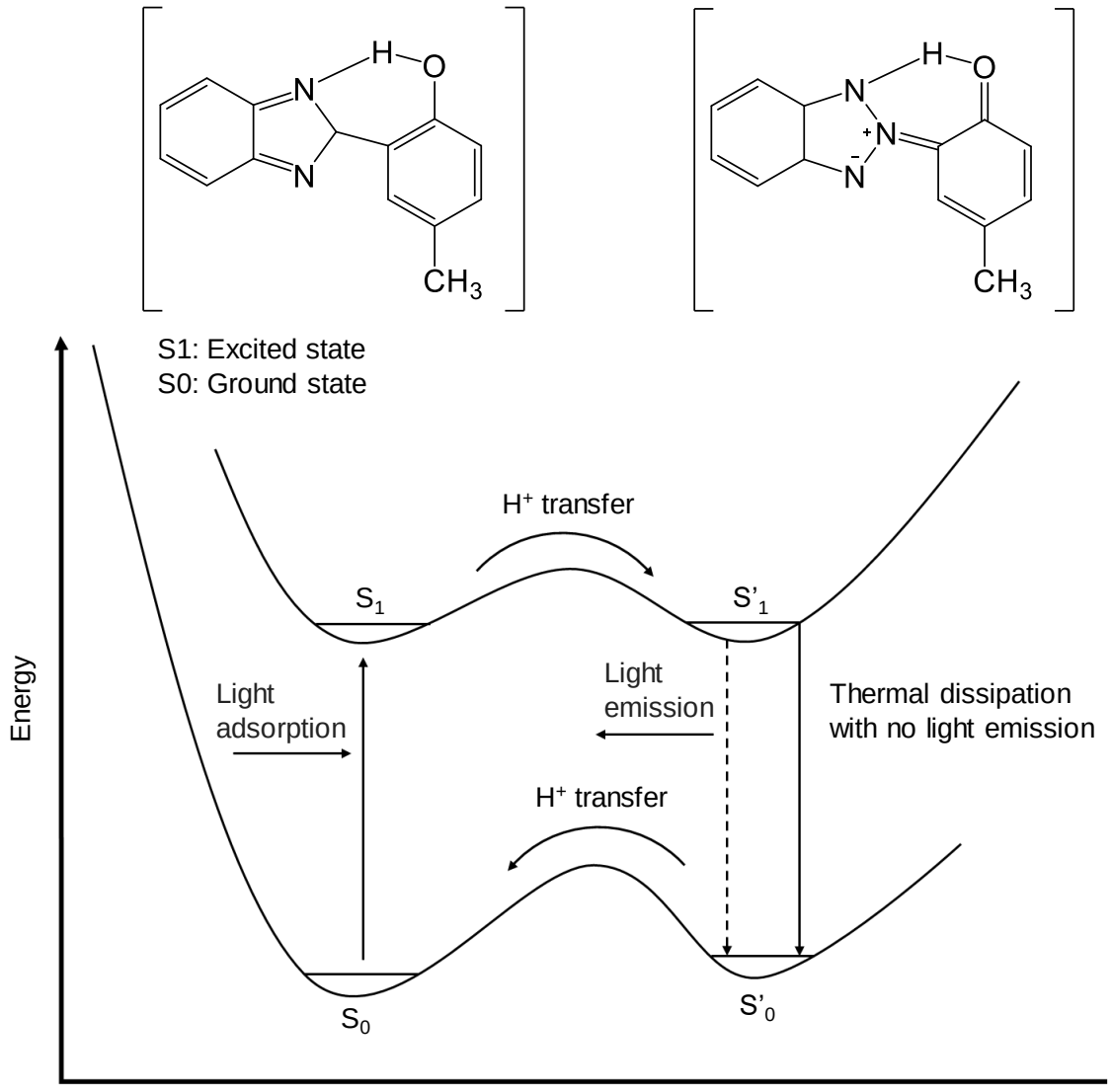

Figure 1.5. Mechanism of an UV absorber quenching light adsorbed.

Phenolic antioxidants scavenge the peroxyl radicals generated by autoxidative degradation and convert them to hydroperoxides, by which they turn into phenoxy

radicals. Phenoxy radicals become carbonyl groups and generate radicals on aromatic rings (Figure 1.6a) [39]. The radicals produced are stabilized by combining with peroxide radicals. Thus, phenolic antioxidants reduce a chance of hydrogen withdrawal from polymer chains by efficiently generating hydroperoxides from peroxyl radicals, which works to inhibit the progression of degradation. Phenolic antioxidants are classified into hindered, semi-hindered, and less hindered types. With respect to reactivity with peroxy radicals, the less hindered type is the most effective, while the opposite is true for the stability of the phenoxy radicals generated by itself: the hindered type is the most stable (Figure 1.6b).

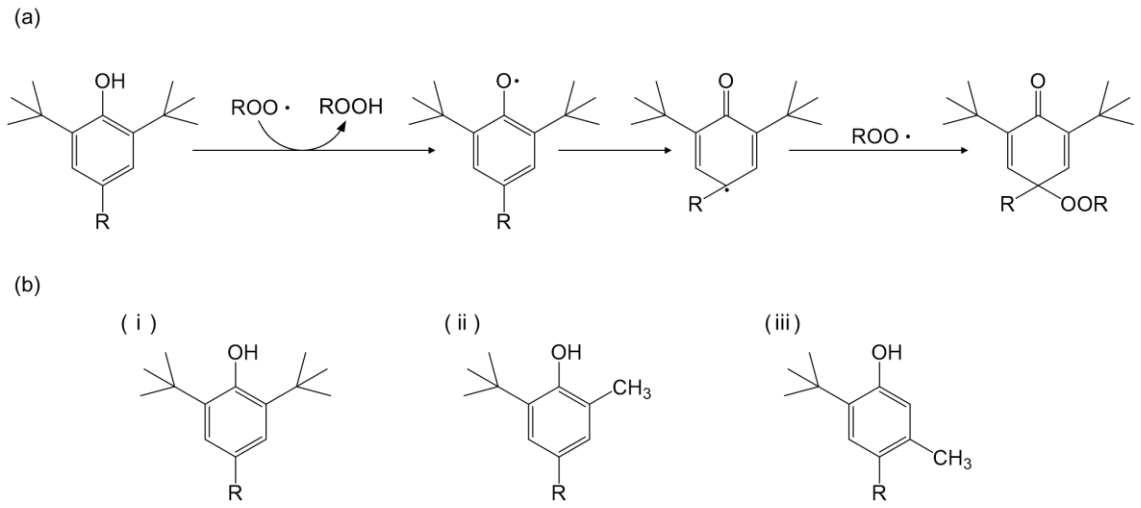

Figure 1.6. (a) Mechanism of stabilization by phenolic type anti-oxidants, and (b) different types of phenolic anti-oxidants: (i) hindered, (ii) semi-hindered, and (iii) less-hindered types.

1.6.3. Stabilizer formulation

Stabilizers are commonly added by polymer producers to give raw polymers durability for the processing or during the processing to give durability as a product. They are used mostly in combination, or as stabilizer formulations, Because combining different types of stabilizers can produce synergistic effects that exceed the sum of the effects of the stabilizers alone [40–42]. However, it is known that the combination of different stabilizers leads to not only synergistic effects but also antagonistic effects. Unfortunately, the interaction of stabilizers during degradation is extremely complex, and the outcome of combination are currently unpredictable.

1.7. Dry-reforming reaction of methane (DRM)

Fossil fuels are our primary source of energy, but the depletion of fossil fuels due to increasing energy demand has become a very serious problem [43]. Therefore, in recent years, methods to produce fuels and chemical products using available resources such as natural gas have been desired.

The dry reforming reaction (DRM) of CH_4 is a catalytic reaction that converts CH_4 and CO_2 into synthetic gas called syngas, which can be used as a starting point for synthesis of chemical products [44]. CO_2 is the most important greenhouse gas resulting from anthropogenic activities. In addition, since CH_4 is 21 times more effective than CO_2 in raising atmospheric temperature [45], it is required to be reduced as a countermeasure

against global warming and climate change. DRM is attracting attention from the viewpoint of effective use of natural gas and deterrence of global warming, because it is a reaction that not only reduces CH_4 and CO_2 emissions into the atmosphere but also converts them into synthesis gas, a valuable product.

1.7.1. Reaction mechanism of DRM

In the DRM process the following reactions can occur,

$$CH_4 + CO_2 \rightarrow 2H_2 + 2CO \quad (1.1),$$

$$2CO \rightarrow CO_2 + C \quad (1.2),$$

$$CH_4 \rightarrow 2H_2 + C \quad (1.3),$$

$$H_2 + CO_2 \rightarrow H_2O + CO \quad (1.4).$$

The last three reactions, called the Boudouard reaction, methane cracking, and the reverse water gas shift reaction, respectively, are the side reactions in DRM, which have detrimental effects such as carbon formation and catalyst deactivation [46]. It has been found that this reaction does not react independently below 640 ºC and that the side reactions, boudoir reaction and reverse water gas shift, occur frequently between 633 and 700 ºC. To minimize these side reactions, the DRM reaction occurs primarily at temperatures above 700 °C [47]. However, theoretical thermodynamic calculations report that the DRM reaction at 300 °C can yield conversion rates of up to about 60% for methane and about 50 % for carbon dioxide. It is also theoretically possible to produce

hydrogen at 100 °C and carbon monoxide at 300 °C [48].

1.7.2. Catalysts of DRM

For the implementation of DRM at an industrial scale, base metals should be selected from a cost perspective [49]. It has been shown that DRM under high conversion conditions of methane and carbon dioxide requires temperatures of at least 700°C. However, most catalysts have the challenge of being susceptible to deactivation by sintering or coking, and the performance of DRM catalysts depends on a variety of factors, including the active metal (type, reduction, particle size), the support (support type, surface area, acidity, basicity, oxygen storage capacity), and the interaction of the two [50–54].

Various active metals have been investigated. Noble metals, such as Pd, Rh, Ru and Ir are known to be highly active with little coking [55–58]. Among base metals, Ni and Co have been proven to be the most active [59,60]. In particular, Ni is the most preferrable in terms of its high activity and low costs. Though Co is considered less active than Ni due to weak metal-support interactions Ni-Co catalysts have been studied extensively due to their high coking resistance.

1.8. Aim of thesis

Human beings have discovered many new materials over a long period of time. In

the early stages of such discovery, the focus of research is concentrated on a specific material, new findings are brought one after another, and significant functional improvements occur. However, once the research progresses to a certain level, only gradual improvements can be expected thereafter, and the research eventually stagnates. To break through this stagnation and bring about breakthroughs in research, it becomes essential to discover materials using new and different approaches. In this thesis, I aim to explore multidimensional materials for controlling chemical reactions by combining combinatorial materials science and materials informatics to conduct an ultra-multidimensional exploration and find a combinatorial rule to guide materials design from a data science perspective. By conducting research for different material systems in different fields, such as stabilizer formulations to control yellowing of polymers and low-temperature dry reforming catalysts for methane, I aim to prove that the methodology proposed in this thesis is universally effective for similar materials designs. My research is mainly comprised of the following three chapters:

In Chapter 2, by establishing an efficient formulation exploration method using a microplate method and the genetic algorithm, a systematic exploration for stabilizer formulations to inhibit light-induced yellowing of transparent plastics was achieved. Furthermore, the obtained dataset was analyzed to learn in detail synergistic combinations of stabilizers that improve the durability of polymers, leading to guidelines for formulation design.

In Chapter 3, a multi-elemental catalyst design for low-temperature DRM was

explored using a combination of high-throughput experimentation and the genetic algorithm. The experimental data obtained were analyzed using various data science techniques to derive guidelines for low-temperature DRM catalyst design.

In Chapter 4, describes the general conclusions of this thesis.

References

[1] The Oxidative Coupling of Methane. *Catal. Letters* **2000**, *68* (3–4), 191–196.

[2] Kobayashi, T.; Yamada, T.; Kayano, K. Effect of Basic Metal Additives on NOx Reduction Property of Pd-Based Three-Way Catalyst. *Appl. Catal. B Environ.* **2001**, *30* (3–4), 287–292.

[3] Carvalho, L. S.; Pieck, C. L.; Rangel, M. C.; Fígoli, N. S.; Grau, J. M.; Reyes, P.; Parera, J. M. Trimetallic Naphtha Reforming Catalysts. I. Properties of the Metal Function and Influence of the Order of Addition of the Metal Precursors on Pt-Re-Sn/γ-Al2O3-Cl. *Appl. Catal. A Gen.* **2004**, *269* (1–2), 91–103.

[4] Wang, A. Q.; Chang, C. M.; Mou, C. Y. Evolution of Catalytic Activity of Au-Ag Bimetallic Nanoparticles on Mesoporous Support for CO Oxidation. *J. Phys. Chem. B* **2005**, *109* (40), 18860–18867.

[5] Liu, X.; Wang, A.; Li, L.; Zhang, T.; Mou, C. Y.; Lee, J. F. Structural Changes of Au-Cu Bimetallic Catalysts in CO Oxidation: In Situ XRD, EPR, XANES, and FT-IR Characterizations. *J. Catal.* **2011**, *278* (2), 288–296.

[6] Xu, J.; White, T.; Li, P.; He, C. H.; Yu, J. G.; Yuan, W. K.; Han, Y.-F. Biphasic Pd - Au Alloy Catalyst for Low-Temperature. *J. Am. Chem. Soc.* **2010**, *132*, 10398–10406.

[7] Wang, X.; Xing, W.; Tang, G.; Hong, N.; Hu, W.; Zhan, J.; Song, L.; Yang, W.; Hu, Y. Synthesis of a Novel Sulfur-Bearing Secondary Antioxidant with a High

Molecular Weight and Its Comparative Study on Antioxidant Behavior in Polypropylene with Two Commercial Sulfur-Bearing Secondary Antioxidants Having Relatively Low Molecular Weight. *Polym. Degrad. Stab.* **2013**, *98* (11), 2391–2398.

[8] Agrawal, A.; Choudhary, A. Perspective: Materials Informatics and Big Data: Realization of the "Fourth Paradigm" of Science in Materials Science. *APL Mater.* **2016**, *4* (5).

[9] Wahler, D.; Reymond, J. High Throughput Enzyme Assays. *Curr. Opin. Biotechnol.* **2001**, *12*, 535–544.

[10] Klumpp, M.; Boettcher, A.; Becker, D.; Meder, G.; Blank, J.; Leder, L.; Forstner, M.; Ottl, J.; Mayr, L. M. Readout Technologies for Highly Miniaturized Kinase Assays Applicable to High-Throughput Screening in a 1536-Well Format. *J. Biomol. Screen.* **2006**, *11* (6), 617–633.

[11] Dai, Q. X.; Xiao, H. Y.; Li, W. S.; Na, Y. Q.; Zhou, X. P. Photodegradation Catalyst Discovery by High-Throughput Experiment. *J. Comb. Chem.* **2005**, *7* (4), 539–545.

[12] Kumar, M.; Husain, M.; Upreti, N.; Gupta, D. Genetic Algorithm: Review and Application. *SSRN Electron. J.* **2020**, *2* (2), 451–454.

[13] Singh, B.; Sharma, N. Mechanistic Implications of Plastic Degradation. *Polym. Degrad. Stab.* **2008**, *93* (3), 561–584.

[14] Göpferich, A. Mechanisms of Polymer Degradation and Erosion1. *Biomater. Silver*

Jubil. Compend. **1996**, *17* (2), 117–128.

[15] Morikawa, T. Thermal Degradation and Stabilization of Polyvinyl Chloride. *Kobunshi Kagaku* **1968**, *25* (281), 602–613.

[16] Karimi, S.; Helal, E.; Gutierrez, G.; Moghimian, N.; Madinehei, M.; David, E.; Samara, M.; Demarquette, N. A Review on Graphene's Light Stabilizing Effects for Reduced Photodegradation of Polymers. *Crystals* **2021**, *11* (1), 1–22.

[17] Bobleter, O. Hydrothermal Degradation of Polymers Derived from Plants. *Prog. Polym. Sci.* **1994**, *19* (5), 797–841.

[18] Allen, N. S. Recent Advances in the Photo-Oxidation and Stabilization of Polymers. *Chem. Soc. Rev.* **1986**, *15* (3), 373–404.

[19] Yousif, E.; Haddad, R. Photodegradation and Photostabilization of Polymers, Especially Polystyrene: Review. *Springerplus* **2013**, *2* (1), 1–32.

[20] Rivaton, A. Recent Advances in Bisphenol-A Polycarbonate Photodegradation. *Polym. Degrad. Stab.* **1995**, *49* (1), 163–179.

[21] Rizzarelli, P.; Rapisarda, M.; Ascione, L.; Innocenti, F. D.; Degli Innocenti, F. Influence of Photo-Oxidation on the Performance and Soil Degradation of Oxo- and Biodegradable Polymer-Based Items for Agricultural Applications. *Polym. Degrad. Stab.* **2021**, *188*, 109578.

[22] Rabek, J. F.; Rånby, B. The Role of Singlet Oxygen in the Photooxidation of Polymers. *Photochem. Photobiol.* **1978**, *28* (4–5), 557–569.

[23] Celina, M. C. Review of Polymer Oxidation and Its Relationship with Materials

Performance and Lifetime Prediction. *Polym. Degrad. Stab.* **2013**, *98* (12), 2419–2429.

[24] Djouani, F.; Richaud, E.; Fayolle, B.; Verdu, J. Modelling of Thermal Oxidation of Phosphite Stabilized Polyethylene. *Polym. Degrad. Stab.* **2011**, *96* (7), 1349–1360.

[25] Gmbh, W. V. Macromol. Symp. 176, 1–15 (2001). **2001**, *15*, 1–15.

[26] Hamskog, M.; Klügel, M.; Forsström, D.; Terselius, B.; Gijsman, P. The Effect of Base Stabilization on the Recyclability of Polypropylene as Studied by Multi-Cell Imaging Chemiluminescence and Microcalorimetry. *Polym. Degrad. Stab.* **2004**, *86* (3), 557–566.

[27] Sadeghifar, H.; Ragauskas, A. Lignin as a Bioactive Polymer and Heavy Metal Absorber- an Overview. *Chemosphere* **2022**, *309* (P1), 136564.

[28] Chirinos Padrón, A. J. Mechanistic Aspects of Polymer Photostabilization. *J. Photochem. Photobiol. A Chem.* **1989**, *49* (1–2), 1–39.

[29] Solera, P. Trends in Polymer Applications. **2008**, *4* (3), 3-1-3–49.

[30] Shahidi, F.; Janitha, P. K.; Wanasundara, P. D. Phenolic Antioxidants. *Crit. Rev. Food Sci. Nutr.* **1992**, *32* (1), 67–103.

[31] Klampfl, C. W.; Himmelsbach, M. Advances in the Determination of Hindered Amine Light Stabilizers – A Review. *Anal. Chim. Acta* **2016**, *933* (2016), 10–22.

[32] Kirschweng, B.; Tátraaljai, D.; Földes, E.; Pukánszky, B. Natural Antioxidants as Stabilizers for Polymers. *Polym. Degrad. Stab.* **2017**, *145*, 25–40.

[33] Geven, M.; d'Arcy, R.; Turhan, Z. Y.; El-Mohtadi, F.; Alshamsan, A.; Tirelli, N.

Sulfur-Based Oxidation-Responsive Polymers. Chemistry, (Chemically Selective) Responsiveness and Biomedical Applications. *Eur. Polym. J.* **2021**, *149* (February), 110387.

[34] Sedlar, J. The Mechanism by Which Hindered Amine Light Stabilisers (HALS) Protect Polymers Involves a Multitude of Functions Which Are Now Critically Reviewed . The High Basicity , Typical for HALS , Enhances the Association of Stabiliser with Hydroperoxides ROO. **1982**, *2*.

[35] Ranaweera, R. P. R.; Scott, G. Mechanisms of Antioxidant Action: Metal Complexes as u.v. Stabilisers in Polyethylene. *Eur. Polym. J.* **1976**, *12* (8), 591–597.

[36] Keck, J.; Kramer, H. E. A.; Port, H.; Hirsch, T.; Fischer, P.; Rytz, G. Investigations on Polymeric and Monomeric Intramolecularly Hydrogen-Bridged UV Absorbers of the Benzotriazole and Triazine Class. *J. Phys. Chem.* **1996**, *100* (34), 14468–14475.

[37] Skoultchi, M. Ultraviolet Stabilizing. **1965**, *9*, 903–910.

[38] Zayat, M.; Garcia-Parejo, P.; Levy, D. Preventing UV-Light Damage of Light Sensitive Materials Using a Highly Protective UV-Absorbing Coating. *Chem. Soc. Rev.* **2007**, *36* (8), 1270–1281.

[39] Pospíšil, J. Mechanistic Action of Phenolic Antioxidants in Polymers-A Review. *Polym. Degrad. Stab.* **1988**, *20* (3–4), 181–202.

[40] Gugumus, F. Possibilities and Limits of Synergism with Light Stabilizers in

Polyolefins 2. HALS in Polyolefins. *Polym. Degrad. Stab.* **2002**, *75*, 295–308.

[41] Bauer, I.; Habicher, W. D.; Rautenberg, C.; AI-Malaika, S. Antioxidant Interaction between Organic Phosphites and Hindered Amine Light Stabilisers during Processing and Thermoxidation of Polypropylene. *Polym. Degrad. Stab.* **1995**, *48* (3), 427–440.

[42] Gugumus, F. Possibilities and Limits of Synergism with Light Stabilizers in Polyolefins 2. UV Absorbers in Polyolefins. *Polym. Degrad. Stab.* **2002**, *75* (2), 309–320.

[43] le Saché, E.; Reina, T. R. Analysis of Dry Reforming as Direct Route for Gas Phase CO2 Conversion. The Past, the Present and Future of Catalytic DRM Technologies. *Prog. Energy Combust. Sci.* **2022**, *89* (March 2020). https://doi.org/10.1016/j.pecs.2021.100970.

[44] Lavoie, J. M. Review on Dry Reforming of Methane, a Potentially More Environmentally-Friendly Approach to the Increasing Natural Gas Exploitation. *Front. Chem.* **2014**, *2* (NOV), 1–17.

[45] Bahraminia, S.; Anbia, M.; Koohsaryan, E. Hydrogen Sulfide Removal from Biogas Using Ion-Exchanged Nanostructured NaA Zeolite for Fueling Solid Oxide Fuel Cells. *Int. J. Hydrogen Energy* **2020**, *45* (55), 31027–31040.

[46] Schwab, E.; Milanov, A.; Schunk, S. A.; Behrens, A.; Schödel, N. Dry Reforming and Reverse Water Gas Shift: Alternatives for Syngas Production? *Chemie-Ingenieur-Technik* **2015**, *87* (4), 347–353.

[47] Aider, N.; Touahra, F.; Bali, F.; Djebarri, B.; Lerari, D.; Bachari, K.; Halliche, D. Improvement of Catalytic Stability and Carbon Resistance in the Process of CO2 Reforming of Methane by CoAl and CoFe Hydrotalcite-Derived Catalysts. *Int. J. Hydrogen Energy* **2018**, *43* (17), 8256–8266.

[48] Nikoo, M. K.; Amin, N. A. S. Thermodynamic Analysis of Carbon Dioxide Reforming of Methane in View of Solid Carbon Formation. *Fuel Process. Technol.* **2011**, *92* (3), 678–691.

[49] Torrez-Herrera, J. J.; Korili, S. A.; Gil, A. Recent Progress in the Application of Ni-Based Catalysts for the Dry Reforming of Methane. *Catal. Rev. - Sci. Eng.* **2021**, *00* (00), 1–58.

[50] Jang, W. J.; Jeong, D. W.; Shim, J. O.; Kim, H. M.; Han, W. B.; Bae, J. W.; Roh, H. S. Metal Oxide (MgO, CaO, and La2O3) Promoted Ni-Ce0.8Zr0.2O2 Catalysts for H2 and CO Production from Two Major Greenhouse Gases. *Renew. Energy* **2015**, *79* (1), 91–95.

[51] Jang, W. J.; Jeong, D. W.; Shim, J. O.; Roh, H. S.; Son, I. H.; Lee, S. J. H2 and CO Production over a Stable Ni-MgO-Ce 0.8Zr0.2O2 Catalyst from CO2 Reforming of CH4. *Int. J. Hydrogen Energy* **2013**, *38* (11), 4508–4512.

[52] Xu, G.; Shi, K.; Gao, Y.; Xu, H.; Wei, Y. Studies of Reforming Natural Gas with Carbon Dioxide to Produce Synthesis Gas. X. The Role of CeO2 and MgO Promoters. *J. Mol. Catal. A Chem.* **1999**, *147* (1–2), 47–54.

[53] Song, J. H.; Han, S. J.; Song, I. K. Hydrogen Production by Steam Reforming of

Ethanol Over Mesoporous Ni–Al2O3–ZrO2 Catalysts. *Catal. Surv. from Asia* **2017**, *21* (3), 114–129.

[54] Marinho, A. L. A.; Toniolo, F. S.; Noronha, F. B.; Epron, F.; Duprez, D.; Bion, N. Highly Active and Stable Ni Dispersed on Mesoporous CeO2-Al2O3 Catalysts for Production of Syngas by Dry Reforming of Methane. *Appl. Catal. B Environ.* **2021**, *281* (May 2020), 119459.

[55] Inui, T.; Saigo, K.; Fujii, Y.; Fujioka, K. Catalytic Combustion of Natural Gas as the Role of On-Site Heat Supply in Rapid Catalytic CO2H2O Reforming of Methane. *Catal. Today* **1995**, *26* (3–4), 295–302.

[56] A. Álvarez, M.; Bobadilla, L. F.; Garcilaso, V.; Centeno, M. A.; Odriozola, J. A. CO2 Reforming of Methane over Ni-Ru Supported Catalysts: On the Nature of Active Sites by Operando DRIFTS Study. *J. CO2 Util.* **2018**, *24* (November 2017), 509–515.

[57] Rostrup-Nielsen, J. R.; Bak Hansen, J. H. CO2-Reforming of Methane over Transition Metals. *Journal of Catalysis*. 1993, pp 38–49.

[58] Claridge, J. B.; Green, M. L. H.; Tsang, S. C.; York, A. P. E.; Ashcroft, A. T.; Battle, P. D. A Study of Carbon Deposition on Catalysts during the Partial Oxidation of Methane to Synthesis Gas. *Catal. Letters* **1993**, *22* (4), 299–30.

[59] Abdullah, B.; Abd Ghani, N. A.; Vo, D. V. N. Recent Advances in Dry Reforming of Methane over Ni-Based Catalysts. *J. Clean. Prod.* **2017**, *162*, 170–185.

[60] Sharifianjazi, F.; Esmaeilkhanian, A.; Bazli, L.; Eskandarinezhad, S.; Khaksar, S.;

Chapter 1

Shafiee, P.; Yusuf, M.; Abdullah, B.; Salahshour, P.; Sadeghi, F. A Review on Recent Advances in Dry Reforming of Methane over Ni- and Co-Based Nanocatalysts. *Int. J. Hydrogen Energy* **2021**, (Article in press).

Chapter 2

Exploring stabilizer formulations for light-induced yellowing for light-induced yellowing of polystyrene by high-throughput experimentation and machine learning

Chapter 2

Abstract

In this chapter, a high-throughput experimental protocol was established for yellowing inhibition of transparent plastics on the basis of solution film casting on microplates and ultraviolet/visible (UV/Vis) spectroscopic evaluation using a microplate reader. A combination of the protocol and a genetic algorithm realized a large-scale exploration of stabilizer formulations that consist of commercially available hindered amine stabilizers and UV absorbers, etc. The found formulations were highly effective in inhibiting the photo-induced yellowing of polystyrene, compared to the most efficient single stabilizer at the fixed concentration. The obtained data, which corresponded to seven years of aging (when sequentially acquired), were analyzed and validated based on decision tree classification, force-directed network visualization, and so on. A formulation design guideline was successfully derived that it is essential to combine as many stabilizers that are complementary and synergistic with each other as possible.

Keywords: stabilizer formulation, light-induced yellowing, transparent plastics, high-throughput experimentation, genetic algorithm, force-directed graph, synergism

Chapter 2

2.1. Introduction

In imparting practical durability to polymeric materials, a combination of synergistic stabilizers called a stabilizer formulation is essential [1–4]. However, a design of stabilizer formulations is hard to generalize, and systematic research has been hampered due to a low throughput of durability tests and a huge number of potential combinations [5,6]. In a recent study, Taniike et al. have proposed a solution to the problems, which is based on a combination of high-throughput chemiluminescence imaging for durability tests and a genetic algorithm for combinatorial optimization [7]. This allowed them to find new formulations that significantly improve the durability of polypropylene in a high-temperature oxidative degradation, out of a huge parameter space consisting of 10^7 formulations [8]. Here, I report a novel high-throughput experimental protocol and a genetic algorithm for efficient discoveries of stabilizer formulations to inhibit a yellowing of transparent plastics during photo aging.

Transparent plastics, such as polymethyl methacrylate (PMMA), polycarbonate (PC), and atactic polystyrene (PS), are amorphous polymers with high transparency and Abbe number [9–11]. They are used as alternatives to inorganic glass due to their advantages of transparency, processability, light weight, and low cost. On the other hand, the weaknesses of transparent plastics are their low scratch hardness and heat resistance, as well as their susceptibility to the yellowing [12–14]. In particular, the yellowing due to outdoor exposure directly damages the high transparency, so its suppression for a long

term is highly desired. Generally, the yellowing of transparent plastics is caused by the formation and accumulation of chromophores, such as ethylene and carbonyl groups, in the polymer structure due to the progress of photo degradation [15,16]. In addition, it is known that the yellowing is intensified when the above chromophores coexist with hydroxy and carboxyl groups [17,18]. This problem is exclusively addressed by an addition of stabilizers. Although the basic strategy is to add a larger amount of stabilizers with higher efficacy, there are limitations to increase the amount of the addition, so the development of synergistic formulations is essential [19–21].

In this chapter, I developed a high-throughput experimental protocol consisting of the following two processes, in order to efficiently explore stabilizer formulations regarding the yellowing inhibition. First, cast films containing different formulations are prepared on glass 96 well-microplates, and the microplates are directly subjected to a photo irradiation, which enables simultaneous photo aging of a large array of samples. Then, the yellowing of the large array of samples is rapidly determined by subjecting the microplates after the irradiation to a microplate reader. For example, in this chapter, three microplates were used to simultaneously evaluate the yellowing resistance of as many as 288 samples in a single test. By combining this high-throughput experimental protocol with a genetic algorithm [22,23], I conducted non-empirical exploration of stabilizer formulations that can suppress the yellowing of atactic PS without increasing the addition amount. Furthermore, the obtained big data corresponding to seven years of photo aging was analyzed in order to understand common features of high-performing formulations

as well as rules of making synergistic combinations.

2.2. Experimental

2.2.1. Materials

Atactic PS pellets ($M_w = 19.2 \times 10^4$) were purchased from Sigma-Aldrich. They were dissolved in dichloromethane and recovered by precipitation from methanol to remove additives contained in original pellets. Figure 2.1 shows a stabilizer library. A total of 24 stabilizers were provided by ADEKA, Toyotsu Chemiplus, and Clariant. They were selected from common UV absorbers (UVAs), hindered amine light stabilizers (HALSs), and phenolic antioxidants, and are colored in Figure 2.1 according to their respective categories. In general, the anti-coloring effect of UVAs for aromatic resins follows in the order of benzotriazole ≈ triazine > benzophenone, while the compatibility is higher for benzophenone > benzotriazole ≈ triazine. Among HALSs, the thermal stability is in the order N–H ≈ N–R > N–OR, while the stability to an acidic substance is in the order N–OR > N–H ≈ N–R [24].

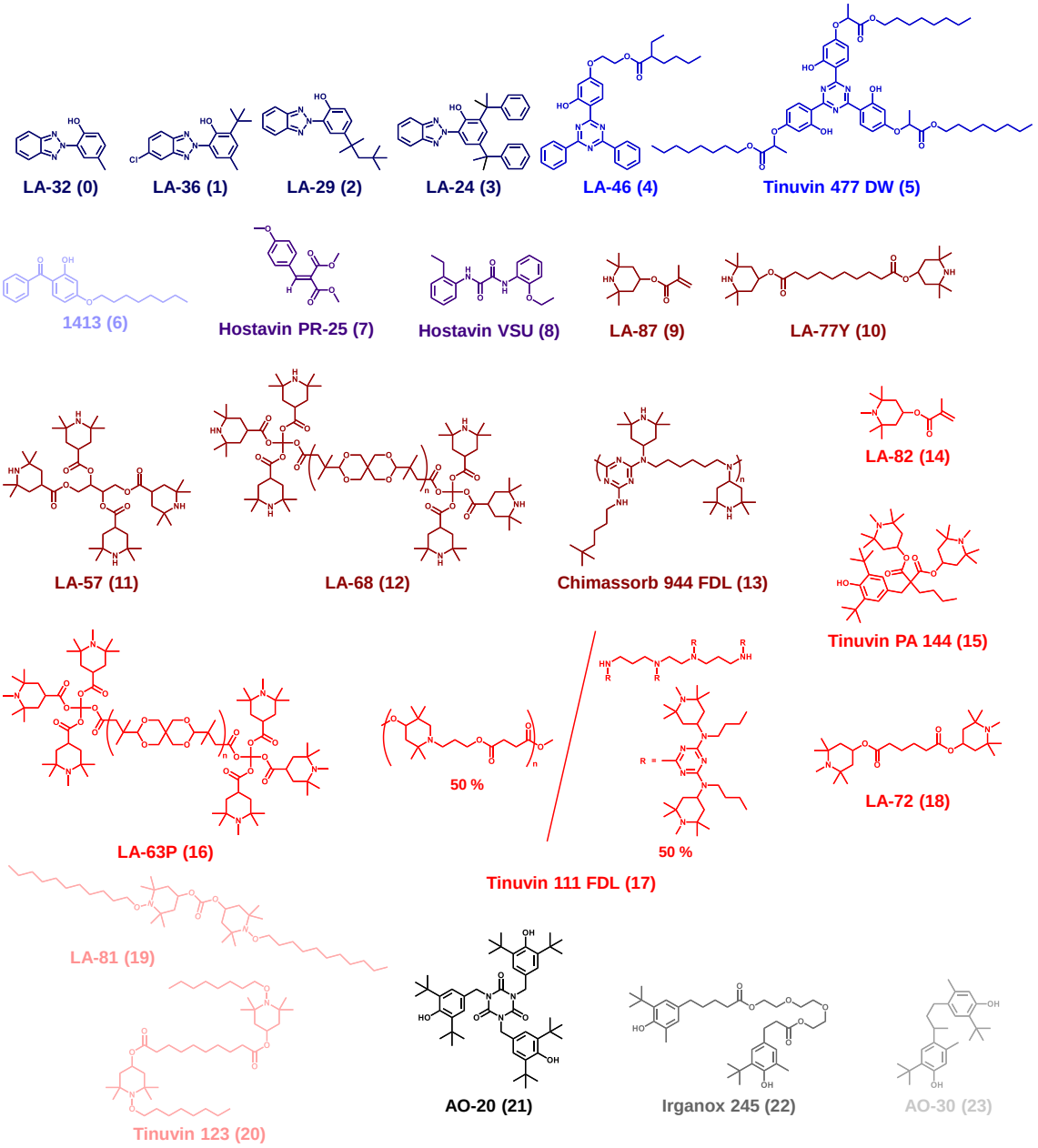

Figure 2.1. Library of stabilizers. The numbers in parentheses correspond to the gene codes used in the genetic algorithm. The colors correspond to the group of stabilizers: dark blue, benzotriazole type; blue, triazine type; light blue, benzophenone type; purple, other types; dark red, N–H type; red, N–R type; light red, N–OR type; black, hindered phenol; gray, semi-hindered phenol; light gray, less-hindered phenol.

2.2.2. Methodology

2.2.2.1. Microplate method

The high-throughput experimental protocol proposed in this chapter consists of the preparation of a large number of cast films on microplates and a quick determination of the photo-induced yellowing of these films using a microplate reader.

2.2.2.2. Film preparation

83 µL of a solution containing PS and stabilizers was cast into each well of a 96-well glass bottom microplate (BMB-1, BM Equipment). The microplate was dried for 12 h at room temperature to obtain 96 cast films with the thickness of 100 µm. Individual solutions were prepared by dissolving 0.10 g of stabilizer-free PS and a specified amount of stabilizers or their formulations in dichloromethane (3.9 g) at room temperature. Apart from this, self-standing films with the thickness of 100 µm were also prepared for validation experiments. The films prepared on petri dishes were peeled off after immersing in water for 4 h. The obtained films were dried in vacuum at 60 °C for 4 h.

2.2.2.3. Photo aging

Photo aging was performed using a xenon lamp accelerator SUNTEST CPS+ (Atlas). Either the microplates or self-standing films were placed in the chamber and irradiated typically for 300 h, during which the power of the irradiance was fixed at 550 W/m^2 and the black panel temperature was set to 83 °C. The black panel temperature indicates the temperature of the polymer exposed to sunlight, which can reach over 80 °C in the

summer season.

2.2.2.4. Characterization

Discoloration due to the light exposure was evaluated by UV/Vis absorption spectroscopy. In case of the microplates, a microplate reader (Epoch 2, BioTek) was used with a wavelength range of 300–800 nm. The spectrum of the blank microplate was subtracted as the background.

UV/vis spectra of the self-standing films were acquired on a V770 spectrometer (JASCO). Fourier transform infrared spectra of the films were recorded in attenuated total reflection (ATR) mode by using a Spectrum 100 spectrometer (Perkin-Elmer).

2.2.3. Exploration of stabilizer formulations

Figure 2.2 represents the methodology used to explore stabilizer formulations. The parametric space explored in this chapter consists of 92,561,040 formulations that can be created by combining any 10 of the 24 stabilizers in the library with duplications allowed. The amount of a formulation added to polystyrene is 0.050 wt%, which is equal to 0.005 wt% multiplied by 10 selections. The amount of a specific stabilizer in the formulation is expressed as $0.005 \times n$ wt%. where n is the number of selections. In the following, the details of the methodology are described in three steps as shown in Figure 2.2.

Step 1: Preparation

Preparation of polystyrene cast films containing given formulations is carried out.

Formulations are obtained by random selection in the case of the 0th generation and by genetic operators thereafter. The preparation of cast films on microplates is described in 2.2.2.2. A total of 288 cast films, consisting of 8 films (N = 8) by 36 formulations were prepared using three 96-well microplates.

Step 2: Evaluation

The three microplates are placed in the sun tester and photo degradation tests are carried out as described in 2.2.2.3. UV/vis absorption characteristics of the films after 300 h of irradiation are acquired on the microplate reader as described in 2.2.2.4. The change in absorbance at 400 nm before and after irradiation was used as an index of the yellowing. The inverse of the absorbance at 400 nm averaged over N = 8 was used to represent the performance of a formulation. The fitness within the genetic algorithm is given according to the following equation,

$$\rho_i = \frac{1/\mathrm{Abs}_i - 1/\mathrm{Abs}_{max}}{1/\mathrm{Abs}_{min} - 1/\mathrm{Abs}_{max}} \quad (2.1),$$

$$f_i = \exp(3\rho_i) \quad (2.2),$$

where $1/\mathrm{Abs}_i$, $1/\mathrm{Abs}_{min}$, and $1/\mathrm{Abs}_{max}$ are the inverse of the absorbance at 400 nm for the i^{th}, the best, and the worst formulations in a generation, respectively. f_i is the fitness of the i^{th} formulation.

Step 3: Evolution

Genetic operators were implemented to create formulations of the next generation. In crossover, the stabilizers which were common to two selected parent formulations were inherited, and the non-common parts were randomly inherited from either of the parent

formulations. In mutation, 10 or 20% of the stabilizers in a selected parent formulation were replaced by stabilizers randomly drawn from the library. The parents were selected by a roulette method using a fitness as a weight. 22 formulations by crossover, 3 formulations by mutation, 8 formulations by elitism, and 3 random formulations created as in the 0^{th} generation led to 36 formulations for the next generation.

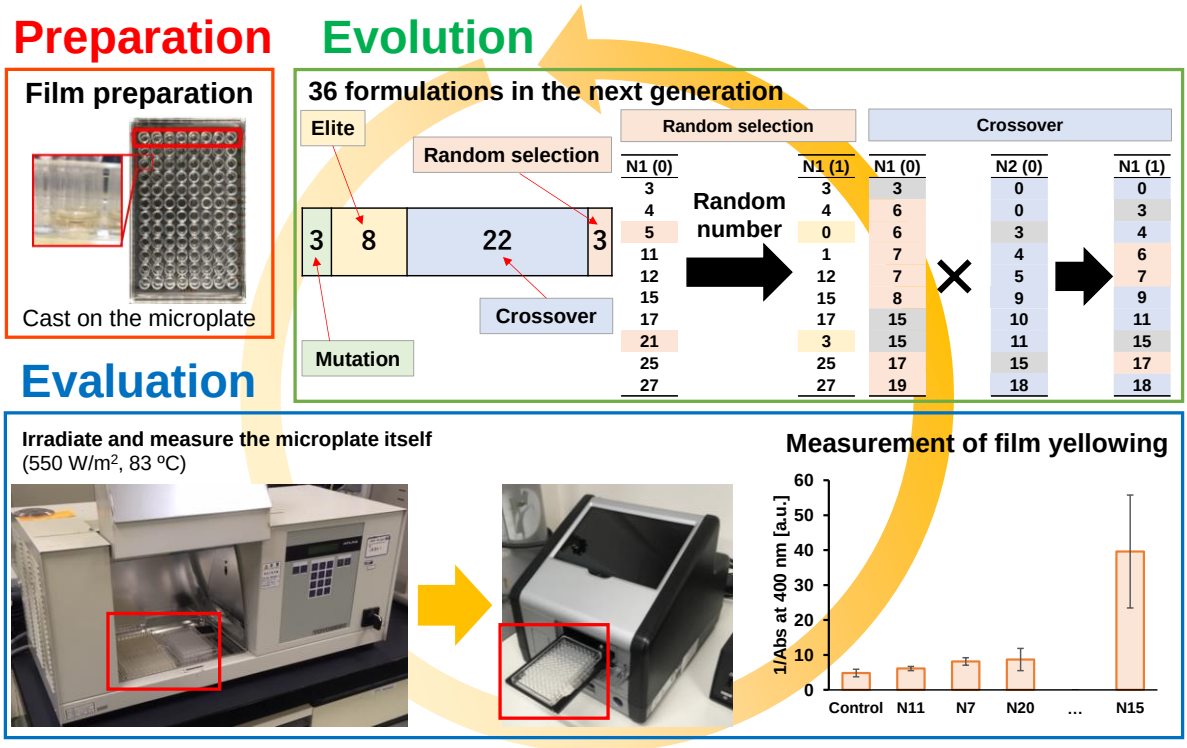

Figure 2.2. Scheme of the exploration of stabilizer formulations based on the genetic algorithm. The scheme consists of three steps: preparation of cast films on microplates, evaluation of their yellowing resistance, and evolution of formulations. Stabilizer formulations are defined as combinations of 10 stabilizers, which are expressed by the gene codes shown in Figure 2.1.

2.2.4. Data analysis

In this chapter, a total of 259 formulations were obtained, excluding duplicates due to elite preservation. This is equivalent to 2590 selections of stabilizers and 11655 selections of binary combinations. The analysis of such a large dataset was conducted to derive insights into a formulation design and a synergism among stabilizers. Most of the analyses can be performed without any special software. The decision tree analysis was implemented using the scikit-learn library in python [25]. Gephi was used for visualizing the interaction among stabilizers. The details of each analysis are described in the corresponding part of Results and Discussion [26,27].

2.3. Results and discussion

2.3.1. Establishment of a microplate method

In this chapter, I propose a high-throughput experimental protocol called a microplate method to evaluate the photo-induced yellowing of transparent plastics. In this protocol, cast films prepared on microplates are directly irradiated with light, and the UV/Vis absorption of the films is evaluated by a microplate reader. In order to establish such the protocol, the photo degradation behavior of unstabilized PS was first compared between microplate-casted films and self-standing films having the identical thickness (Figure 2.3).

The IR and UV/vis spectra of the self-standing PS film were tracked every 50 h of light irradiation, and are shown in Figures 2.3a and 2.3b, respectively. In the IR spectra, the absorbance of the stretching vibration of methine (1494 cm^{-1}) decreased along with the irradiation time, and this accompanied an increase in the absorbance of C=O at 1734 cm^{-1}. This corresponds to the C–H cleavage at tertiary carbons in PS and the formation of C=O groups mediated by the decomposition of peroxide radical intermediates [28]. In the UV/Vis spectra, the absorbance below 450 nm increased along with the irradiation time. This reflects the formation of chromophores such as hydroperoxides, carbonyls, unsaturated bonds, and so on [28]. Chromophores are functional groups for the discoloration of polymers, and when auxiliary chromophores such as amino and carboxyl groups coexist with chromophores, the discoloration can be largely promoted [29].

Following these results, the progress of photo degradation of the self-standing PS was plotted using two markers (Figure 2.3c): increases in the absorbance of C=O in IR and in the absorbance at 400 nm with respect to the unirradiated film. The former is widely used as a marker for the oxidative degradation of polymers. The latter is an indicator of the yellowness. In Figure 2.3c, both of the markers exhibited similar exponential increase with the irradiation time, as these changes are consequences of the same auto-oxidation. Figure 2.3d compares the increase in absorbance at 400 nm upon photo irradiation between the self-standing and microplate-casted films. This verified that the films prepared on the microplate underwent a similar photo degradation as the self-standing films.

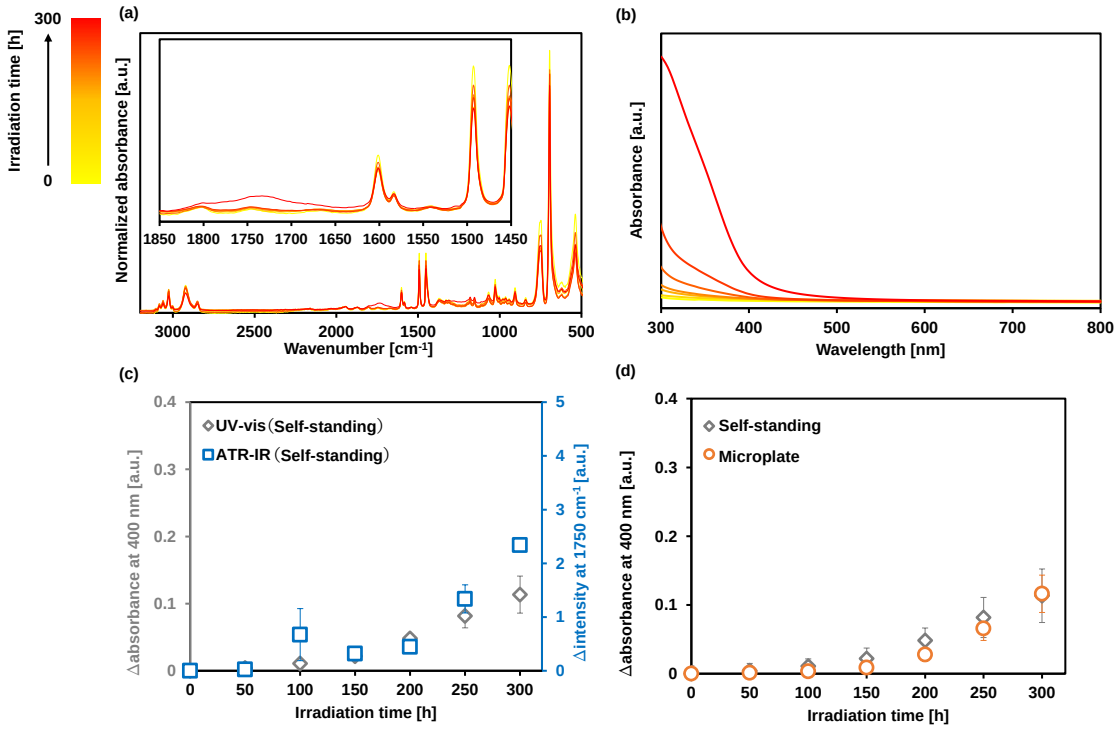

Figure 2.3. Comparison of the photo degradation of self-standing and microplate-casted PS films. a, b) Changes in the IR and UV/Vis spectra of the self-standing films along with photo irradiation. c) Increases in the absorbance of C=O and in the absorbance at 400 nm are plotted against the irradiation time for the self-standing film. d) Increase in the absorbance at 400 nm upon photo irradiation for the microplate-casted films compared to that of self-standing films.

2.3.2. Evolution of formulations

Figure 2.4 plots the evolution of the best and average performance of formulations along with the generation. The performance of the formulations was determined on the basis of the absorbance at 400 nm of PS after 300 hours of light exposure. Within 9 generations, the best performance and average performance improved 2.7 times and 3.6 times, respectively. When each of the 24 stabilizers in the library was added to PS at the maximum concentration (0.05 wt%), Tinuvin PA 144 (No. 15) showed the best performance (Figure 2.5). From Figure 2.4, it can be seen that most of the formulations perform much better than that of Tinuvin PA 144 (No. 15). This fact clearly indicates the importance of synergistic combinations for the yellowing suppression.

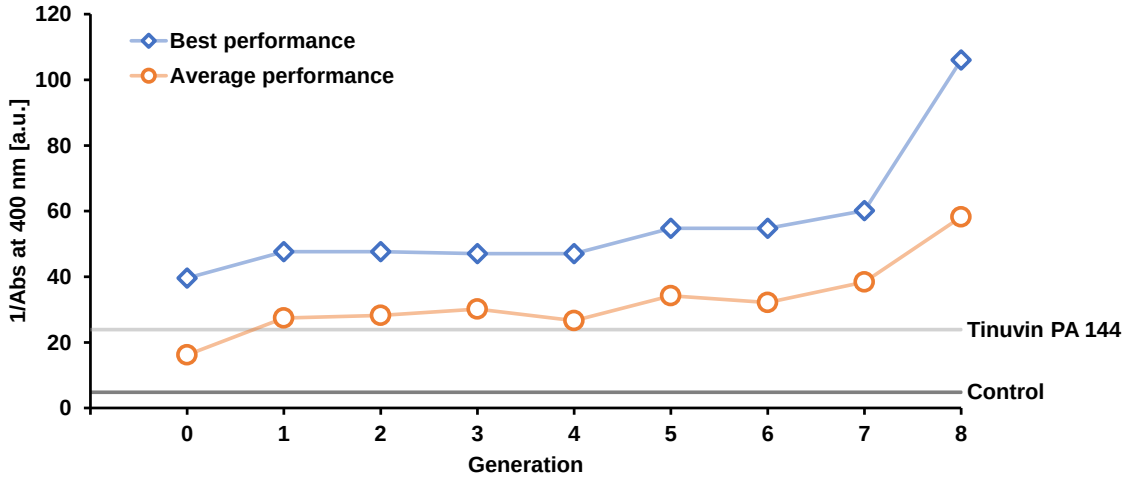

Figure 2.4. The evolution of the best and average performance of formulations along with the generation. The performance of a stabilizer formulation was evaluated as 1/Abs during photo degradation of PS after 300 h irradiation. Control corresponds to PS without stabilizer, and Tinuvin PA 144 (No.15) shows the highest performance as an individual stabilizer in the library.

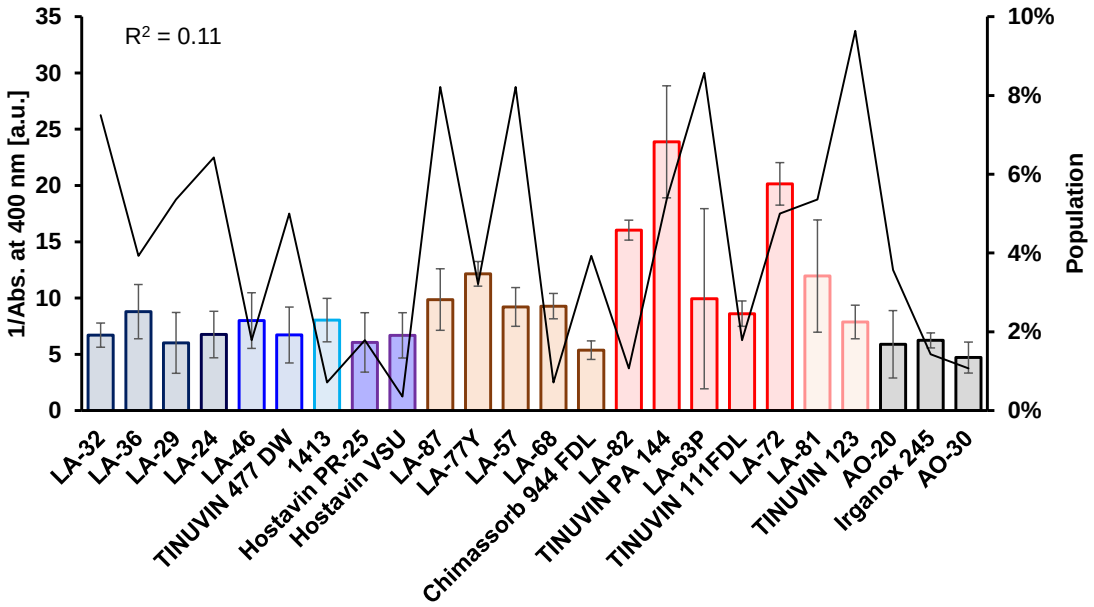

Figure 2.5. Performance of the 24 stabilizers in the library. Films containing only one

stabilizer at 0.050 wt% were prepared on a microplate and the performance was determined with the absorbance at 400 nm after 300 h of light exposure. The right axis corresponds to the population of each stabilizer in the last generation of the genetic algorithm. A low R^2 value indicates little correlation between the performance of stabilizers on their own (the left axis) and being selected in the genetic algorithm (the right axis).

2.3.3. Formulations and their performance

A total of 259 formulations were obtained as a result of evolution over 8 generations (note that duplicates due to the elitism are not counted). Table 2.1 lists the 259 formulations and their performance. The formulation code, G*x*-*y*, refers to the y^{th} best formulation in the x^{th} generation. There are 10 genes per formulation, and the value in each gene corresponds to the number of stabilizers as defined in Figure 2.1. Table 2.2 lists the 10 best performing formulations out of the 259 formulations. It can be seen that these formulations commonly contain certain stabilizers: LA-87 (No. 9), LA-63P (No. 16), Tinuvin 123 (No. 20) > Tinuvin 477 DW (No. 5), LA-57 (No. 11), LA-81 (No. 19) > LA-32 (No. 0) in the order of the frequency of appearance. A breakdown by the type of stabilizers is LA-87: HALS (N–H), LA-63P: HALS (N–R), Tinuvin 123: HALS (N–OR), Tinuvin 477 DW: UVA (triazine), LA-57: HALS (N–H), LA-81: HALS (N–OR), and LA-32: UVA (benzophenone). Thus, many of the stabilizers frequently contained in good

performing formulations belong to different types, which suggests the complementary action of different types of stabilizers in inhibiting the photo degradation. A similar result was obtained in the thermo-oxidative degradation of PP [6]. On the other hand, LA-86 and LA-57, which were selected from the same N–H type, differ significantly in the molecular weight. This likely corresponds to a well-known synergism between a high molecular weight HALS with a superior retainability and a low molecular weight HALS with a superior mobility [30-32].

Table 2.1. List of formulations[a].

Formulation code[a]	Stabilizers[b]										1/Abs[c]
G0-1	1	2	2	2	6	9	9	10	10	20	39.6
G0-2	2	6	8	9	13	14	17	17	20	21	35.4
G0-3	1	4	4	4	9	16	18	18	20	22	29.4
G0-4	1	8	8	11	11	14	14	15	16	21	23.5
G0-5	0	3	9	13	16	16	18	19	20	20	20.7
G0-6	0	1	1	2	4	9	9	11	18	20	19.8
G0-7	0	0	1	1	9	13	15	16	17	17	19.2
G0-8	7	10	10	13	17	19	21	21	22	23	19.1
G0-9	1	1	1	9	9	11	13	14	16	17	18.6
G0-10	1	2	3	3	3	11	13	14	18	21	18.1
G0-11	3	6	10	14	16	17	18	18	20	23	17.8
G0-12	2	5	5	9	13	15	17	18	19	21	17.7
G0-13	1	4	5	7	14	15	16	17	21	21	15.8
G0-14	2	2	4	5	9	10	14	19	19	20	15.6
G0-15	1	1	5	9	10	10	13	16	16	22	15.5
G0-16	1	2	5	8	11	16	16	20	22	22	15.4
G0-17	3	4	7	9	10	12	18	19	21	22	15.3
G0-18	0	0	2	6	8	13	15	15	20	20	15.3
G0-19	0	4	6	9	10	10	12	14	17	22	14.8
G0-20	0	0	4	6	11	14	14	15	20	22	14.8
G0-21	3	5	6	10	11	15	18	19	20	23	14.1
G0-22	0	7	12	15	16	17	17	17	18	22	14.1
G0-23	1	2	2	2	8	9	10	12	18	21	13.3
G0-24	0	1	2	6	12	13	14	15	22	23	13.2
G0-25	2	2	6	7	11	12	15	16	20	21	12.5
G0-26	1	4	5	10	12	15	15	18	22	23	12.2

G0-27	1	7	11	17	17	20	20	20	21	23	11.6
G0-28	0	2	2	4	5	11	13	14	14	23	11.3
G0-29	8	8	11	13	14	17	17	19	20	20	11.2
G0-30	3	9	10	14	17	19	20	22	23	23	10.1
G0-31	0	3	4	5	7	18	18	19	23	23	10.0
G0-32	0	5	8	10	13	16	19	20	23	23	9.2
G0-33	1	3	5	6	6	7	11	12	12	19	8.7
G0-34	0	6	6	7	8	16	16	17	19	23	8.1
G0-35	0	2	3	3	4	5	7	8	16	22	6.1
G1-1	0	0	5	5	11	13	15	15	15	23	47.6
G1-2	1	2	2	8	8	9	10	12	18	21	44.9
G1-3	2	2	2	6	9	9	10	17	20	21	44.4
G1-4	1	2	5	8	11	16	19	20	22	22	44.0
G1-5	1	2	4	9	14	14	14	16	16	17	40.8
G1-6	1	1	2	7	9	15	16	18	18	20	37.2
G1-7	2	6	8	9	12	13	14	18	20	21	36.5
G1-8	1	1	1	4	5	5	9	10	15	18	34.8
G1-9	0	1	4	4	9	11	18	18	20	22	34.3
G1-10	1	1	2	2	2	9	9	9	13	15	34.0
G1-11	1	2	6	7	7	10	10	17	20	22	33.8
G1-12	1	2	2	5	7	11	16	16	16	20	33.3
G1-13	0	1	1	13	14	15	16	17	18	23	32.7
G1-14	2	6	6	9	9	13	18	18	19	20	32.7
G1-15	1	10	10	10	11	14	15	16	16	16	29.3
G1-16	7	11	12	12	16	17	17	18	20	22	29.1
G1-17	2	6	8	9	13	14	17	17	20	21	28.0
G1-18	1	4	8	9	9	9	11	16	20	22	26.8
G1-19	0	2	6	10	10	13	14	14	17	20	26.1
G1-20	2	8	9	9	9	10	11	11	18	21	24.2
G1-21	1	1	4	5	5	6	6	11	14	20	23.7
G1-22	1	2	2	6	9	9	10	14	14	20	22.9
G1-23	1	2	2	2	6	9	9	10	10	20	22.2
G1-24	0	1	8	9	11	12	14	16	18	22	21.4
G1-25	0	3	9	16	18	19	20	20	22	23	15.3
G1-26	1	5	7	7	10	16	20	20	22	23	14.9
G1-27	0	3	7	7	7	13	18	19	20	23	13.1
G1-28	1	1	2	2	2	6	6	11	20	23	12.8
G2-1	1	2	5	7	11	16	16	16	20	22	47.1
G2-2	0	4	5	5	9	11	15	17	19	21	40.4
G2-3	1	2	5	8	11	11	19	20	22	22	38.6
G2-4	4	5	5	9	12	14	17	19	20	20	32.0
G2-5	0	9	13	13	16	16	19	19	19	20	30.3
G2-6	1	2	2	4	9	14	15	16	16	17	29.4
G2-7	1	5	8	11	15	15	16	20	22	22	29.4
G2-8	1	1	1	1	4	5	9	10	15	18	28.1
G2-9	0	1	2	13	14	17	17	18	18	20	27.5
G2-10	3	3	5	8	13	13	14	20	20	21	27.3

G2-11	1	2	8	9	11	16	16	18	19	19	26.4
G2-12	0	0	5	5	11	13	15	15	15	23	25.0
G2-13	1	2	6	6	9	9	10	16	20	22	24.0
G2-14	1	2	2	9	9	13	14	15	20	21	22.4
G2-15	1	1	1	2	2	4	8	8	9	9	22.0
G2-16	2	2	2	6	7	10	17	20	21	22	21.9
G2-17	1	1	8	8	10	12	12	12	15	18	21.3
G2-18	7	8	8	8	10	12	12	16	18	20	20.8
G2-19	1	2	2	2	6	7	10	10	17	20	20.8
G2-20	1	2	2	7	9	9	9	9	10	20	20.0
G2-21	2	2	6	6	9	14	16	17	20	20	19.4
G2-22	0	1	1	1	2	5	11	20	22	22	18.5
G2-23	1	2	6	13	14	15	15	16	18	21	17.7
G2-24	1	4	9	11	11	14	14	16	22	22	17.1
G2-25	2	2	2	8	9	10	11	12	18	21	16.4
G2-26	1	2	4	6	9	9	9	16	16	20	15.4
G2-27	1	2	2	2	2	6	8	9	10	21	13.5
G2-28	2	2	9	9	9	9	10	11	11	21	12.3
G3-1	0	0	0	2	5	9	11	16	19	20	38.5
G3-2	1	2	2	5	7	11	15	16	16	19	37.9
G3-3	1	2	7	9	9	16	16	16	20	22	37.6
G3-4	1	1	1	2	2	9	10	10	16	18	35.4
G3-5	2	3	7	7	13	14	16	16	19	20	34.5
G3-6	5	8	9	11	11	15	15	19	20	22	34.0
G3-7	1	2	2	2	9	9	18	18	20	21	32.4
G3-8	0	0	1	2	9	15	16	16	19	19	31.5
G3-9	0	0	4	5	5	9	11	11	19	22	31.0
G3-10	1	2	2	2	5	11	16	16	20	23	30.5
G3-11	2	5	7	11	13	13	13	15	16	22	29.0
G3-12	0	0	0	1	5	12	13	18	20	22	28.8
G3-13	2	16	16	17	17	19	20	21	21	21	27.4
G3-14	1	1	5	8	10	12	16	16	18	20	27.3
G3-15	0	1	2	13	14	17	17	18	18	20	27.0
G3-16	0	1	2	3	8	10	11	20	20	22	26.9
G3-17	1	2	5	7	11	16	16	16	20	22	26.8
G3-18	1	5	9	11	14	14	15	15	17	22	26.7
G3-19	0	2	9	9	9	13	14	18	19	20	26.1
G3-20	2	5	12	14	14	16	16	17	17	20	25.7
G3-21	1	2	10	11	16	16	16	17	20	22	25.2
G3-22	1	2	2	7	8	10	19	19	20	22	24.0
G3-23	1	1	8	8	10	10	12	12	14	18	23.8
G3-24	0	1	3	7	7	7	9	11	14	22	22.8
G3-25	7	10	10	13	17	18	18	18	21	23	22.0
G3-26	2	3	7	7	16	16	19	20	22	23	19.6
G3-27	1	3	5	7	13	16	20	21	21	21	16.4
G3-28	0	1	1	1	5	5	19	20	20	22	14.4
G4-1	0	2	5	7	7	11	12	14	15	16	37.7

G4-2	0	1	2	7	7	9	10	19	20	22	30.8
G4-3	0	3	9	13	16	18	19	20	20	23	29.5
G4-4	0	2	5	7	7	9	11	16	20	22	29.5
G4-5	0	5	5	9	11	13	13	13	15	19	29.3
G4-6	1	5	11	12	12	15	16	19	20	20	29.2
G4-7	4	5	8	9	12	14	17	19	20	21	26.8
G4-8	0	4	5	9	11	11	17	19	20	21	26.5
G4-9	2	3	7	11	16	16	19	20	22	23	26.3
G4-10	0	0	2	9	13	13	18	19	20	23	25.7
G4-11	1	6	7	12	15	16	20	21	22	23	25.2
G4-12	1	2	5	10	11	11	16	20	22	22	24.1
G4-13	3	3	3	6	6	9	18	20	22	23	22.9
G4-14	0	5	9	15	16	18	18	19	20	21	22.9
G4-15	2	5	11	16	17	17	17	17	19	20	22.7
G4-16	0	3	13	14	14	16	17	18	19	20	22.4
G4-17	1	2	2	4	5	9	9	11	19	22	22.3
G4-18	0	1	2	3	6	7	12	13	17	22	21.2
G4-19	0	3	9	13	16	18	19	20	22	23	21.1
G4-20	0	9	11	11	11	11	13	16	19	20	19.6
G4-21	2	2	2	5	9	11	12	14	16	17	18.7
G4-22	7	10	11	13	17	21	21	21	22	23	18.0
G4-23	1	2	5	10	10	11	16	20	20	23	18.0
G4-24	2	3	9	13	16	18	19	20	22	22	16.6
G4-25	1	2	3	3	7	11	16	20	20	22	16.6
G4-26	9	9	16	17	18	18	18	19	20	21	16.1
G4-27	0	1	5	9	11	15	17	19	20	21	15.5
G4-28	5	8	9	11	15	19	20	20	21	22	14.0
G5-1	0	3	9	13	13	16	18	19	20	23	54.8
G5-2	0	2	4	5	11	12	14	14	15	16	52.6
G5-3	0	1	5	9	11	15	16	17	20	21	51.3
G5-4	1	2	5	5	7	11	16	16	20	22	51.0
G5-5	0	2	2	9	13	13	13	16	19	20	45.2
G5-6	0	3	3	7	9	12	13	13	13	16	43.5
G5-7	2	6	7	16	16	18	18	18	19	21	38.1
G5-8	3	9	9	10	11	15	17	18	19	21	37.7
G5-9	0	3	9	13	16	16	18	19	20	22	37.6
G5-10	0	0	2	5	9	9	11	16	19	20	36.9
G5-11	0	2	3	13	16	17	18	18	19	20	34.8
G5-12	2	5	7	10	11	16	19	20	22	23	32.9
G5-13	5	5	5	7	7	16	18	19	20	22	30.7
G5-14	0	2	5	11	14	16	19	19	19	20	30.4
G5-15	0	2	5	7	11	15	16	19	20	22	29.9
G5-16	0	4	5	11	12	14	16	16	20	20	29.2
G5-17	0	3	9	16	18	19	20	20	22	23	28.3
G5-18	0	5	5	9	13	16	18	19	19	20	27.4
G5-19	0	4	4	5	9	11	13	15	17	19	27.4
G5-20	2	4	7	9	12	12	14	14	14	15	27.3

G5-21	2	5	7	7	7	11	12	14	15	16	24.7
G5-22	0	2	5	7	9	11	16	19	19	20	22.5
G5-23	0	2	3	9	13	18	19	20	22	23	22.4
G5-24	2	4	5	7	16	17	17	20	22	22	21.4
G5-25	0	1	1	2	11	12	13	16	16	19	20.2
G5-26	2	5	7	7	11	12	14	16	19	20	19.1
G5-27	4	4	5	5	9	13	16	17	19	20	18.4
G5-28	0	2	5	5	9	11	11	11	19	20	18.2
G6-1	1	2	3	3	3	9	11	16	18	20	54.1
G6-2	0	0	0	2	5	9	11	16	19	20	45.7
G6-3	0	2	7	11	15	15	15	16	19	20	39.4
G6-4	0	2	2	9	11	13	13	16	19	20	38.6
G6-5	0	0	3	5	9	13	15	18	19	21	38.5
G6-6	0	4	5	5	9	13	16	18	19	20	31.6
G6-7	0	5	9	11	11	13	16	18	19	20	31.5
G6-8	0	2	5	12	12	14	14	16	18	20	30.0
G6-9	6	7	8	14	14	15	16	18	19	19	29.4
G6-10	0	1	2	2	9	13	16	20	22	22	28.8
G6-11	0	2	5	9	11	11	13	16	19	20	28.1
G6-12	2	5	9	9	9	10	11	19	20	22	26.8
G6-13	1	5	7	9	9	11	16	17	20	21	26.7
G6-14	0	5	5	9	11	13	16	17	19	20	26.0
G6-15	0	2	5	7	7	9	11	12	16	20	25.9
G6-16	0	3	9	13	16	18	19	20	23	23	25.6
G6-17	0	0	0	2	11	15	15	17	19	20	25.2
G6-18	0	2	5	9	11	15	16	17	20	21	25.0
G6-19	0	2	2	7	9	10	10	13	19	20	23.4
G6-20	0	9	11	11	16	18	18	19	19	20	22.5
G6-21	0	0	0	5	9	16	18	19	20	22	21.3
G6-22	0	9	10	13	15	15	16	18	22	23	20.8
G6-23	0	3	10	13	13	18	19	20	21	23	19.1
G6-24	0	0	0	2	5	9	11	14	19	20	19.1
G6-25	0	1	2	2	5	9	11	16	20	21	19.1
G6-26	0	1	2	5	5	5	11	13	16	19	18.9
G6-27	0	2	9	13	16	19	20	23	23	23	17.7
G6-28	0	3	9	13	16	18	19	20	22	22	17.6
G7-1	0	3	5	5	5	7	9	11	16	20	60.2
G7-2	0	2	5	9	10	10	11	16	19	20	58.8
G7-3	0	5	9	11	11	13	13	16	18	20	49.1
G7-4	0	2	5	14	14	14	16	18	18	20	49.1
G7-5	1	2	5	7	9	11	15	16	20	21	47.1
G7-6	0	5	9	9	11	15	15	16	19	20	45.5
G7-7	0	5	9	11	15	17	19	19	20	21	44.9
G7-8	0	11	11	15	16	16	16	18	19	20	44.2
G7-9	1	3	7	9	11	13	16	16	17	22	42.3
G7-10	1	2	3	3	3	9	11	16	18	20	41.2
G7-11	0	0	2	5	9	11	16	19	20	22	41.0

G7-12	0	2	5	5	11	15	17	17	19	20	40.6
G7-13	0	5	9	11	13	13	13	16	19	20	37.4
G7-14	0	2	5	5	9	11	16	19	20	23	37.4
G7-15	0	2	5	9	11	15	16	20	21	21	35.1
G7-16	0	2	5	5	5	9	16	18	19	20	34.8
G7-17	1	2	3	3	9	11	11	16	18	23	33.3
G7-18	0	2	9	11	11	11	13	16	19	20	32.0
G7-19	0	2	7	9	10	10	13	16	19	20	29.2
G7-20	1	2	3	5	5	11	16	19	20	22	25.7
G7-21	1	1	2	3	5	11	13	14	20	21	24.8
G7-22	0	0	2	9	11	11	13	16	19	20	24.8
G7-23	0	1	1	10	10	13	15	16	20	21	23.9
G7-24	1	2	3	3	3	9	11	16	18	20	21.7
G7-25	0	9	10	10	10	13	16	22	22	23	21.5
G7-26	0	9	11	11	13	13	16	18	19	20	20.1
G7-27	0	5	9	11	11	11	13	16	19	20	19.6
G7-28	0	2	4	4	6	7	10	21	21	23	16.6
G8-1	0	3	5	9	13	16	18	18	19	20	106.1
G8-2	0	3	5	9	9	11	15	16	19	20	98.8
G8-3	0	9	11	13	15	15	16	18	19	20	98.6
G8-4	0	2	5	9	9	11	11	16	18	20	93.3
G8-5	0	1	5	9	11	15	16	17	19	20	87.5
G8-6	1	2	5	7	9	11	15	16	20	21	81.6
G8-7	0	3	3	3	5	9	11	16	19	20	78.7
G8-8	0	2	5	9	10	10	11	16	19	20	73.7
G8-9	0	3	3	5	7	9	10	11	16	20	73.4
G8-10	1	2	5	9	11	15	16	19	20	21	70.0
G8-11	0	2	4	5	11	14	16	18	20	20	66.7
G8-12	0	2	4	4	4	4	6	7	15	23	63.1
G8-13	1	2	7	9	11	15	16	18	20	21	60.6
G8-14	2	8	9	15	17	19	20	20	21	21	58.8
G8-15	0	1	1	10	13	15	16	19	20	21	56.9
G8-16	0	3	5	12	13	16	18	21	22	22	52.3
G8-17	0	2	2	5	9	11	13	16	19	20	52.2
G8-18	0	5	9	9	11	15	17	19	20	21	48.2
G8-19	0	0	1	2	5	9	11	16	18	20	48.2
G8-20	1	2	3	3	3	9	11	19	20	22	47.0
G8-21	2	3	7	10	10	10	13	14	20	21	43.7
G8-22	0	6	10	11	12	16	18	18	21	23	42.1
G8-23	1	3	9	11	13	16	16	17	17	22	41.7
G8-24	1	1	3	11	15	15	16	18	20	23	40.6
G8-25	0	2	11	14	15	16	18	18	20	20	32.8
G8-26	0	3	3	9	10	13	13	16	19	20	28.6
G8-27	0	3	3	9	13	15	16	18	19	20	27.2
G8-28	0	2	9	11	11	11	13	16	19	20	21.7

[a]G*x*-*y* refers to the y^{th} best formulation in the x^{th} generation.

[b]Correspond to the numbers of stabilizers in Figure 2.1.

[c]Correspond to the inverse of the absorbance at 400 nm of polystyrene films after 300 hours of light exposure.

Table 2.2. 10 best performing formulations.

Formulation code[a]	Stabilizers[b]										1/Abs[c]
G8-1	0	3	5	9	13	16	18	18	19	20	106.1
G8-2	0	3	5	9	9	11	15	16	19	20	98.8
G8-3	0	9	11	13	15	15	16	18	19	20	98.6
G8-4	0	2	5	9	9	11	11	16	18	20	93.3
G8-5	0	1	5	9	11	15	16	17	19	20	87.5
G8-6	1	2	5	7	9	11	15	16	20	21	81.6
G8-7	0	3	3	3	5	9	11	16	19	20	78.7
G8-8	0	2	5	9	10	10	11	16	19	20	73.7
G8-9	0	3	3	5	7	9	10	11	16	20	73.4
G8-10	1	2	5	9	11	15	16	19	20	21	70.0

[a]G*x*-*y* refers to the y^{th} best formulation in the x^{th} generation.
[b]Correspond to the numbers of stabilizers in Figure 2.1.
[c]Correspond to the inverse of the absorbance at 400 nm of polystyrene films after 300 hours of light exposure.

2.3.4. Selection of individual stabilizers

The evolution process changes formulations in a way to increase the performance, where stabilizers that have a positive effect on the performance will be selected more, and vice versa. Figure 2.6 shows the change in the selection of individual stabilizers in the course of evolution. The 0th generation is fully based on random selection, so that the percentage of the selection is relatively similar among the stabilizers, varying in a narrow range (3−6%). Stabilizers which gained the selection by the evolution are Tinuvin 123 (No. 20) > LA-57 (No. 11) > LA-87 (No. 9) > LA-63P (No.16). Those which lost the selection are Hostavin VSU (No. 8) > 1413 (No. 6) > LA-82 (No. 14) > LA-68 (No. 12) >

AO-30 (No. 23) > Irganox 245 (No. 22). Such results have a little correlation with the performance of the stabilizers when they are used alone (Figure 2.5). For example, Tinuvin 123 (No. 20) and Hostavin VSU (No. 8) are the most selected and most rejected stabilizers in the course of evolution. The performance of these stabilizers when used alone ranks 14th and 18th, respectively, among 24. Thus, the selection of stabilizers occurs based on whether or not a specific stabilizer is synergistic when used in combination with other stabilizers. Here, it is important to note that although the evolution has eliminated certain stabilizers, it has rarely eliminated the family of stabilizers. This means that the selection is not caused by the difference in the mechanism (how stabilizers interrupt degradation), but by the difference in the details of molecular structures.

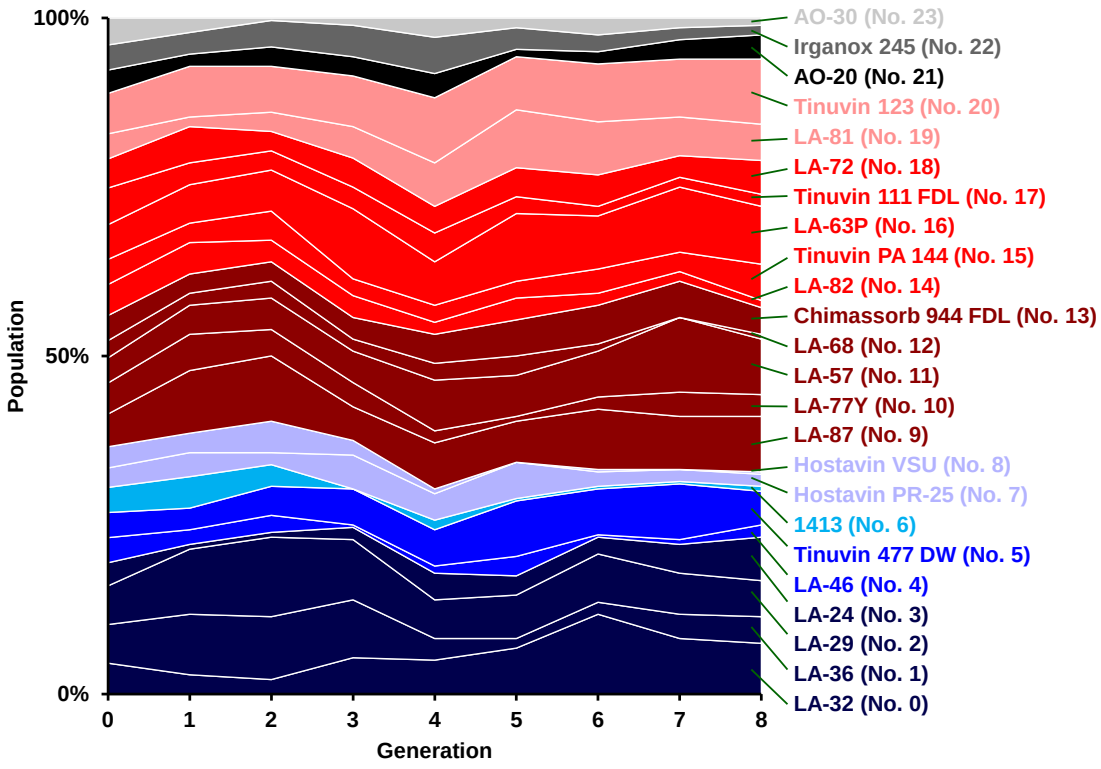

Figure 2.6. Percent stacked area chart for the selection of individual stabilizers along with the generation. The color scheme is as defined in Figure 2.1.

2.3.5. Decision tree analysis

A decision tree classification was implemented to visualize the guideline of designing stabilizer formulations (Figure 2.7). The top 25 percentiles out of 259 formulations were classified as good formulations and the rest as non-good formulations. The content of individual stabilizers was used as features, and the split was performed based on the Gini index until each leaf became completely pure. For visible clarity, the obtained tree was pruned with a restriction of more than 30 samples to each split. The entire tree without pruning is also shown in Figure 2.8. In Figure 2.7, out of the 65 formulations in the top 25 percentiles, 72% selected LA-57 at least once. Of these, 83% included LA-63P, and 60% included LA-87 together. This result is reasonable in a sense that these three HALSs correspond to those frequently selected along with the evolution. On the other hand, frequently selected UVAs were not used as decisive features. This fact suggests that the selection of UVAs is not as molecular structure-specific as that of HALSs, i.e., it is necessary to include UVAs [33], but its molecular structure is less restricted. Of the non-performant formulations, 55% did not contain LA-57, and did not contain Chimassorb 944 FDL, LA-82, and LA-63P more than three times. Chimassorb 944 FDL and LA-63P are stabilizers whose selection rate increased during the evolution. Some of

the positive stabilizers may have adverse effects on the formulation performance if the amount exceeds a certain level.

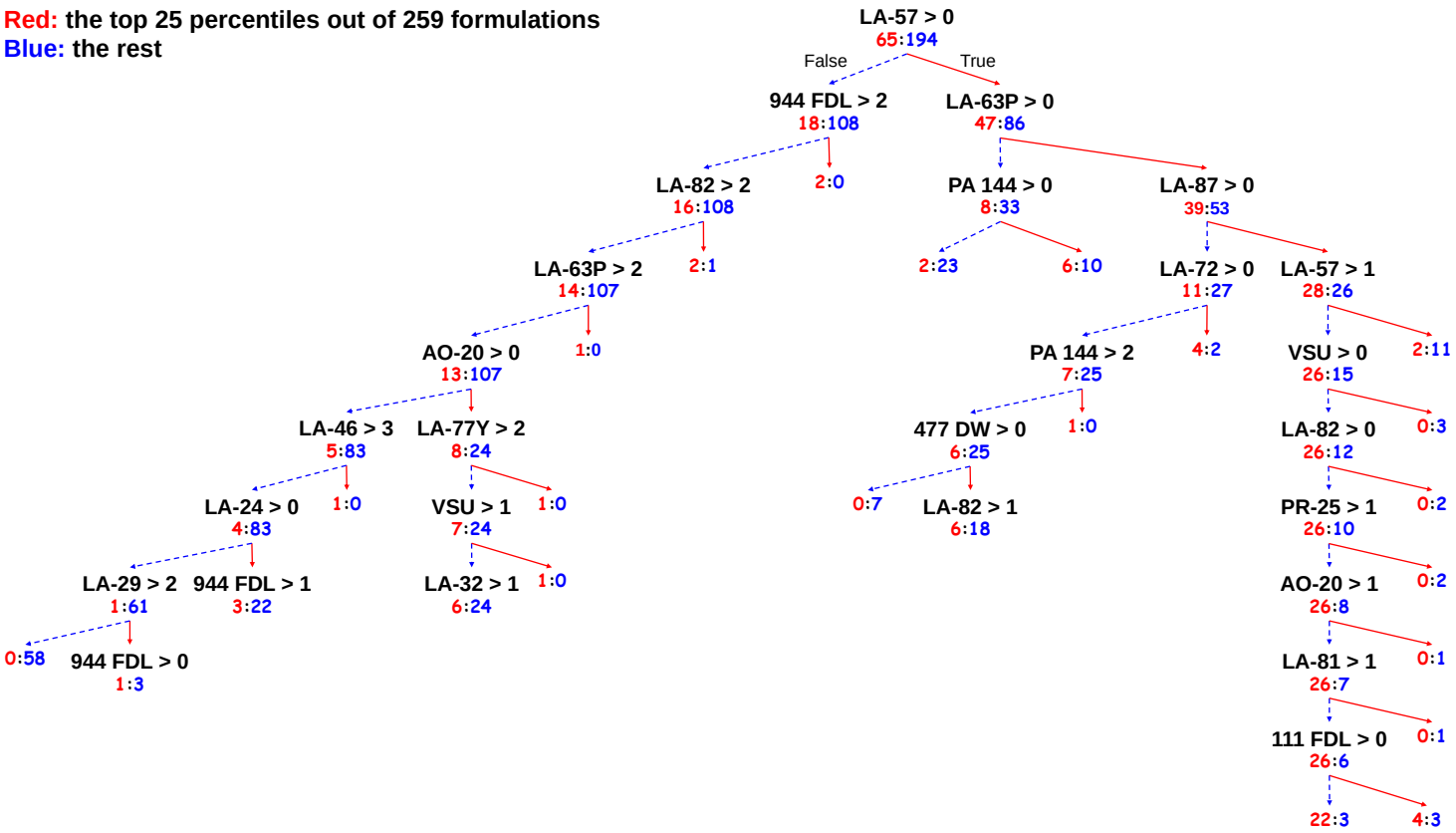

Figure 2.7. Formulation design guideline visualized by decision tree classification. 259 formulations are classified into the top 25 percentiles (red) and the rest (blue) using the number of times each stabilizer is selected in a formulation. The numbers in each split and leaf correspond to the numbers of formulations for the two classes.

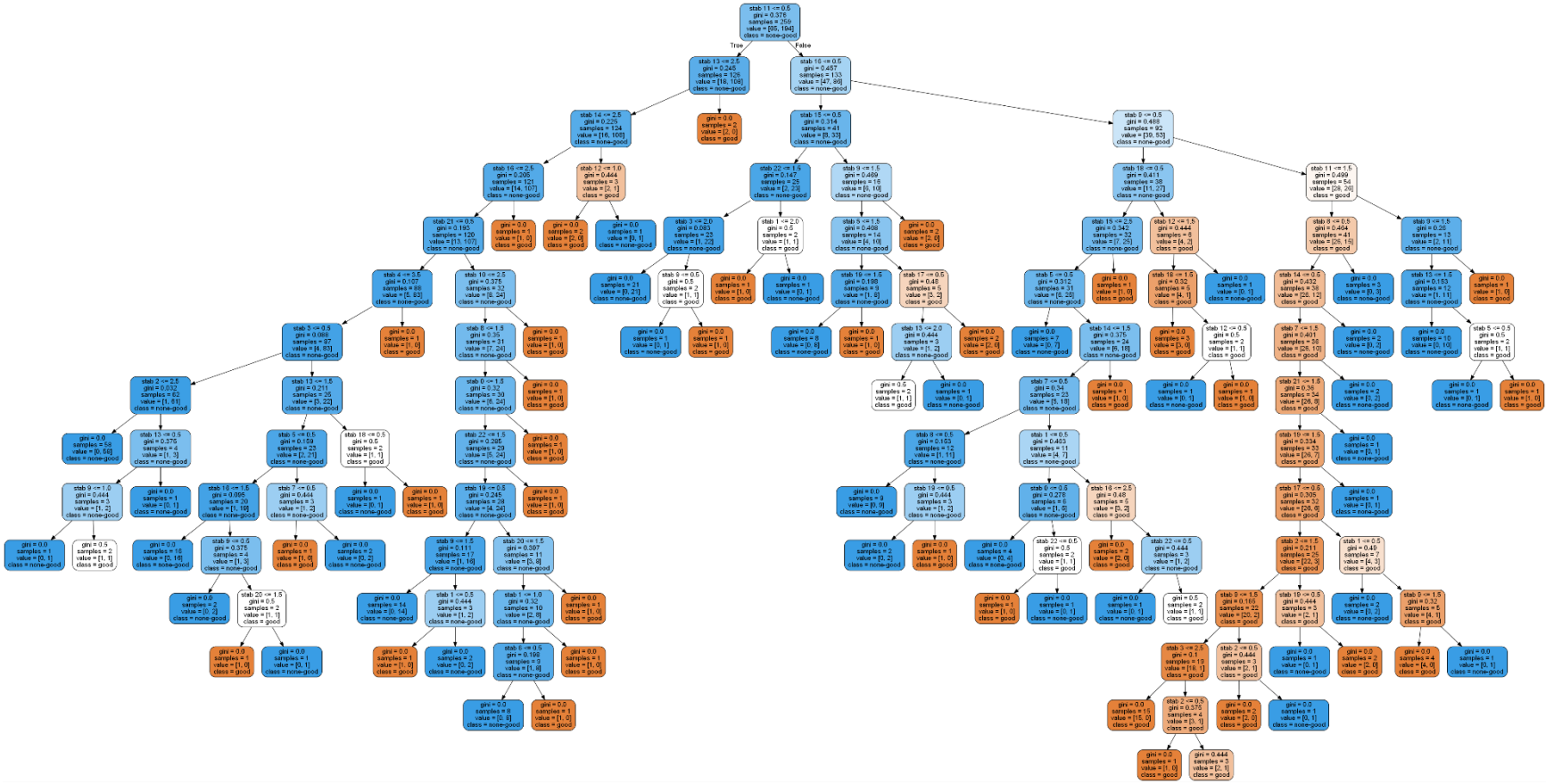

Figure 2.8. Entire decision tree. The 259 formulations are classified into the top 25 percentiles (red) or the rest (blue) using the number of times each stabilizer is selected in a formulation.

2.3.6. Synergism and formulation performance

In order to evaluate the interaction between stabilizers, I introduced a synergy value as defined in Equation (2.3),

$$\text{Synergy}(\alpha,\beta) = \langle 1/\text{Abs}\rangle_{\alpha\cap\beta}/\langle 1/\text{Abs}\rangle_{\alpha\Delta\beta} \quad (2.3).$$

This is the ratio of the performance averaged among formulations containing both stabilizers α and β (α∩β) to that among combinations containing either of α and β (αΔβ). When the value is greater than 1, the combination is regarded synergistic, and vice versa.

A strong positive correlation is seen ($R^2 = 0.84$) between the synergy value and the performance of formulation (Figure 2.9). This suggests that the performance of formulations is determined by synergistic combinations rather than the inclusion of a stabilizer which is high performing by its own [34-38]. A similar conclusion was obtained for the design of stabilizer formulations against thermo-oxidative degradation [8].

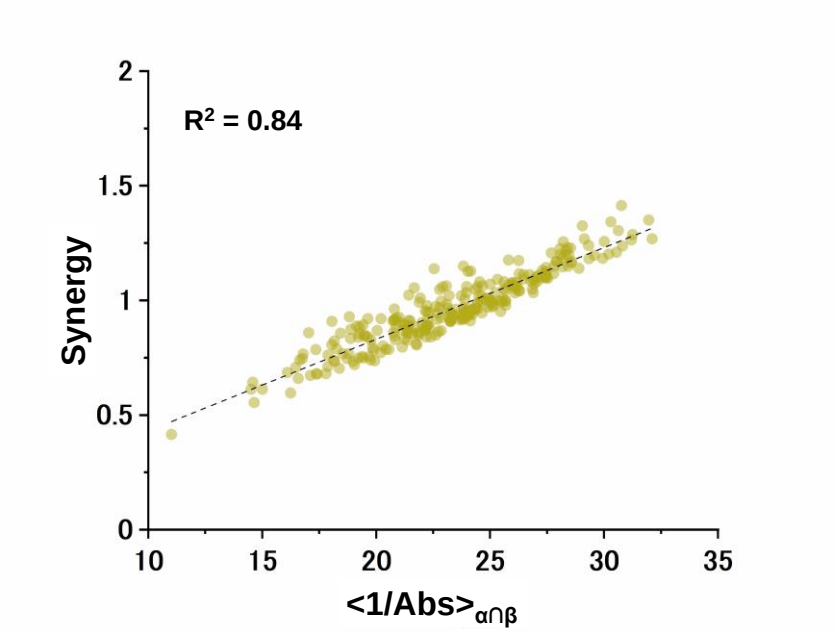

Figure 2.9. Impact of synergistic combinations on the performance of stabilizer formulations. The synergy is evaluated based on Equation (3). It compares the average performance of formulations between when both of stabilizers α and β are contained and when either of α and β is contained. $<1/Abs>_{\alpha\cap\beta}$ corresponds to the former case, i.e., the average 1/Abs of formulations having both of α and β.

2.3.7. Synergistic and antagonistic combinations

Table 2.3 lists the most synergistic and antagonistic combinations. In the synergy side, stabilizers that frequently appeared are LA-87 (No. 9) > LA-57 (No. 11) > Tinuvin PA 144 (No. 15), Tinuvin 123 (No. 20) in this order. These are all HALSs (but of different types), and correspond to frequently selected ones as a result of the evolution (cf. Figure 2.6). Many of the synergistic combinations were derived from UVA × HALS, in particular,

benzotriazole/triazine × N–H/N–OR, and from HALS (N–H) × HALS (N–R/N–OR). These results suggest that a combination of stabilizers with different mechanisms or complementary features has a synergistic effect on the inhibition of photo degradation. In the antagonist side, 1413 (No. 6) > AO-30 (No. 23) >> LA-32 (No. 0), Hostavin PR-25 (No. 8), LA-81 (No. 19) were frequently observed in this order. Frequent antagonistic combinations were UVA (benzotriazole) × UVA (others) > UVA (benzophenone) × HALS (N–R/N–OR) > HALS (any) × hindered phenol (less hindered one).

Table 2.3. Synergistic and antagonistic combinations of stabilizers[a]

Ranking	Synergistic combination				Antagonistic combination			
	α	β	Synergy	$\langle 1/\mathrm{Abs}\rangle_{\alpha\cap\beta}$	α	β	Synergy	$\langle 1/\mathrm{Abs}\rangle_{\alpha\cap\beta}$
1	11	16	1.41	30.8	0	8	0.42	11.0
2	15	19	1.35	32.0	6	11	0.55	14.6
3	0	11	1.34	30.3	8	16	0.60	16.2
4	5	11	1.33	29.0	6	19	0.61	15.0
5	5	9	1.30	30.6	4	7	0.61	14.5
6	7	9	1.29	31.3	17	23	0.64	14.6
7	9	15	1.27	32.1	5	23	0.66	16.6
8	0	9	1.27	29.1	0	6	0.67	17.1
9	11	15	1.26	31.2	5	8	0.68	17.4
10	9	11	1.26	30.0	19	23	0.68	17.4
11	16	20	1.26	28.2	6	15	0.68	17.8
12	9	16	1.24	29.3	14	22	0.69	16.1
13	3	15	1.24	30.8	6	16	0.70	18.4
14	5	20	1.23	28.4	4	22	0.71	16.5
15	9	20	1.23	28.5	3	7	0.71	17.9
16	0	20	1.23	28.1	20	23	0.72	19.1
17	2	19	1.22	28.3	0	23	0.73	19.0
18	15	16	1.21	30.5	12	19	0.73	18.2
19	2	20	1.21	27.7	12	15	0.74	19.9
20	11	18	1.20	30.2	1	6	0.74	18.1

[a]An impact of combining two stabilizers, α and β, is evaluated based on Equation (3). The stabilizer codes correspond to those in Figure 2.1. The larger the synergy value, the more synergistic the combination, and vice versa. $\langle 1/\mathrm{Abs}\rangle_{\alpha\cap\beta}$ indicates the average 1/Abs value for formulations which contain both of the stabilizers (α and β).

2.3.8. Visualization by force-directed graph

In order to derive heuristics on the design of more complex formulations, binary interactions between stabilizers were visualized using a force-directed graph (Figure 2.10). In general, a force-directed graph consists of nodes repelling each other like charged particles and edges connecting nodes like springs, with a purpose to visualize relationships between the nodes. Takahashi et al. proposed a visual catalyst design method by using force-directed graphs to visualize relationships between active elements, supports, their combinations, and the target yield in methane oxidation coupling [39]. Bryan et al. have visualized the effect of tyrosine kinase knockdown on the MCF-7 proteome, where nodes are the knocked-down tyrosine kinases and the proteins that are increased or decreased by them [40]. Figure 2.10 shows a force-directed graph where the nodes represent the individual stabilizers, and the edges reflect the synergy value (appropriately scaled) for the corresponding combination of stabilizers. Note that the higher the synergy value is, the more the corresponding nodes or stabilizers attract each other. It can be seen that there is a cluster of stabilizers that are located close to each other (Nos. 0, 5, 9, 11, 15, 16, 19, 20). The formation of a cluster indicates that the stabilizers as members of the cluster are synergistic with each other. In fact, these 8 stabilizers were commonly included in the 10 best performing formulations in Table 2.2, leading to a hypothesis that formulations containing a large number of synergistic combinations have

high performance. Such a trend was also observed in the design of stabilizer formulations in the thermal oxidative degradation of PP. Far from the cluster, some stabilizers are located in an isolated fashion (Nos. 4, 6, 8, 10, 12, 14, 17, 22, 23). These correspond to the stabilizers that were eliminated in the evolution (Figure 2.5), and the reason for the elimination is that they are antagonistic to the others.

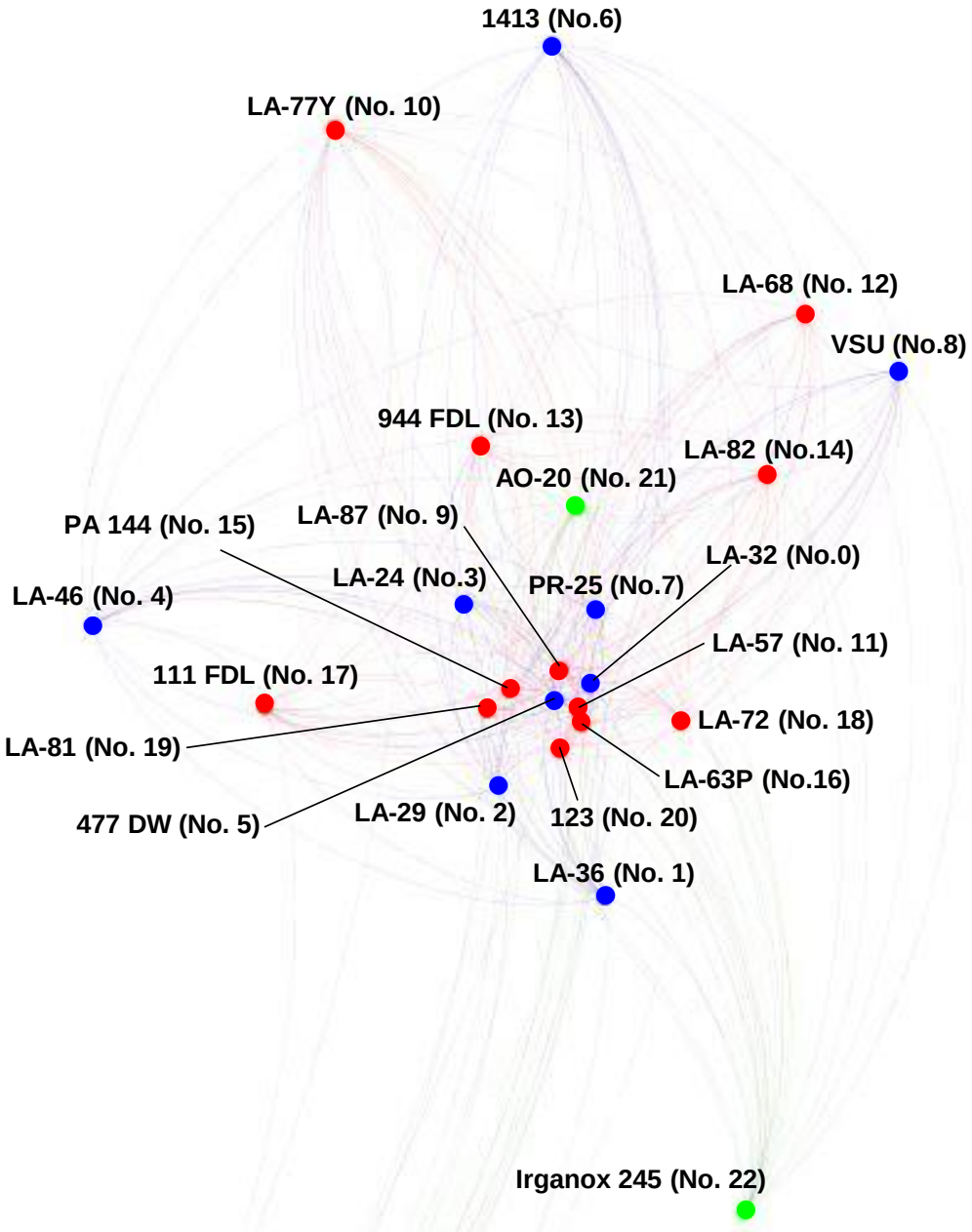

Figure 2.10. Visualization of binary interactions based on a force-directed graph. The nodes represent individual stabilizers (blue: UVA, red: HALS, green: hindered phenol). An edge reflects the synergy value between the correspondent stabilizers, where the closer the nodes are, the more synergistic the stabilizers are.

2.3.9. Validation of combinatorial effects

Care must be taken in understanding the results of the interaction analysis between stabilizers. The problem is related to the sampling bias introduced by the genetic algorithm: in order to fairly evaluate the interaction between stabilizers α and β, the other stabilizers contained in the formulations must be selected without bias or randomly. Note that a formulation can contain up to 10 different stabilizers. The genetic algorithm inherits genes that contribute to improve the performance in a simultaneous and parallel manner. For example, when evolution results in the predominance of formulations that simultaneously contain α, β, and γ, formulations that contain both α and β are more likely to occur in a late stage of the evolution and have a higher probability of containing γ compared to those that contain only one of α or β, which are more likely to occur in an early stage of the evolution. This leads to an overestimation of the synergy value, and vice versa. Thus, the results of the interaction analysis between stabilizers are considered to be strongly influenced by the sampling bias brought by the genetic algorithm. Besides, there is no guarantee that the interaction between two stabilizers will be the same in the presence of different stabilizers that can interact with them. In light of the said limitations, additional experiments were conducted to evaluate the synergistic combinations found in Table 2.3 and the hypothesis that a key for high-performing formulations is to add up many synergistic combinations. The detailed experimental content is described as follows. Formulations consisting of a limited number of stabilizers were assumed, and the

performance of the formulations was estimated by the score defined in,

$$\text{Score} = \sum_{a<\beta}\text{Synergy}(\alpha,\beta) \quad (2.4).$$

Synergy(α,β) is as defined in Equation (2.3). Top-scored 6 formulations were selected from the formulations containing the specified number of stabilizers, as summarized in Table 2.4. For example, among formulations consisting of only 2 stabilizers, the best formulation, namely that with the highest score, consists of LA-57 (No. 11) and LA-63P (No. 16), which correspond to the most synergistic binary combination in Table 2.3. Among formulations consisting of 3 stabilizers, the best formulation consists of Tinuvin 477 DW (No. 5), LA-57 (No. 11), and LA-63P (No. 16), which were shown mutually synergistic in Figure 2.10. The performance of the selected formulations was experimentally evaluated using the procedure and conditions identical to those employed for the GA part. These results are summarized in Table 2.4. Note that the amount of a formulation to PS was fixed at 0.05 wt%, which was equally divided by the constituent stabilizers.

The average performance of the top-scored 6 formulations was derived for each number of constituent stabilizers. The relationship between the number of constituent stabilizers and the average performance is plotted in Figure 2.11. It can be seen that the performance of the formulations tended to increase as the number of constituent stabilizers increased. This is consistent with the increase in the score value, and more importantly, with the hypothesis that formulations containing a large number of synergistic combinations have high performance. On the other hand, the performance of

individual formulations did not necessarily correspond to the score value (Table 2.4). This plausibly reflects the conditional nature of binary interactions, which is caused by the sampling bias of the genetic algorithm. For example, the performance of formulations that commonly contain LA-57 (No. 11) and LA-63P (No. 16), namely 2C-1, 3C-1, 3C-2, C3-3, and 3C-5, was largely affected by the choice of the third stabilizer.

Table 2.4. Top-scored formulations containing 2 to 6 stabilizers.

Formulation code[a]	Stabilizers[b]						Score[c]	1/Abs[d]
2C-1	11	16					1.41	5.9
2C-2	15	19					1.35	15.0
2C-3	0	11					1.34	11.1
2C-4	5	11					1.33	8.5
2C-5	5	9					1.30	14.1
2C-6	7	9					1.29	10.6
3C-1	5	11	16				3.94	14.2
3C-2	0	11	16				3.92	15.5
3C-3	9	11	16				3.91	30.0
3C-4	5	9	11				3.89	6.5
3C-5	11	15	16				3.88	19.4
3C-6	0	5	11				3.87	23.6
4C-1	5	9	11	16			7.74	18.3
4C-2	0	5	9	11			7.70	27.9
4C-3	0	9	11	16			7.69	13.4
4C-4	0	5	11	16			7.65	19.1
4C-5	9	11	15	16			7.65	21.9
4C-6	5	11	16	20			7.63	14.2
5C-1	0	5	9	11	16		12.72	33.1
5C-2	5	9	11	15	16		12.66	20.0
5C-3	5	9	11	16	20		12.66	31.0
5C-4	0	9	11	15	16		12.63	52.3
5C-5	0	5	9	11	15		12.61	45.5
5C-6	0	9	11	16	20		12.61	88.9
6C-1	0	5	9	11	16	20	18.87	63.0
6C-2	0	5	9	11	15	16	18.84	58.0
6C-3	5	9	11	15	16	20	18.76	54.8
6C-4	0	9	11	15	16	20	18.73	28.9
6C-5	0	5	9	11	15	20	18.68	77.7
6C-6	0	5	11	15	16	20	18.60	71.4

[a]*x*C-*y* refers to the y^{th} scored formulation out of formulations consisting of *x* stabilizers.
[b]Correspond to the numbers of stabilizers in Figure 2.1.
[c]As defined in Equation (4).
[d]Correspond to the inverse of the absorbance at 400 nm of polystyrene films after 300 hours of light exposure.

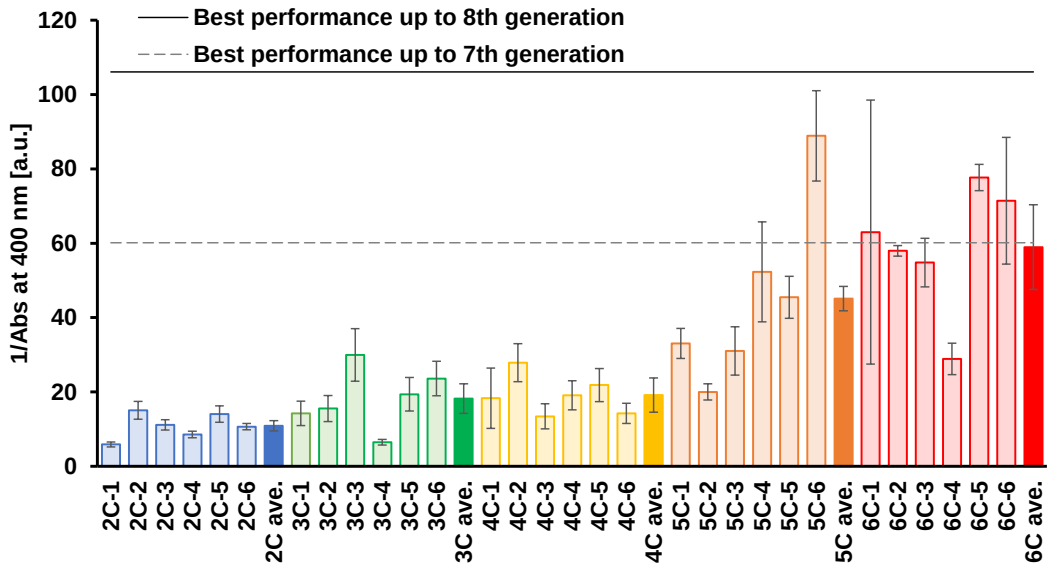

Figure 2.11. The relationship between the performance of formulations and the number of constituent stabilizers therein. Note that the performance of formulations corresponds to the average of the performance of the top-scored 6 formulations for each number of constituent stabilizers.

2.4. Conclusions

A systematic study on stabilizer formulations for inhibiting light-induced yellowing of transparent plastics has been hardly implemented due to the low throughput of experiments with respect to a huge number of potential combinations. In this chapter, I developed a high-throughput experimental protocol that enables to evaluate the light-induced yellowing of 288 samples in a single experiment, which consists of the preparation of a large number of cast films on microplates and quick determination of the photo-induced yellowing of these films using a microplate reader. This protocol was used in conjunction with a genetic algorithm to explore stabilizer formulations, which were made by combining 10 of 24 commercially available stabilizers. Furthermore, the obtained dataset was analyzed to derive formulation design guidelines. Major findings are as follows.

- Polystyrene films cast on a microplate exhibited a degradation behavior similar to a self-standing film. This supports the usefulness of the established high-throughput experimental protocol for screening purposes.
- The best formulation found in the genetic algorithm performed five times better than the best performing stabilizer by its own. This proves the superiority of formulating multiple stabilizers for improving the durability of polymers.
- Most of synergistic combinations were identified between stabilizers that play complementary roles in suppressing the degradation, such as a combination of HALS

and UVA, or between stabilizers of the same class but with different reactivity and stability, such as HALS of N–H type and that of N–OR type.

- A visualization based on a force-directed graph led to a hypothesis that the inclusion of as many mutually synergistic stabilizers as possible is important in the design of high performing formulations, which was successfully proven by additional experiments.

The methodology proposed in this chapter can be used for a wide range of applications involving changes in light absorption. The data provided by a combination of the high-throughput experiment and the genetic algorithms is useful not only for simple optimization for the target variable, but also for extracting heuristics of materials design.

References

[1] Djouani, F.; Richaud, E.; Fayolle, B.; Verdu, J. Modelling of Thermal Oxidation of Phosphite Stabilized Polyethylene. *Polym. Degrad. Stab.* **2011**, *96*, 1349−1360.

[2] Vulic, I.; Vitarelli, G.; Zenner, J. M. Structure-Property Relationships: Phenolic Antioxidants with High Efficacy and Low Color Contribution. *Macromol. Symp.* **2001**, *176*, 1−16.

[3] Matta, A.; Katada, I.; Kawazoe, J.; Chammingkwan, P.; Terano, M.; Taniike, T. Stabilization of Polypropylene-Based Materials via Molecular Retention with Hyperbranched Polymer. *Polym. Degrad. Stab.* **2017**, *142*, 50−54.

[4] Hamskog, M.; Klügel, M.; Forsström, D.; Terselius, B.; Gijsman, P. The Effect of Base Stabilization on the Recyclability of Polypropylene as Studied by Multi-cell Imaging Chemiluminescence and Microcalorimetry. *Polym. Degrad. Stab.* **2004**, *86*, 557−566.

[5] Bauer, D. R. Interpreting Weathering Acceleration Factors for Automotive Coatings Using Exposure Models. *Polym. Degrad. Stab.* **2000**, *69*, 307–316.

[6] Pickett, J. E.; Gibson, D. A.; Gardner, M. M. Effects of Irradiation Conditions on the Weathering of Engineering Thermoplastics. *Polym. Degrad. Stab.* **2008**, *93*, 1597–1606.

[7] Aratani, N.; Katada, I.; Nakayama, K.; Terano, M.; Taniike, T. Development of High Throughput Chemiluminescence Imaging Instrument for Parallel Evaluation of Polymer Lifetime. *Polym. Degrad. Stab.* **2015**, *121*, 340−347.

[8] Taniike, T.; Kitamura, T.; Nakayama, K.; Takimoto, K.; Aratani, N.; Wada, T.; Thakur, A.; Chammingkwan, P. Stabilizer Formulation Based on High-Throughput Chemiluminescence Imaging and Machine Learning. *ACS Appl. Polym. Mater.* **2020**, *2*, 3319−3326.

[9] Pankasem, S.; Kuczynski, J.; Thomas, J. K. Photochemistry and Photodegradation of Polycarbonate. *Macromolecules* **1994**, *27*, 3773–3781.

[10] Ali, U.; Karim, K. J. B. A.; Buang, N. A. A Review of the Properties and Applications of Poly (Methyl Methacrylate) (PMMA). *Polym. Rev.* **2015**, *55*, 678–705.

[11] Lü, C.; Yang, B. High Refractive Index Organic-Inorganic Nanocomposites: Design, Synthesis and Application. *J. Mater. Chem.* **2009**, *19*, 2884–2901.

[12] Diepens, M.; Gijsman, P. Photodegradation of Bisphenol A Polycarbonate. *Polym. Degrad. Stab.* **2007**, *92*, 397–406.

[13] Monsores, K. G. D. C.; Silva, A. O. Da; De Sant'Ana Oliveira, S.; Rodrigues, J. G. P.; Weber, R. P. Influence of Ultraviolet Radiation on Polymethylmethacrylate (PMMA). *J. Mater. Res. Technol.* **2019**, *8*, 3713–3718.

[14] Kaczmarek, H.; Kamińska, A.; Światek, M.; Sanyal, S. Photoinitiated Degradation of Polystyrene in the Presence of Low-Molecular Organic Compounds. *Eur. Polym. J.* **2000**, *36*, 1167–1173.

[15] Yazdan Mehr, M.; Van Driel, W. D.; Jansen, K. M. B.; Deeben, P.; Boutelje, M.; Zhang, G. Q. Photodegradation of Bisphenol A Polycarbonate under Blue Light Radiation and Its Effect on Optical Properties. *Opt. Mater. (Amst).* **2013**, *35*, 504–508.

[16] Ammala, A.; Bateman, S.; Dean, K.; Petinakis, E.; Sangwan, P.; Wong, S.; Yuan, Q.; Yu, L.; Patrick, C.; Leong, K. H. An Overview of Degradable and Biodegradable Polyolefins. *Progress in Polymer Science.* **2011**, *36*, 1015–10

[17] Xiao, L.; Zhao, Y.; Jin, B.; Zhang, Q.; Chai, Z.; Peng, R. Synthesis of Novel Ultraviolet Stabilizers Based on [60]Fullerene and Their Effects on Photo-Oxidative Degradation of Polystyrene. *Fullerenes Nanotub. Carbon Nanostructures* **2020**, *28*, 465–473.

[18] Feldman, D. Polymer Weathering: Photo-Oxidation. *J. Polym. Environ.* **2002**, *10*, 163–173.

[19] Muller, F.; Salonen, A.; Glatter, O. Monoglyceride-Based Cubosomes Stabilized by Laponite: Separating the Effects of Stabilizer, pH and Temperature. *Colloids Surf., A* **2010**, 358, 50−56.

[20] Földes, E. Study of the Effects Influencing Additive Migration in Polymers. *Angew. Makromol. Chem.* **1998**, *261*, 65−76.

[21] Park, D.; Kobayashi, D.; Suh, H.; Cho, Y.; Lee, A. Synthesis of (3-tert-butyl-4-hydroxy-5 methylphenyl) Propionate Derivatives and Their Thermal Antioxidation Behavior for POM. *J. Appl. Polym. Sci.* **2012**, *124*, 1731−1736.

[22] Heard, C. J.; Heiles, S.; Vajda, S.; Johnston, R. L. $Pd_nAg_{(4-n)}$ and $Pd_nPt_{(4-n)}$ Clusters on MgO (100): A Density Functional Surface Genetic Algorithm Investigation. *Nanoscale* **2014**, *6*, 11777−11788.

[23] Takasao, G.; Wada, T.; Thakur, A.; Chammingkwan, P.; Terano, M.; Taniike, T. Machine Learning-Aided Structure Determination for $TiCl_4$-Capped $MgCl_2$ Nanoplate of Heterogeneous Ziegler-Natta Catalyst. *ACS Catal.* **2019**, *9*, 2599−2609.

[24] Gijsman, P. A Review on the Mechanism of Action and Applicability of Hindered Amine Stabilizers. *Polym. Degrad. Stab.* **2017**, *145*, 2–10.

[25] Pedregosa, F.; Varoquaux, G.; Gramfort, A.; et al. Scikit-learn: Machine learning in Python. *J. Mach. Learn. Res.* **2011**, *12*, 2825− 2830.

[26] Bastian, M.; Heymann, S.; Jacomy, M. Gephi: An Open Source Software for Exploring and Manipulating Networks. *Proceedings of the International AAAI Conference on Web and Social Media* **2009**, *3*, 361–362.

[27] An, M.; Chang, D.; Hong, D.; Fan, H.; Wang, K. Metabolic Regulation in Soil Microbial Succession and Niche Differentiation by the Polymer Amendment under Cadmium Stress. *J. Hazard. Mater.* **2021**, *416*, 126094.

[28] Yousif, E.; Haddad, R. Photodegradation and Photostabilization of Polymers, Especially Polystyrene: Review. *Springerplus* **2013**, *2*, 1–32.

[29] Al-Malaika, S. Antioxidants: An Overview. *Plastics Atdditives* **1998**, 55–72.

[30] Gugumus, F. Possibilities and Limits of Synergism with Light Stabilizers in Polyolefins 1. HALS in Polyolefins. *Polym. Degrad. Stab.* **2002**, *75*, 295–308.

[31] Gugumus, F.; Lelli, N. Light Stabilization of Metallocene Polyolefins. *Polym. Degrad. Stab.* **2001**, *72*, 407–421.

[32] Gugumus, F. The Performance of Light Stabilizers in Accelerated and Natural Weathering. *Polym. Degrad. Stab.* **1995**, *50*, 101–116.

[33] Kurumada, T.; Ohsawa, H.; Yamazaki, T. Synergism of Hindered Amine Light Stabilizers and UV-Absorbers. *Polym. Degrad. Stab.* **1987**, *19*, 263–272.

[34] Cai, R.; Ding, X. Research Progress in Enhancing the Radiation Resistance of Polymer Material. *American Journal of Science and Technology* **2015**, *2*, 195–201.

[35] Maringer, L.; Roiser, L.; Wallner, G.; Nitsche, D.; Buchberger, W. The Role of Quinoid Derivatives in the UV-Initiated Synergistic Interaction Mechanism of HALS and Phenolic Antioxidants. *Polym. Degrad. Stab.* **2016**, *131*, 91–97.

[36] Volponi, J. E.; Mei, L. H. I.; Dos Santos Rosa, D. The Use of Differential Photocalorimetry to Measure the Oxidation Induction Time of Isotatic Polypropylene. *Polym. Test.* **2004**, *23*, 461–465.

[37] Lucki, J.; Rabek, J. F.; Rånby, B. Photostabilizing Effect of Hindered Piperidine Compounds: Interaction between Hindered Phenols and Hindered Piperidines. *Polym. Photochem.* **1984**, *5*, 351–384.

[38] Allen, N. S. Photo-Stabilising Performance of a Hindered Piperidine Compound in Polypropylene Film: Anti-Oxidant/Light Stabiliser Effects. *Polym. Degrad. Stab.* **1980**, *2*, 129–135.

[39] Takahashi, L.; Ohyama, J.; Nishimura, S.; Takahashi, K. Representing the Methane Oxidation Reaction via Linking First-Principles Calculations and Experiment with Graph Theory. *J. Phys. Chem. Lett.* **2021**, *12*, 558–568.

[40] Bryan, K.; Jarboui, M. A.; Raso, C.; Bernal-Llinares, M.; McCann, B.; Rauch, J.; Boldt, K.; Lynn, D. J. HiQuant: Rapid Postquantification Analysis of Large-Scale MS-Generated Proteomics Data. *J. Proteome Res.* **2016**, *15*, 2072–2079.

Chapter 3

Derivation of catalyst design guidelines for low-temperature dry-reforming reaction of methane by combinatorial exploration

Chapter 3

Abstract

In this chapter, multi-elemental catalyst design was explored for low-temperature dry reforming of methane by means of combined high-throughput experimentation and genetic algorithm. The composition of catalysts, consisting of up to 16 elements (Mg, Al, Ca, V, Mn, Fe, Co, Ni, Cu, Zn, Ce Sr, Zr, Mo, Pd, La, Ce) supported on γ-Al_2O_3 was optimized in order to maximize the H_2 yield at 500 °C. A huge amount of data generated by high-throughput experimentation was subjected to various data science techniques, in order to acquire catalyst design and process optimization guidelines.

Keywords: high-throughput experimentation, genetic algorithm, dry-reforming reaction, multidimensional exploration, machine learning

Chapter 3

3.1. Introduction

Since most chemical reactions are composed of multiple elementary reactions, the design of catalysts to control them tends to be multidimensional. Especially for solid catalysts, it is common to design catalysts by integrating multiple components that play different roles on the surface [1–3]. In such multicomponent design, predicting the outcome of adding a component is challenging as the component can interact with all the chemical species present in the chemical system such as the other components in the catalysts as well as reactants, intermediates, and products of the catalysis. To address this challenge, materials informatics (MI) is emerging in the field of catalysis, which attempts to surrogate a complex interaction network by a machine learning model [4–6].

The implementation of machine learning necessitates data sufficient in the quantity and quality, but such data is scarcely present in materials science. The research group of Taniike has addressed this challenge by means of high-throughput experimentation (HTE), which can produce a large amount of experimental data in a short period [7–14]. For example, they developed a high-throughput screening instrument that can acquire 4000 catalyst data a day for the oxidation coupling reaction of methane. The generated catalyst big data were exploited for predicting the performance of catalysts based on random forest regression, decision tree classification, and other methods [10–12]. They also developed a high-throughput chemiluminescence imaging instrument that can evaluate the thermal-oxidation degradation of 100 polymer samples. Moreover, as described in Chapter 2, a microplate-based HTE protocol was developed for evaluating yellowing resistance of 288 polymer samples. The protocol was combined. These techniques enabled exploration of stabilizer formulations at an unprecedent scale [13,14].

Chapter 3

Low-temperature dry reforming (DRM), which is a reaction that converts CH_4 and CO_2 to syngas, i.e. H_2 and CO, attracts increasing attention from the viewpoints of effective utilization of CH_4 and carbon dioxide capture utilization and storage [15–17]. DRM is an exothermic reaction, but it requires high temperature (>800 ºC) due to the low reactivity of the reactants, where catalyst deactivation due to carbon deposition and sintering, and the by-production of water molecules that causes reverse reactions are the major concerns [18–20]. This has motivated the development of low-temperature DRM catalysts that can operate at lower temperatures (<600 °C) [21–23]. Elements widely used in DRM are late transition metals such as Ni, Co, Pt, Pd, Ru, Rh, and Ir [24–30]. In particular, Ni/γ-Al_2O_3 is the most preferred choice because it is inexpensive and relatively abundant, although the catalyst is prone to deactivation by carbon deposition and sintering [31]. In order to improve the performance of the Ni/γ-Al_2O_3, catalyst modification has been extensively studied [32–36]. For example, the addition of a basic oxide to γ-Al_2O_3 as the main support is known to enhance the adsorption of CO_2 to improve the activity [37]. Moreover, $MgAl_2O_4$ and prevents the formation of inactive $NiAl_2O_4$ [38]. Another direction of the modification is the addition of a secondary element. A combination of Ni with Fe was reported to enhance both the activity and the durability of the catalyst by suppressing carbon formation, where the redox effect of Fe and the interaction of Fe with Ni were proposed as potent reasons [39]. Thus, the multi-component design is an effective strategy to improve the performance of DRM catalysts, but catalysts containing more than 4 components have not been explored.

In this chapter, truly multi-component design of catalysts was explored by combining HTE and genetic algorithm for low-temperature DRM. The catalysts consisted of up to 16 elements (Mg, Al, Ca, V, Mn, Fe, Co, Ni, Cu, Zn, Sr, Zr, Mo, Pd, La, Ce) that

were co-supported on γ-Al_2O_3. The performance of the catalysts was evaluated in the previously developed HTE apparatus. The catalyst composition was evolved by using GA, where the H_2 yield at 500 °C was used as the target variable. The generated data were subjected to a variety of data analysis in order to derive catalyst design guidelines.

3.2. Experimental

3.2.1 Materials

The metal precursors were $Mg(NO_3)_2 \cdot 6H_2O$, $Al(NO_3)_3 \cdot 9H_2O$, $Ca(NO_3)_2 \cdot 4H_2O$, $VOSO_4 \cdot xH_2O$ (x=3–5), $Mn(NO_3)_2 \cdot 6H_2O$, $Fe(NO_3)_3 \cdot 9H_2O$, $Co(NO_3)_2 \cdot 6H_2O$, $Ni(NO_3)_2 \cdot 6H_2O$, $Cu(NO_3)_2 \cdot 3H_2O$, $Zn(NO_3)_2 \cdot 6H_2O$, $Sr(NO_3)_2$, $ZrO(NO_3)_2 \cdot xH_2O$ (x = 2), $(NH_4)_6Mo_7O_{24} \cdot 4H_2O$, $Pd(CH_3COO)_2$, $La(NO_3)_3 \cdot 6H_2O$, and $Ce(NO_3)_3 \cdot 6H_2O$. These were purchased from Wako Pure Chemical Industries, Kanto Chemical, or Sigma-Aldrich. Aluminum oxide in a powder form (γ-Al_2O_3, 164 m^2/g, Sumitomo Chemical Industry) was used as a support.

3.2.2. Catalyst preparation

Catalysts were prepared based on a co-impregnation method, where γ-Al_2O_3 (1.0 g) was impregnated with 5.0 mL of an aqueous solution dissolving specified precursors at specified concentrations at 50 ºC for 6 h under stirring. Followed by vacuum drying at 90 ºC for 4 h, the catalysts were calcinated at 500 ºC under air for 6 h, thoroughly ground, and subjected to the catalytic test.

3.2.3. Catalytic test

The DRM performance of the catalysts was evaluated by using a previously developed HTE instrument [10]. The instrument is briefly described as below. A

CH_4/CO_2/Ar mixture is supplied from a gas generator, where the flow rates of the three gases are controlled individually and Ar works as a balance gas. The gas mixture is equally split into 20 reaction quartz tubes (4 mm to 2 mm of I.D.) bearing catalyst beds of 10 mm height. The reaction tubes are arranged symmetrically in a hollow electric furnace. The effluent gas from the 20 tubes is sampled sequentially by an autosampler and transferred to a quadruple mass spectrometer (Transpector CPM, INFICON). Mass signals are converted to relative pressure of individual gases based on external calibrations. The system can evaluate the performance of 20 catalysts under programmed conditions. Two programs were used here. One is for activating the catalyst with H2 reduction (Figure 3.1). The other is for evaluating catalyst performance with gas for the DRM reaction. Both were pre-fired inline. The temperature was increased stepwise from 400 to 500, 600, 700°C, and 800 °C. At each temperature, the total flow rate (Q = 10, 15, 20 mL/min/channel) and CH_4/CO_2 ratio (0.50, 0.75, 1.00, 1.25, 1.50 mol/mol) were changed stepwise (Figure 3.1).

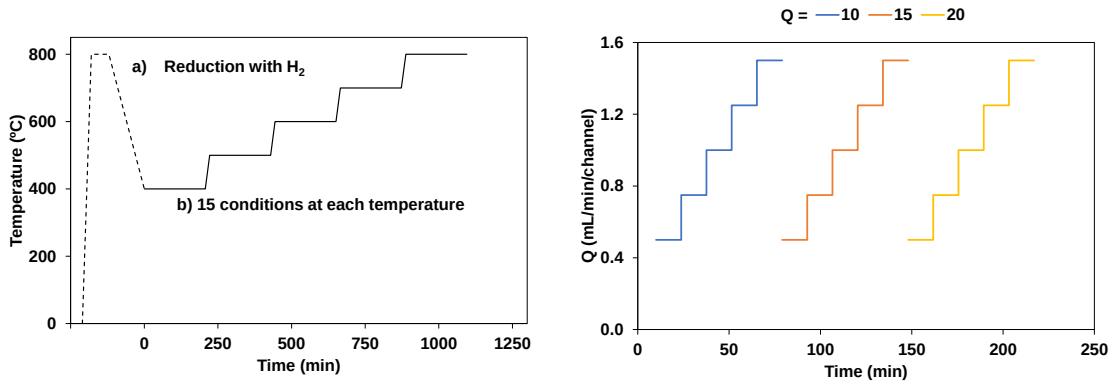

Figure 3.1. Two programmed sequences of reaction conditions: a) used for catalyst activation, and b) used for catalyst evaluation. Please note that each temperature step in b) includes a program for the gas flow volume and composition.

3.2.4. Exploration of catalysts

Figure 3.2 represents the methodology used to explore catalysts. A catalyst is composed by selecting either of Mg, Al, Ca, V, Mn, Fe, Co, Ni, Cu, Zn, Ce Sr, Zr, Mo, Pd, La, Ce and "None" 20 times with repetitive selection allowed. Namely, the catalyst is represented by a chromosome with 20 genes. The values of the genes are the elements in the library or "None". The maximum amount of the elements per gram of the support was set to 3.5 mmol/g-support, which corresponded to the addition of 0.175 mmol/g-support per selection except for “None”. “None” corresponds to not to add any element, and functions to vary the total amount of elements per gram of the support. The selection rate of “None” was appropriately adjusted. The parametric space as defined above includes 80^{13} combinations.

In the following, the procedure of the catalyst exploration is described according to the three steps shown in Figure 3.2.

Step 1: Preparation

Catalyst compositions were determined based on random selection in the case of the 0th generation and by genetic operators thereafter. The catalysts were prepared according to the method described in 3.2.2.

Step 2: Evaluation

The number of data points obtained is 8720. The conversion and yield values were derived based on Eqs. (3.1)–(3.4),

$$CH_4\ conversion\ (\%) = \frac{CH_4\ output - CH_4\ input}{CH_4\ input} \times 100 \quad (3.1),$$

$$CO_2\ conversion\ (\%) = \frac{CO_2\ output - CO_2\ input}{CO_2\ input} \times 100 \quad (3.2),$$

$$H_2\ yield\ (\%) = \frac{H_2\ output}{CH_4\ input} \times 100 \quad (3.3),$$

$$CO\ yield\ (\%) = \frac{CO\ output}{CH_4\ input} \times 100 \quad (3.4).$$

The catalysts prepared in Step 1 were subjected to the catalytic test as described in 3.2.3. The H_2 yield at 500 °C was used to derive the fitness of the individual catalysts based on Eqs. (3.5) and (3.6),

$$\rho_i = \frac{H_2\ \text{yield}_i - H_2\ \text{yield}_{min}}{H_2\ \text{yield}_{max} - H_2\ \text{yield}_{min}} \quad (3.5),$$

$$f_i = \exp(3\rho_i) \quad (3.6),$$

where H_2 yield$_i$, H_2 yield$_{min}$, and H_2 yield$_{max}$ are the H_2 yield for the i^{th}, the best, and the worst catalyst in a generation, respectively. f_i is the fitness of the i^{th} catalyst.

Step 3: Evolution

Genetic operators were introduced to evolve the catalyst composition. In crossover, the common genes were inherited from two selected parent catalysts, and the non-common part was randomly inherited from either parent catalyst. In this study, two types of mutations with different degrees were used to counter early convergence of evolution. In normal mutation, 5–20% of the genes in a selected parent catalyst were replaced by elements randomly drawn from the library. In another mutation, called big mutation, random replacement of the genes was performed for 20–50% of the genes. The parents were selected by a roulette selection method using the fitness as the weight. The catalysts with excellent performance were utilized as elite catalysts to carry over to the next

generation. 12 catalysts by the crossover, 4 by the normal mutation, 4 by the big mutation, and 4 by the elitism led to a total of 24 catalysts for the next generation.

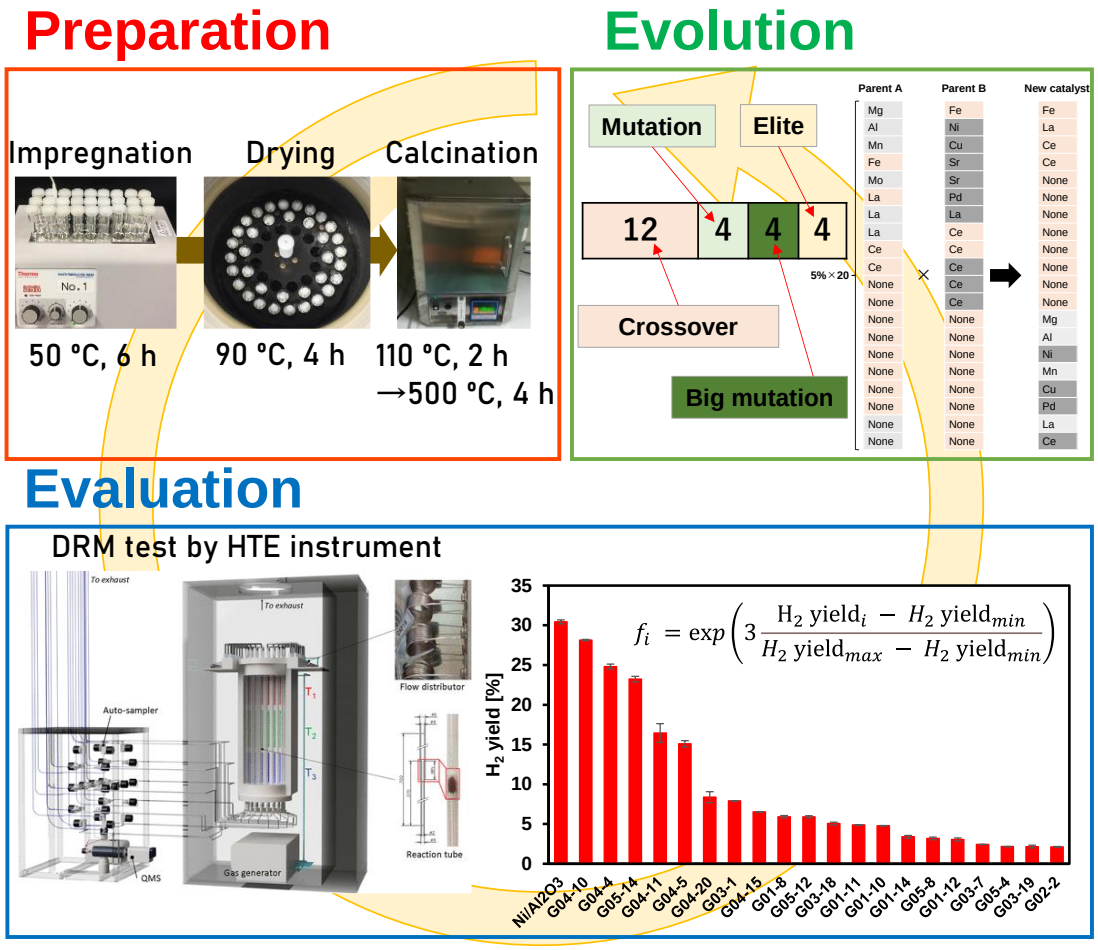

Figure 3.2. flow of the exploration of dry-reforming catalysts based on the genetic algorithm. The scheme consists of three steps: preparation of catalysts, evaluation of catalytic performance, and evolution of catalysts.

3.2.5. Data analysis

In order to derive insights into catalyst design, the data derived in the course of the evolution was analyzed by different techniques. The principal component analysis and classification tree analysis were implemented using the scikit-learn library in python [40,41]. Gephi was used for visualizing the interaction among elements [42,43]. The details of each analysis are described in the corresponding part of Results and Discussion.

3.3. Results and discussion

3.3.1. Pre-conditioning

When evolving catalysts in GA, H2 yield ≈ 0% means that the fitness is zero, and these individuals are synonymous with non-existence. Therefore, it was necessary to create many random catalyst compositions and evaluate their performance. Temperatures other than 500 °C were also considered to determine trends in gas conditions and experimental conditions that are efficient for DRM. In this chapter, I explored DRM catalysts using the HTE instrument and GA. To evolve catalysts while maintaining diversity in GA, random catalysts were created and evaluated (100 catalysts) until 20 catalysts exhibiting H_2 yield (>1% H_2 yield) were obtained. Table 3.1 lists the performance of the 139 catalysts. The catalyst code E*x* refers to the x^{th} catalyst explored. Each catalyst has 20 genes, and the number of elements or "none" in each gene determines the total loading amount and the ratio of each element to the total loading. Table 3.1 shows that only 15.1% of the catalyst prepared in random (Table 3.1, E1–99) exhibited catalytic performance (>1% H_2 yield). In addition, only 3.6% of those catalysts had ≥10% H_2 yield. Figure 3.3 is a visualization of these data points based on scatter plots. Figure 3.3 shows that H_2 yield, CH_4 conversion, and CO_2 conversion are proportional (Figure 3.3a). It was observed that H_2 yield decreased and CO yield increased with increasing temperature (Figure 3.3b). This suggests the influence of reverse water gas shift ($H_2 + CO_2 \rightarrow H_2O + CO$), a side reaction of DRM [44]. When CO_2 flow rate was increased, H_2 yield decreased and CO yield increased (Figure 3.3c), which may also be due to the reverse water gas shift. It was also found that CH_4/CO_2 should be close to 1 to obtain high H_2 yield and CO

yield. Figure 3.3d shows that Loading amount, H_2 yield, and CO yield were not correlated. This fact means that the loading amount is not an important factor in designing multidimensional catalysts. The catalyst became easier to clogging during the evolutionary process, making it difficult to evaluate 20 catalysts simultaneously at the 2^{nd}. This is likely due to the increase in carbon precipitation as well as the improvement in catalyst performance during the evolution (Figure 3.4).

Table 3.1. List of catalysts in the 0th (E1–99), 1st (E100–119) and 2nd (E120–139) generations[a]. Each catalyst performance is at 500 °C.

						Catalyst composition (%)														
Cat. code[a]	CH_4 conv.	CO_2 conv.	H_2 yield	CO yield	Total loading (mmol/g-support)	Mg	Al	Ca	V	Mn	Fe	Co	Ni	Cu	Zn	Sr	Zr	Mo	Pd	La	Ce
E1	1.5	-3.8	0.1	0.4	1.23	0	5	5	5	5	0	0	0	0	0	0	0	5	5	5	0
E2	2.7	-1.8	0.1	0.3	1.75	5	5	0	0	5	5	0	0	0	0	0	0	5	0	15	10
E3	4.8	0.4	0.8	5.1	1.75	0	0	0	0	0	5	0	5	5	0	10	0	0	5	5	15
E4	-1.4	-6.3	0.1	0.2	1.75	5	0	10	5	10	0	0	0	0	0	0	5	10	0	5	0
E5	3.3	0.3	0.1	0.4	2.45	0	0	5	5	10	10	0	10	10	10	0	0	0	0	0	10
E6	2.6	-1.3	0.1	0.2	2.10	0	5	0	0	15	5	0	5	0	10	5	0	15	0	0	0
E7	2.7	-1.0	0.1	0.3	1.93	0	0	0	10	0	0	5	5	5	0	5	10	5	5	5	0
E8	3.4	8.8	5.9	11.3	2.45	0	0	5	0	0	5	10	5	10	5	15	5	5	5	0	0
E9	2.2	-2.4	0.1	0.3	1.93	0	0	10	0	0	0	15	0	5	0	0	5	10	0	0	10
E10	2.4	5.9	4.9	9.4	2.10	5	5	0	0	0	0	0	10	5	5	0	0	5	5	10	10
E11	2.9	6.6	5.0	9.5	1.93	5	5	5	0	5	5	5	5	10	0	0	0	0	10	0	0
E12	10.2	6.8	3.1	11.6	2.28	5	0	0	0	10	5	0	5	5	5	5	10	0	5	5	5
E13	3.3	-1.8	0.1	0.5	1.75	5	10	0	10	5	5	0	0	0	0	10	5	0	0	0	0
E14	1.2	2.8	3.2	7.1	2.45	15	10	0	0	15	0	0	5	5	5	0	0	5	5	5	0
E15	2.8	-2.0	0.1	0.5	1.40	0	0	5	10	0	0	5	0	5	5	5	0	0	0	5	0
E16	2.1	-2.1	0.1	0.4	1.05	0	5	5	0	0	5	5	0	5	0	0	5	0	0	0	0
E17	-1.6	-7.7	0.1	0.2	2.45	0	10	0	5	5	15	0	0	0	5	0	5	15	0	10	0
E18	1.7	-1.8	0.1	0.3	1.93	5	5	0	5	0	5	5	5	0	5	5	0	0	5	5	5
E19	2.5	-1.5	0.1	0.6	1.58	5	0	5	5	0	5	0	0	10	5	0	0	0	0	0	10
E20	-1.3	-5.5	0.3	1.2	2.28	0	5	0	0	0	0	0	10	10	5	5	5	15	0	5	5
E21	0.0	4.0	0.1	0.3	1.75	5	5	10	0	5	5	0	0	5	0	5	0	0	0	5	5
E22	-4.2	6.1	2.2	5.8	1.40	5	5	5	0	0	0	0	5	5	0	0	0	5	5	0	5
E23	-29.4	-3.2	0.1	0.3	1.40	10	10	5	0	0	0	0	0	5	5	0	0	5	0	0	0
E24	-6.7	1.8	0.1	0.1	1.93	0	0	0	10	10	0	5	10	0	0	5	5	5	5	0	0
E25	-7.3	2.0	0.1	2.7	2.10	0	0	20	10	5	0	5	0	0	0	5	5	0	10	0	0
E26	-8.7	1.1	0.1	0.1	1.93	0	5	0	0	5	5	10	0	0	0	5	0	5	0	15	5
E27	-7.5	2.1	0.1	0.2	1.58	0	5	0	5	0	5	0	5	5	0	0	0	5	5	5	5
E28	-66.4	-16.7	0.1	3.5	2.28	10	0	5	10	0	10	0	5	5	0	5	5	0	5	0	5
E29	3.9	4.9	0.1	0.0	1.58	5	5	0	5	0	0	5	0	0	0	15	5	0	5	0	0
E30	4.8	5.9	0.1	0.1	2.10	10	0	5	0	0	5	0	5	0	10	0	5	0	0	15	5
E31	0.0	5.4	0.1	0.1	1.58	0	0	5	0	0	0	0	5	0	0	5	10	0	5	10	5

E32	3.0	5.2	0.1	0.3	1.23	0	0	0	0	5	0	0	5	5	0	5	5	0	10	0	0
E33	-7.6	-0.2	0.1	3.2	2.10	0	5	5	0	0	0	5	0	0	5	5	10	5	5	10	5
E34	1.8	12.9	1.6	6.1	2.28	0	5	5	5	5	0	5	5	5	0	5	5	0	5	10	5
E35	-1.4	3.8	0.1	0.1	2.28	0	5	5	0	5	0	5	5	0	0	5	10	0	10	10	5
E36	3.8	5.5	0.1	0.2	1.05	0	0	0	0	5	0	0	10	0	0	5	5	0	0	0	5
E37	3.0	4.2	0.1	0.1	1.23	10	0	0	0	0	5	5	0	0	0	5	0	0	5	0	5
E38	-6.5	-0.1	0.1	1.1	1.23	5	5	5	0	0	0	0	5	0	5	0	0	0	0	5	5
E39	3.2	4.9	0.1	0.6	1.93	0	0	0	0	0	5	5	5	0	5	0	5	5	10	10	5
E40	10.6	10.3	8.1	11.7	1.23	0	0	0	0	0	0	5	10	5	5	0	0	5	5	0	0
E41	2.5	-1.4	0.1	0.2	1.23	0	5	0	5	5	0	0	0	0	0	0	5	5	5	0	5
E42	3.2	-2.6	0.1	0.1	1.75	0	0	0	0	5	10	5	0	0	0	5	0	15	10	0	0
E43	6.2	0.2	0.1	0.5	2.10	0	5	0	5	5	0	0	0	5	5	10	0	5	5	0	15
E44	5.5	-0.2	0.1	0.4	1.75	5	0	5	10	5	0	0	0	5	0	0	0	0	5	5	10
E45	3.2	-0.8	0.1	0.2	2.10	0	15	10	5	0	0	0	0	0	10	0	0	5	10	0	5
E46	8.1	4.7	2.5	5.7	2.28	10	0	10	0	0	10	0	10	5	0	0	10	5	0	5	0
E47	1.1	-4.0	0.1	0.2	1.58	5	0	10	0	10	10	0	5	0	0	0	0	0	0	5	0
E48	3.0	-1.0	0.1	0.2	1.05	5	0	5	0	0	0	0	5	0	0	0	5	5	0	0	5
E49	4.1	-0.2	0.3	2.1	1.40	0	0	0	0	0	5	0	0	0	5	5	15	0	10	0	0
E50	6.2	1.3	1.4	6.5	2.63	10	15	5	15	0	0	5	5	0	0	0	5	0	5	5	5
E51	1.2	-3.0	0.1	0.3	1.75	0	0	0	0	10	10	0	0	0	5	0	10	5	0	0	10
E52	0.2	-5.4	0.1	0.2	1.58	0	5	5	5	5	0	5	15	0	5	0	0	0	0	0	0
E53	1.3	-3.2	0.1	0.3	1.58	10	5	0	0	0	5	0	0	5	0	0	0	5	5	10	0
E54	3.3	-1.1	0.1	0.2	1.40	0	5	0	5	10	5	5	0	0	0	5	0	0	5	0	0
E55	7.0	-1.0	0.1	0.4	1.93	0	0	10	5	5	5	5	5	0	5	5	0	5	0	0	5
E56	4.9	0.0	1.6	5.0	1.40	0	0	5	0	5	5	0	0	5	0	0	0	10	5	5	0
E57	8.0	2.9	5.2	13.4	1.58	0	5	0	0	0	0	0	5	5	0	5	0	5	5	5	10
E58	6.7	1.8	2.2	7.3	1.58	5	5	0	0	0	5	5	5	0	5	0	0	5	10	0	0
E59	3.9	0.4	0.1	1.5	2.45	5	5	0	0	0	0	5	0	5	5	10	0	10	5	10	10
E60	3.4	-6.8	0.3	0.7	1.40	5	5	5	0	0	0	0	0	0	0	0	0	10	5	10	0
E61	2.7	-4.6	0.1	0.3	1.75	5	10	5	5	0	5	5	5	5	0	0	0	0	0	0	5
E62	2.0	-4.0	0.1	0.3	2.10	10	0	10	10	0	0	0	10	0	5	0	15	0	0	0	0
E63	30.4	17.6	25.3	38.9	1.05	0	0	0	0	5	0	0	5	0	0	5	5	0	5	0	5
E64	20.3	10.6	15.4	26.6	1.05	0	0	0	0	0	0	0	5	0	0	5	5	5	5	5	0
E65	1.8	-8.5	0.3	0.8	1.58	0	0	5	10	0	0	5	0	5	0	5	5	0	5	5	0
E66	0.9	-9.1	0.1	0.4	1.58	5	10	0	0	0	10	5	0	0	0	5	5	0	0	5	0
E67	2.4	-8.6	0.1	0.3	2.63	0	5	5	5	5	10	5	0	5	0	5	15	5	5	5	0

E68	4.7	-2.6	0.1	0.2	1.40	5	5	0	0	15	0	0	10	0	0	0	5	0	0	0	0
E69	37.8	23.3	28.7	41.4	2.10	0	5	5	0	0	0	5	5	0	0	5	10	0	10	10	5
E70	23.3	13.6	16.8	30.9	1.23	5	5	0	0	0	5	0	10	0	5	0	0	0	0	5	0
E71	1.3	-5.3	0.1	0.3	1.93	0	10	0	5	0	0	10	5	0	5	5	0	0	0	10	5
E72	2.0	-4.7	0.1	0.3	1.40	0	5	5	5	5	0	0	0	5	5	5	5	0	0	0	0
E73	5.1	-4.5	0.8	4.7	1.75	5	0	0	0	5	0	0	5	5	5	5	5	0	0	5	10
E74	16.3	5.2	9.1	17.2	2.28	10	10	0	0	5	0	0	10	10	10	0	0	0	10	0	0
E75	0.2	-7.7	0.1	0.2	1.75	0	0	0	0	0	5	20	0	0	0	5	0	15	0	5	0
E76	2.6	-7.4	0.1	1.0	1.23	0	0	0	5	0	0	5	5	5	0	0	5	0	5	5	0
E77	0.0	-6.5	0.1	0.3	1.93	5	0	10	0	0	0	5	0	0	0	5	10	0	0	20	0
E78	3.4	-3.2	0.1	0.4	1.40	10	0	5	0	0	0	5	5	0	10	0	0	0	0	5	0
E79	12.1	3.4	8.5	19.9	1.40	5	0	0	0	0	5	5	5	0	5	0	0	5	5	0	5
E80	3.6	0.3	-5.4	0.0	1.75	0	0	0	0	0	0	10	5	5	5	5	10	0	0	0	10
E81	0.3	0.3	-6.4	0.2	1.40	10	5	0	0	0	5	0	0	5	5	0	0	0	5	5	0
E82	1.8	0.2	0.8	0.5	1.58	5	5	0	0	0	5	5	5	0	5	0	0	5	5	5	0
E83	5.6	0.4	0.5	0.8	1.23	0	0	0	0	0	0	5	5	5	5	0	0	0	5	5	5
E84	5.1	0.2	-3.3	0.5	1.58	5	5	0	0	0	5	5	0	0	5	5	0	5	5	5	0
E85	2.7	0.3	-6.4	0.5	1.58	0	5	0	5	0	0	0	5	5	0	0	5	0	5	5	10
E86	0.8	0.8	-7.0	1.2	1.58	0	5	0	0	0	0	5	0	5	5	5	5	0	5	5	5
E87	6.4	0.1	-1.4	0.5	1.93	5	5	5	0	0	0	5	0	0	0	5	10	5	5	10	0
E88	0.7	0.7	-5.1	0.7	1.58	0	5	0	5	0	0	5	5	5	5	5	0	0	0	10	0
E89	0.5	0.2	-5.6	0.2	1.75	5	0	0	5	0	0	5	5	0	0	5	10	0	0	15	0
E90	-1.6	0.2	-7.0	0.3	1.23	0	5	0	5	0	5	5	0	5	5	0	5	0	0	0	0
E91	11.5	0.4	4.8	0.5	1.58	0	0	0	0	0	5	5	5	5	0	10	0	0	5	5	5
E92	1.1	0.0	-4.5	0.1	1.93	0	10	0	5	0	0	10	5	5	5	5	0	0	0	5	5
E93	30.8	0.4	19.6	0.8	2.45	0	0	5	0	0	5	10	5	10	0	15	5	5	10	0	0
E94	-0.1	0.0	-5.6	0.2	1.58	0	10	5	5	0	5	5	5	5	0	0	0	0	0	0	5
E95	2.1	0.3	-3.6	0.4	1.93	0	15	0	5	0	0	10	5	0	5	5	0	0	0	5	5
E96	0.1	0.8	-5.2	0.7	1.93	0	0	5	10	15	0	5	10	5	0	0	0	5	0	0	0
E97	0.0	0.4	-8.9	0.3	1.93	0	5	0	5	0	15	5	0	5	5	0	5	5	0	5	0
E98	0.1	0.3	-5.6	0.2	2.63	10	0	5	10	10	0	5	5	0	10	10	10	0	0	0	0
E99	1.1	0.3	-6.6	0.6	2.63	15	15	0	20	0	5	5	0	0	5	0	0	0	0	0	10
E100	1.0	-8.8	0.1	0.5	1.93	0	5	5	0	0	0	5	0	0	0	5	10	5	5	10	5
E101	8.9	-1.0	2.7	8.5	2.10	5	10	0	0	0	0	0	10	10	5	0	0	0	10	5	5
E102	19.1	9.5	12.3	25.0	1.75	5	5	5	0	0	5	0	5	0	5	0	0	0	10	10	0
E103	16.7	7.3	9.9	21.9	1.58	0	5	0	0	0	0	5	5	0	0	5	10	0	5	5	5

E104	17.0	7.0	9.6	21.7	1.93	5	5	5	0	0	0	0	5	0	5	5	5	0	10	5	5
E105	14.2	4.6	8.5	20.1	1.05	0	0	0	0	5	0	0	5	0	0	5	5	0	5	5	0
E106	5.9	-0.5	2.6	5.4	1.58	0	0	0	0	0	0	5	5	10	0	5	5	5	10	0	0
E107	5.8	-0.4	2.4	6.2	1.93	0	0	5	0	0	5	10	5	5	0	15	0	5	5	0	0
E108	5.2	3.3	2.4	6.6	1.58	0	0	0	0	0	5	10	5	0	0	5	5	5	5	5	0
E109	23.3	12.6	17.2	31.2	1.40	0	0	5	0	0	0	0	5	0	0	5	5	0	5	10	5
E110	30.9	18.4	24.1	38.1	1.58	0	0	0	0	0	0	5	5	0	0	5	10	0	10	10	0
E111	22.1	11.6	16.4	30.8	1.23	0	0	0	0	0	5	5	5	0	0	5	5	0	5	0	5
E112	2.6	-3.7	0.5	1.5	1.75	5	0	0	0	0	5	5	5	0	5	5	0	10	5	0	5
E113	23.2	12.1	18.6	32.0	2.10	10	10	0	0	0	0	0	10	10	10	0	0	0	10	0	0
E114	20.1	8.8	13.4	23.1	1.75	0	5	5	0	0	0	5	5	0	0	5	10	0	5	10	0
E115	28.0	15.5	22.5	36.2	1.05	0	0	0	0	5	0	0	5	0	0	5	5	0	5	0	5
E116	24.1	13.9	15.5	29.5	1.75	0	5	5	0	0	5	0	5	0	5	0	5	0	5	10	5
E117	3.2	-0.3	3.8	7.5	1.58	0	0	0	0	0	0	5	5	5	0	10	5	5	5	0	5
E118	9.3	1.2	3.1	10.6	1.93	5	0	5	0	0	5	5	0	5	0	15	0	0	10	5	0
E119	18.0	8.4	9.7	20.3	2.63	0	5	5	0	10	0	10	5	0	0	5	10	5	10	5	5
E120	8.2	0.8	1.4	6.8	1.75	5	5	0	0	0	5	5	0	0	5	0	5	0	10	10	0
E121	24.6	9.2	13.4	29.9	1.93	0	0	5	0	0	0	10	5	5	0	5	5	0	5	10	5
E122	18.9	10.8	10.1	22.6	1.58	5	5	0	0	0	5	0	5	0	5	0	10	0	5	5	0
E123	16.8	8.0	6.7	14.1	1.58	10	10	0	0	0	0	0	10	5	0	0	0	0	10	0	0
E124	32.5	20.8	23.4	37.0	1.75	5	10	0	0	0	0	5	10	0	5	0	0	0	5	10	0
E125	5.3	5.8	3.6	8.8	1.05	0	0	0	0	5	0	5	0	0	0	0	5	0	5	5	5
E126	32.4	21.2	23.0	37.0	1.75	0	0	5	0	5	0	5	5	0	0	5	10	0	10	5	0
E127	35.3	22.9	26.1	40.0	1.23	0	0	0	0	5	5	0	5	0	0	5	5	0	5	0	5
E128	8.6	-1.7	2.1	3.8	1.75	5	0	0	0	5	5	0	5	0	0	5	5	10	5	0	5
E129	22.8	13.6	13.9	27.4	1.40	0	5	0	0	5	5	0	5	0	5	0	5	0	5	0	5
E130	38.4	22.9	30.9	45.3	1.58	0	0	5	0	0	0	0	5	0	0	5	10	0	5	10	5
E131	21.1	3.7	10.9	18.7	1.23	0	0	0	0	5	0	0	5	5	0	5	5	0	10	0	0
E132	7.1	8.1	5.0	9.8	2.10	0	5	5	0	0	0	5	0	0	5	5	10	5	5	10	5
E133	3.0	-4.4	0.1	0.2	2.28	0	5	5	5	5	0	5	5	5	0	5	5	0	5	10	5
E134	35.1	20.8	28.6	43.1	2.28	0	5	5	0	5	0	5	5	0	0	5	10	0	10	10	5
E135	40.5	23.8	33.9	48.1	1.05	0	0	0	0	5	0	0	10	0	0	5	5	0	0	0	5
E136	34.6	22.2	25.8	40.0	1.23	10	0	0	0	0	5	5	0	0	0	5	0	0	5	0	5
E137	3.0	-7.7	0.1	0.2	1.23	5	5	5	0	0	0	0	5	0	5	0	0	0	0	5	5
E138	2.9	-3.0	0.4	1.7	1.93	0	0	0	0	0	5	5	5	0	5	0	5	5	10	10	5
E139	10.3	14.4	8.6	14.2	1.75	0	0	0	0	5	0	5	5	0	0	10	0	5	10	10	0

[a]E*x* refers to the x^{th} catalyst explored.

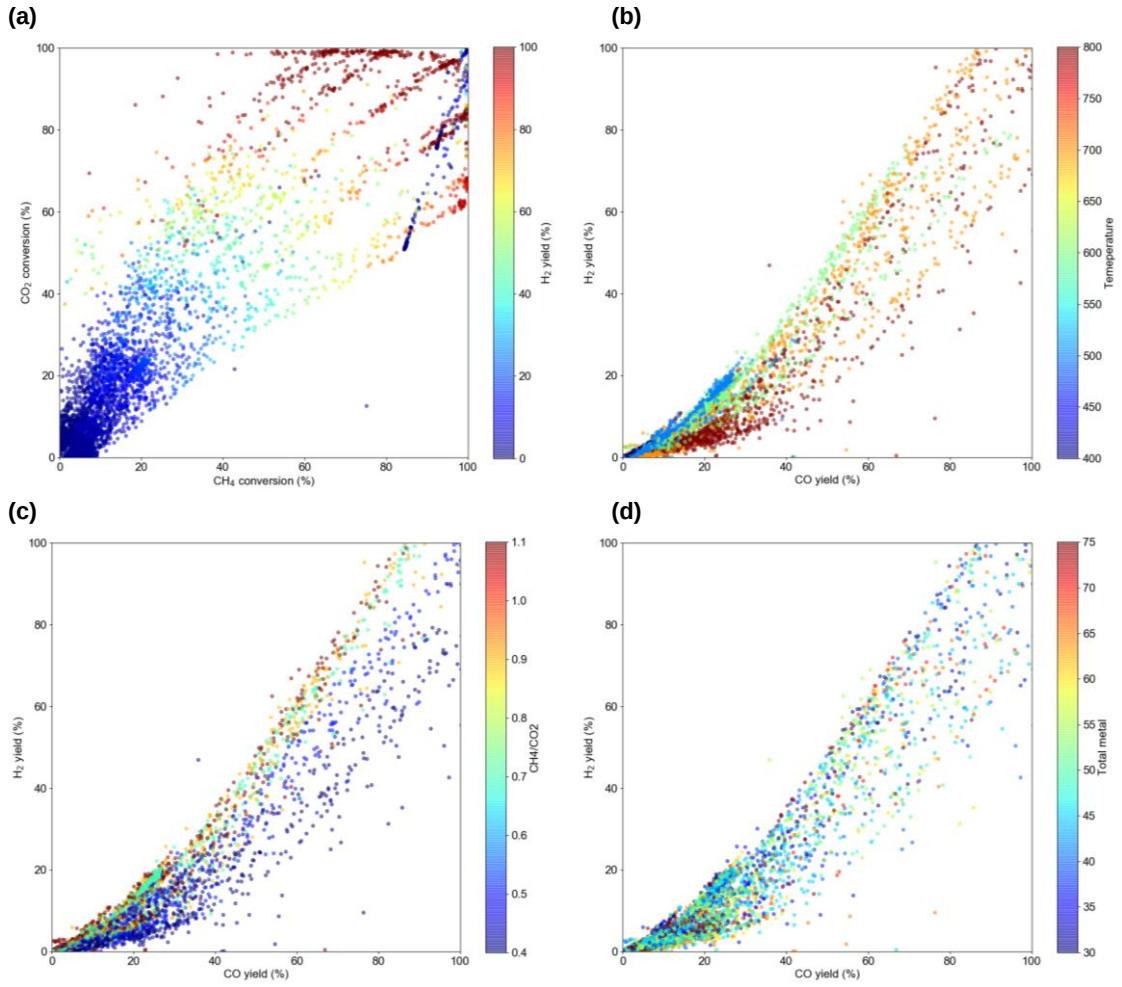

Figure 3.3. Visualization of 8720 data points based on scatter plots. (a) CH_4 conversion vs CO_2 conversion with the H_2 yield indicated by the color. CO yield vs H_2 yield with (b) the temperature, (c) the CH_4/CO_2 and (d) the total loading amount indicated by the color.

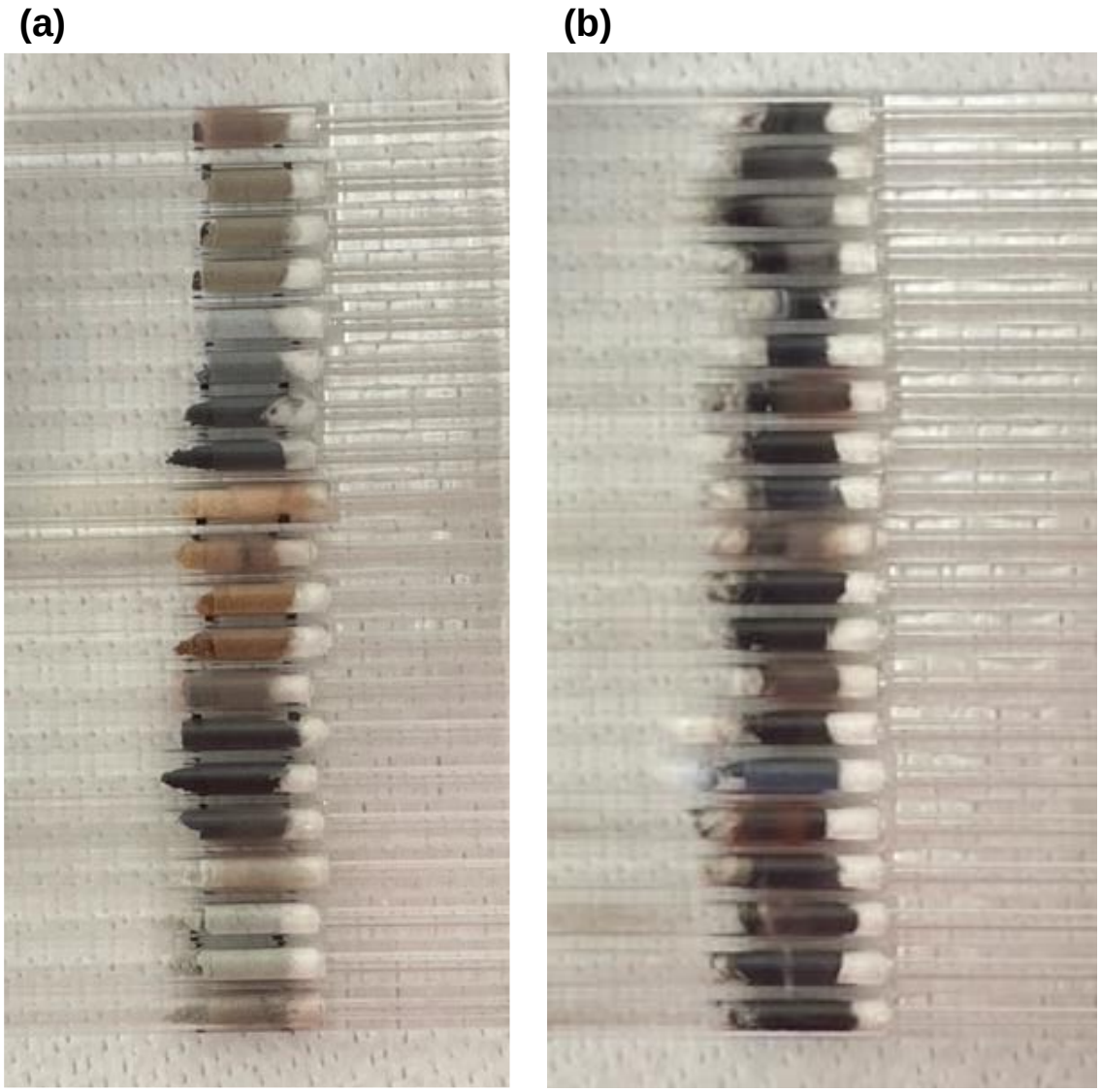

Figure 3.4. Color change of catalyst after the catalytic test: (a) Before the experiment. Please note that, the black lines shown in both ends of the catalyst are markers for aligning the height of the catalyst, not the color of the catalyst. (b) After the experiment. Each catalyst has turned black suggesting coking.

3.3.2. Catalyst stability and new experimental conditions

Based on the problem in 3.3.1, the reaction temperature (500 ºC), total flow rate (Q

= 20 mL/channel), and CH_4/CO_2 ratio (1.00 mol/mol) were changed, and the catalysts were evaluated for 20000 sec. The top 20 catalysts in Table 3.1 and the 20 catalysts in 2nd were re-evaluated under the above conditions. Experimental results showed that there was no catalyst clogging due to catalyst coking, and all catalysts were evaluated without any problems. Figure 3.5 shows the H_2 yield change for each catalyst over time. Figure 3.5 shows that there are differences in stability among the catalysts. Catalytic performance should consider not only H_2 yield but also stability. Therefore, the catalytic performance was defined as the H_2 yield averaged over 15000-20000 sec, where the catalytic performance is relatively stable.

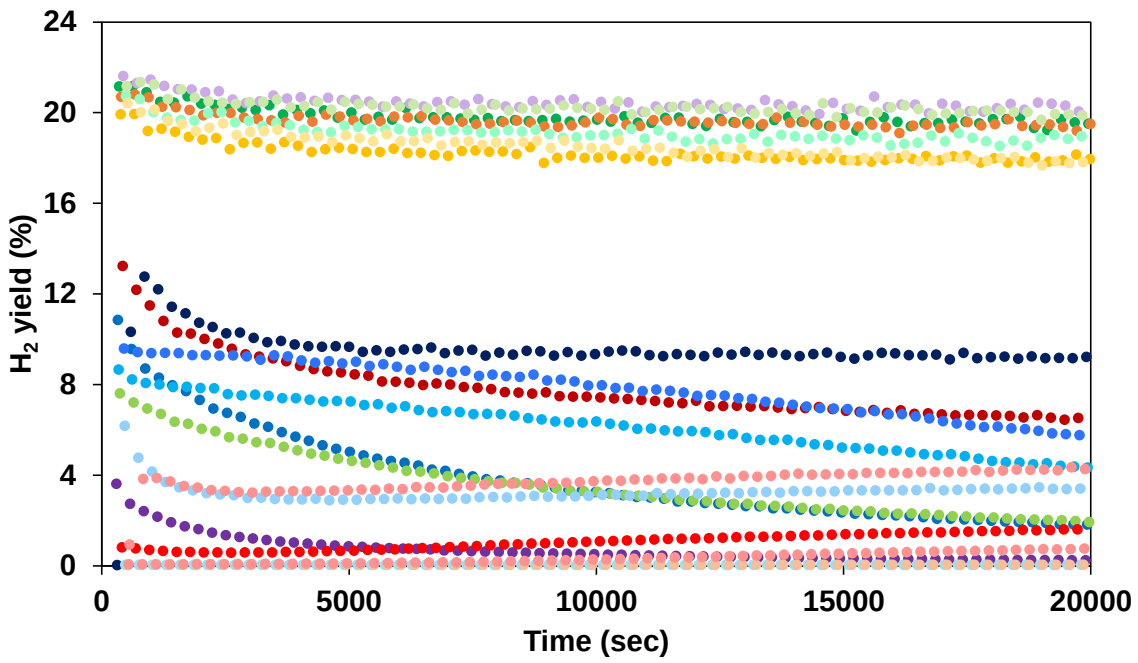

Figure 3.5. H_2 yield change over time in 20 catalysts.

3.3.3. Evolution of catalysts

Figure 3.6 shows the box-and-whisker plot of catalyst performance trends by generation. Within 9 generations, the performance improved 1.7 time, and the variation in performance between catalysts became smaller. It was also able to achieve a large scale exploration and confirm the evolution. The results consisted of 160 catalysts, 5120 element selections and 160208 combinations.

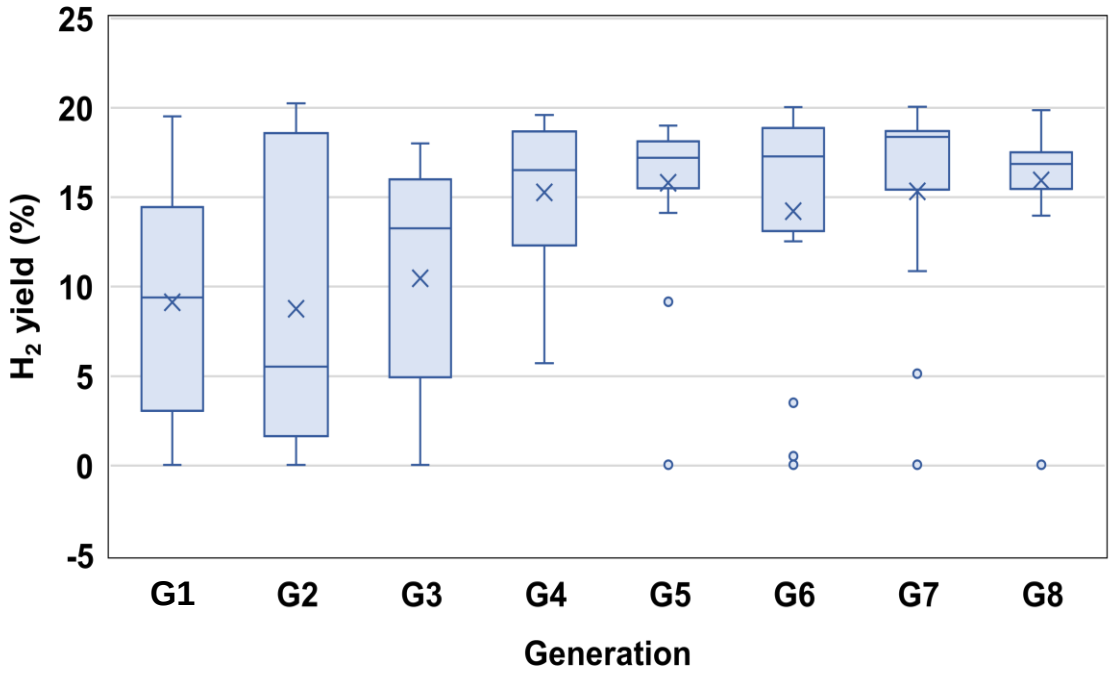

Figure 3.6. The evolution of the best and average performance of catalysts along with the generation.

3.3.4. Catalysts and their performance

A total of 160 catalysts were obtained from as a result of evolution over 8 generations

(note that duplicates due to the elitism are not counted). Table 3.2 lists the catalyst composition and performance of the obtained catalysts. The catalyst code G*x*–*y* refers to the y^{th} catalyst in the *x* generation and R*x* refers to the x^{th} reference catalyst, which was evaluated separately from the catalyst obtained by GA. Table 3.3 shows the 10 best catalysts in the 160 catalysts. These catalysts were found to contain common elements in the order Ni > Pd > Al, Co, La > Sr, Ce > Zr > Mg, Ca, Mn, Zn. Although the most selected Ni is a highly active element, it has the disadvantage of easy to carbon deposition. Transition elements, particularly Ni, Co and Fe, have been reported to exhibit catalytic activity [22,23,39], but Fe is not included in the high performance catalysts. This suggests that other elements may inhibit Fe, or that Fe may inhibit elements that are superior to itself. Pd improves the dispersibility and reducibility of Ni through its hydrogen spillover effect [27]. Lanthanides of La and Ce promote metal dispersion and CO_2 adsorption on γ-Al_2O_3 [45].

Table 3.2. List of catalyst from 2nd generations. Note that top 20 catalysts of the 0th and 1st catalysts were re-evaluated using new protocol.

Cat. code[a]	CH_4 conv.	CO_2 conv.	H_2 yield	CO yield	Total loading (mmol/g-support)	Catalyst composition (%)															
						Mg	Al	Ca	V	Mn	Fe	Co	Ni	Cu	Zn	Sr	Zr	Mo	Pd	La	Ce
G1-1	20.2	23.8	19.5	26.4	2.10	0	5	5	0	0	0	5	5	0	0	5	10	0	10	10	5
G1-2	20.0	24.1	19.4	26.1	1.23	0	5	0	5	0	5	5	0	5	5	0	5	0	0	0	0
G1-3	19.9	23.4	19.0	25.6	1.93	0	15	0	5	0	0	10	5	0	5	5	0	0	0	5	5
G1-4	18.5	21.6	17.0	23.6	1.58	0	10	5	5	0	5	5	5	5	0	0	0	0	0	0	5
G1-5	16.7	20.1	14.7	21.9	1.05	0	0	0	0	5	0	0	5	0	0	5	5	0	5	0	5
G1-6	16.4	18.3	13.6	20.5	2.45	0	0	5	0	0	5	10	5	10	0	15	5	5	10	0	0
G1-7	15.5	17.2	12.4	19.3	1.75	5	0	0	5	0	0	5	5	0	0	5	10	0	0	15	0
G1-8	15.0	14.6	11.5	16.7	2.45	0	0	5	0	0	5	10	5	10	0	15	5	5	10	0	0
G1-9	13.8	13.4	10.9	16.5	1.05	0	0	0	0	0	0	0	5	0	0	5	5	5	5	5	0
G1-10	13.5	14.4	9.8	16.8	1.40	5	0	0	0	0	5	5	5	0	5	0	0	5	5	0	5
G1-11	12.6	13.0	9.0	15.8	1.58	5	5	0	0	0	5	5	5	0	5	0	0	5	5	5	0
G1-12	10.8	9.5	5.6	11.8	1.58	5	5	0	0	0	5	5	0	0	5	5	0	5	5	5	0
G1-13	9.6	6.1	5.5	9.8	1.23	0	0	0	0	0	0	5	10	5	5	0	0	5	5	0	0
G1-14	9.4	7.2	4.1	9.7	1.58	0	0	0	0	0	5	5	5	5	0	10	0	0	5	5	5
G1-15	8.8	5.5	3.2	8.5	1.23	0	0	0	0	0	0	5	5	5	5	0	0	0	5	5	5
G1-16	8.4	5.2	3.0	8.3	1.23	5	5	0	0	0	5	0	10	0	5	0	0	0	0	5	0
G1-17	7.4	3.1	2.1	6.5	1.58	0	5	0	5	0	0	0	5	5	0	0	5	0	5	5	10
G1-18	6.9	0.5	2.1	4.5	2.28	10	10	0	0	5	0	0	10	10	10	0	0	0	10	0	0
G1-19	4.6	-5.4	0.0	0.3	1.93	0	0	5	10	15	0	5	10	5	0	0	0	5	0	0	0
G1-20	4.4	-5.6	0.0	0.2	2.63	15	15	0	20	0	5	5	0	0	5	0	0	0	0	0	10
G2-1	5.4	-2.9	0.3	1.8	1.75	5	5	0	0	0	5	5	0	0	5	0	5	0	10	10	0
G2-2	13.3	14.2	9.2	39.0	1.93	0	0	5	0	0	0	10	5	5	0	5	5	0	5	10	5
G2-3	7.9	3.2	2.0	6.2	1.58	5	5	0	0	0	5	0	5	0	5	0	10	0	5	5	0
G2-4	10.8	5.8	4.8	7.5	1.58	10	10	0	0	0	0	0	10	5	0	0	0	0	10	0	0
G2-5	19.9	23.9	19.6	26.2	1.75	5	10	0	0	0	0	5	10	0	5	0	0	0	5	10	0
G2-6	7.9	3.7	2.2	6.6	1.05	0	0	0	0	5	0	5	0	0	0	0	5	0	5	5	5
G2-7	18.7	22.1	17.9	24.2	1.75	0	0	5	0	5	0	5	5	0	0	5	10	0	10	5	0
G2-8	20.1	23.8	19.4	26.1	1.23	0	0	0	0	5	5	0	5	0	0	5	5	0	5	0	5
G2-9	7.1	0.5	1.5	4.4	1.75	5	0	0	0	5	5	0	5	0	0	5	5	10	5	0	5
G2-10	12.0	10.8	6.7	12.9	1.40	0	5	0	0	5	5	0	5	0	5	0	5	0	5	0	5
G2-11	20.7	24.4	20.3	26.8	1.58	0	0	5	0	0	0	0	5	0	0	5	10	0	5	10	5
G2-12	12.4	8.0	6.3	9.3	1.23	0	0	0	0	5	0	0	5	5	0	5	5	0	10	0	0
G2-13	8.6	5.3	3.4	8.2	2.10	0	5	5	0	0	0	5	0	0	5	5	10	5	5	10	5
G2-14	4.9	-5.6	0.0	0.2	2.28	0	5	5	5	5	0	5	5	5	0	5	5	0	5	10	5
G2-15	20.1	23.1	18.8	25.7	2.28	0	5	5	0	5	0	5	5	0	0	5	10	0	10	10	5
G2-16	20.7	23.8	20.0	26.5	1.05	0	0	0	0	5	0	0	10	0	0	5	5	0	0	0	5
G2-17	19.2	22.3	17.9	24.8	1.23	10	0	0	0	0	5	5	0	0	0	5	0	0	5	0	5
G2-18	4.1	-5.7	0.0	0.2	1.23	5	5	5	0	0	0	0	5	0	5	0	0	0	0	5	5
G2-19	6.1	-0.9	0.7	3.3	1.93	0	0	0	0	0	5	5	5	0	5	0	5	5	10	10	5
G2-20	9.6	6.8	4.2	9.5	1.75	0	0	0	0	5	0	5	5	0	0	10	0	5	10	10	0

G3-1	18.3	21.1	15.9	23.0	1.05	0	0	0	0	0	0	0	5	0	0	5	5	0	5	5	5
G3-2	18.2	21.5	15.8	23.0	1.75	5	5	0	0	0	0	5	10	0	0	5	5	0	5	10	0
G3-3	17.9	21.0	16.0	23.2	1.23	0	0	0	0	5	5	0	5	0	0	5	5	0	5	0	5
G3-4	19.3	22.4	17.4	24.5	1.58	0	5	5	0	0	0	5	5	0	5	0	5	0	5	10	0
G3-5	9.4	6.7	4.1	9.8	2.10	0	0	0	0	0	5	10	5	5	0	10	5	5	10	5	0
G3-6	19.2	22.0	17.2	23.7	1.75	0	0	5	0	5	0	5	5	0	0	5	10	0	10	5	0
G3-7	10.4	7.8	4.9	10.5	1.75	0	5	5	0	0	0	0	5	0	5	5	5	0	10	10	0
G3-8	12.7	12.3	8.1	14.7	1.58	0	0	5	0	0	0	5	5	0	0	5	10	0	5	10	0
G3-9	11.6	10.0	6.8	12.6	1.40	0	0	5	0	5	0	0	5	0	0	5	10	0	5	5	0
G3-10	17.9	20.5	15.3	22.5	1.40	5	5	0	0	5	5	0	5	0	0	5	0	0	5	0	5
G3-11	12.2	11.4	7.7	13.5	1.93	0	0	5	0	5	0	5	5	0	0	5	10	0	10	10	0
G3-12	16.9	19.1	14.3	21.6	1.23	0	0	0	0	5	5	0	5	0	0	5	5	0	5	0	5
G3-13	17.0	19.2	14.4	21.7	1.23	0	0	0	0	5	5	0	5	0	0	5	5	0	5	0	5
G3-14	19.4	22.9	18.0	25.0	1.05	0	0	0	0	5	0	0	5	0	0	5	5	0	5	0	5
G3-15	4.9	-6.0	0.0	0.1	1.05	0	0	0	0	5	0	0	10	0	0	5	5	0	0	0	5
G3-16	10.3	6.5	5.0	9.4	1.75	0	0	0	0	5	0	5	5	0	0	10	0	5	10	10	0
G3-17	4.8	-5.6	0.0	0.1	1.05	0	0	0	0	5	0	0	10	0	0	5	5	0	0	0	5
G3-18	15.4	17.1	12.2	18.9	1.75	0	0	5	0	5	0	5	5	0	0	5	10	0	10	5	0
G3-19	18.3	20.9	16.1	23.0	1.05	0	0	0	0	5	0	0	5	0	0	5	5	0	5	0	5
G3-20	4.5	-5.7	0.0	0.1	1.05	0	0	0	0	5	0	0	10	0	0	5	5	0	0	0	5
G4-1	20.3	23.2	19.0	26.0	2.10	5	5	5	0	0	0	5	5	0	0	5	10	0	5	10	5
G4-2	35.3	34.6	10.9	100	1.40	0	5	0	0	0	5	0	5	0	5	0	5	0	5	10	0
G4-3	19.2	21.8	17.2	23.7	1.23	0	5	0	0	0	0	5	5	0	0	5	5	0	5	5	0
G4-4	20.1	21.9	18.2	24.3	1.75	5	5	0	0	0	0	5	10	0	0	5	10	0	5	5	0
G4-5	10.9	7.8	5.7	10.8	1.40	0	0	5	0	5	0	0	5	0	0	5	10	0	5	5	0
G4-6	15.9	16.6	12.3	18.9	1.93	0	0	5	0	5	0	5	5	0	0	5	10	0	10	10	0
G4-7	20.0	22.8	18.4	25.4	1.58	0	5	0	0	0	0	5	5	0	0	5	10	0	5	5	5
G4-8	18.7	20.4	16.0	22.6	1.58	5	10	0	0	0	0	5	5	0	5	0	0	0	5	10	0
G4-9	18.0	19.5	15.0	22.2	1.23	0	0	0	0	5	5	0	5	0	0	5	5	0	5	0	5
G4-10	18.0	18.9	15.0	21.6	1.40	0	0	5	0	5	0	0	5	0	0	5	5	0	10	0	5
G4-11	21.1	23.7	19.6	26.4	1.40	0	5	0	0	0	0	5	5	0	0	5	5	0	10	0	5
G4-12	20.6	23.0	18.4	25.3	1.58	0	0	5	0	5	0	5	5	0	0	5	5	0	5	5	5
G4-13	19.5	21.3	17.0	23.8	1.05	0	0	0	0	5	0	0	5	0	0	5	5	0	5	0	5
G4-14	17.3	18.7	14.1	21.3	1.05	0	0	0	0	5	0	0	10	0	0	5	5	0	0	0	5
G4-15	14.2	12.7	9.2	15.4	1.75	0	0	5	0	5	0	5	5	0	0	5	10	0	10	5	0
G4-16	13.9	12.5	9.3	15.4	1.75	0	0	5	0	5	0	5	5	0	0	5	10	0	10	5	0
G4-17	21.5	23.3	19.6	25.3	1.75	5	10	0	0	0	0	5	10	0	5	0	0	0	5	10	0
G4-18	20.3	23.1	18.8	25.6	1.58	0	5	5	0	0	0	5	5	0	5	0	5	0	5	10	0
G4-19	16.0	17.2	12.4	19.7	1.23	0	0	0	0	5	5	0	5	0	0	5	5	0	5	0	5
G4-20	20.9	23.6	19.3	26.0	1.05	0	0	0	0	0	0	0	5	0	0	5	5	0	5	5	5
G5-1	20.9	23.0	18.2	25.5	1.75	5	10	0	0	0	0	5	10	0	0	0	5	0	10	5	0
G5-2	18.9	21.4	15.3	23.4	1.23	0	10	0	0	5	0	5	5	0	0	5	0	0	0	5	0
G5-3	19.9	21.4	17.0	24.2	1.58	0	5	0	0	5	0	5	10	0	0	5	5	0	5	5	0
G5-4	18.2	18.4	14.1	20.7	1.23	0	5	0	0	5	0	0	5	0	0	5	5	0	5	0	5
G5-5	20.5	21.4	17.6	24.3	1.93	0	0	5	0	5	0	5	5	0	0	5	10	0	5	10	5
G5-6	19.6	20.4	16.0	22.6	1.93	0	5	5	0	0	0	5	5	0	0	5	10	0	5	10	5

G5-7	20.4	21.5	17.1	23.7	1.75	5	10	0	0	0	0	5	10	0	0	5	5	0	5	5	0
G5-8	18.1	18.6	14.1	21.2	1.23	0	0	0	0	0	0	5	10	0	0	5	0	0	0	10	5
G5-9	20.5	22.2	17.4	24.9	1.75	5	5	5	0	0	0	5	5	0	0	5	0	0	5	10	5
G5-10	20.5	22.6	17.6	25.5	1.40	0	0	0	0	5	0	5	5	0	0	5	5	0	5	10	0
G5-11	21.6	23.1	19.0	25.7	1.23	0	5	0	0	0	0	5	5	0	0	5	5	0	10	0	0
G5-12	5.5	-6.2	0.0	0.1	1.75	5	5	0	0	0	0	5	10	0	5	5	0	0	5	10	0
G5-13	21.0	23.6	18.3	26.1	1.05	0	0	0	0	0	0	0	5	0	0	5	5	0	5	5	5
G5-14	19.8	20.7	16.4	23.2	1.75	5	5	0	0	0	0	5	10	0	0	5	10	0	5	5	0
G5-15	19.8	20.1	16.4	22.9	1.75	5	10	0	0	0	0	5	10	0	5	0	0	0	5	10	0
G5-16	21.5	23.4	18.7	25.8	1.40	0	5	0	0	0	5	0	5	0	5	0	5	0	5	10	0
G5-17	20.5	22.2	17.7	25.1	1.40	0	5	0	0	0	0	5	5	0	0	5	5	0	10	0	5
G5-18	21.0	23.0	18.3	25.2	2.10	0	5	5	0	0	0	5	5	0	0	5	10	0	10	10	5
G5-19	20.4	22.2	17.8	25.0	1.75	5	10	0	0	0	0	5	10	0	5	0	0	0	5	10	0
G5-20	14.5	13.3	9.2	15.9	1.40	0	0	5	0	5	0	0	5	0	0	5	10	0	5	5	0
G6-1	18.6	20.8	16.3	23.3	1.58	0	5	0	0	0	0	5	10	0	0	5	10	0	5	5	0
G6-2	19.0	21.3	16.3	22.8	1.75	5	10	0	0	0	0	5	10	0	5	0	0	0	5	10	0
G6-3	5.8	-2.0	0.5	2.9	1.05	0	0	0	0	5	0	0	5	0	0	5	5	0	0	5	5
G6-4	20.6	23.8	18.8	26.3	1.93	5	5	5	0	5	0	5	5	0	0	5	5	0	5	5	5
G6-5	19.8	23.0	18.2	25.6	1.58	0	5	0	0	0	0	0	5	0	5	5	5	0	5	10	5
G6-6	8.6	5.7	3.5	9.1	1.23	0	5	0	0	5	0	0	10	0	0	5	5	0	0	0	5
G6-7	18.8	21.2	16.5	23.7	1.75	5	10	0	0	0	0	5	5	0	0	5	0	0	5	10	5
G6-8	17.6	19.5	14.9	22.1	1.75	0	10	0	0	0	0	5	5	0	0	5	5	0	5	10	5
G6-9	18.1	19.4	15.1	21.7	1.58	0	5	5	0	5	0	5	5	0	0	5	0	0	5	10	0
G6-10	5.7	-3.0	0.4	2.3	1.23	0	5	0	0	5	0	5	5	0	0	5	0	0	0	5	5
G6-11	4.6	-5.7	0.1	0.4	1.40	5	0	0	0	5	0	0	10	0	5	5	5	0	0	5	0
G6-12	21.4	24.5	20.0	26.5	1.58	0	10	0	0	0	0	5	10	0	0	5	0	0	5	5	5
G6-13	20.8	24.1	18.7	25.9	1.40	0	5	0	0	0	0	5	5	0	0	5	5	0	10	0	5
G6-14	20.2	22.7	18.4	24.8	1.75	5	10	0	0	0	0	5	10	0	5	0	0	0	5	10	0
G6-15	20.6	23.1	18.9	25.5	1.75	5	10	0	0	0	0	5	10	0	5	0	0	0	5	10	0
G6-16	16.4	16.8	12.5	19.3	1.58	0	5	0	0	5	0	5	10	0	0	5	5	0	5	5	0
G6-17	20.8	23.6	19.1	25.5	1.75	5	5	0	0	0	0	5	10	0	5	5	0	0	5	10	0
G6-18	20.6	23.6	19.1	25.7	1.75	5	10	0	0	0	0	5	10	0	5	0	0	0	5	10	0
G6-19	20.3	23.9	19.0	26.2	1.40	0	5	0	0	0	0	5	5	0	0	5	5	0	10	0	5
G6-20	20.2	23.1	18.1	25.0	1.75	5	5	0	0	0	0	5	10	0	0	5	10	0	5	5	0
G7-1	20.7	23.3	18.6	26.3	1.40	5	5	0	0	0	0	0	5	0	0	5	5	0	10	0	5
G7-2	18.9	20.7	15.8	23.0	1.75	5	10	0	0	0	0	5	10	0	0	0	10	0	5	5	0
G7-3	21.1	22.7	18.7	25.4	1.58	0	10	0	0	0	0	5	10	0	5	5	0	0	5	5	0
G7-4	5.2	-6.8	0.0	0.1	1.58	5	5	0	0	5	0	5	10	0	0	5	5	0	0	0	5
G7-5	18.8	19.2	15.3	22.2	1.75	5	5	0	0	0	0	5	10	0	5	5	0	0	5	10	0
G7-6	10.9	7.7	5.1	11.1	1.58	5	5	0	0	0	0	0	5	0	5	5	10	0	5	5	0
G7-7	20.8	22.5	18.6	25.6	1.75	5	5	0	0	0	0	5	10	0	0	5	5	0	5	5	5
G7-8	19.2	20.6	16.4	23.4	1.58	0	10	0	0	5	0	5	5	0	0	5	0	0	5	10	0
G7-9	15.3	15.2	10.9	18.2	1.75	0	10	0	0	5	0	5	10	0	0	5	5	0	0	5	5
G7-10	20.1	22.3	17.9	25.5	1.58	0	10	0	0	0	0	5	5	0	0	5	0	0	10	5	5
G7-11	21.5	23.7	19.5	26.5	1.58	0	10	0	0	0	0	5	10	0	0	0	0	0	5	10	5
G7-12	4.8	-6.8	0.0	0.1	1.40	5	0	0	0	0	0	5	10	0	0	5	5	0	0	5	5

G7-13	20.5	23.0	18.4	26.1	1.40	0	5	0	0	0	0	5	5	0	0	5	5	0	10	0	5
G7-14	21.1	22.7	18.7	25.4	1.75	5	10	0	0	0	0	5	10	0	5	0	0	0	5	10	0
G7-15	20.1	21.5	17.4	24.4	1.58	0	5	0	0	5	0	5	10	0	0	5	5	0	5	5	0
G7-16	21.1	22.6	18.5	25.3	1.75	5	10	0	0	0	0	5	10	0	5	0	0	0	5	10	0
G7-17	22.0	24.0	20.1	26.5	1.58	0	10	0	0	0	0	5	10	0	0	5	0	0	5	5	5
G7-18	21.5	23.4	19.1	25.9	1.58	0	10	0	0	0	0	5	10	0	0	5	0	0	5	5	5
G7-19	21.1	23.1	19.1	25.8	1.75	5	10	0	0	0	0	5	10	0	5	0	0	0	5	10	0
G7-20	20.6	23.1	18.3	26.0	1.40	0	5	0	0	0	0	5	5	0	0	5	5	0	10	0	5
G8-1	19.7	21.3	17.1	23.9	1.75	5	10	0	0	0	0	5	10	0	0	0	5	0	5	10	0
G8-2	18.0	19.8	14.7	21.7	1.75	5	10	0	0	0	0	5	10	0	0	0	5	0	5	10	0
G8-3	19.0	19.6	15.8	22.0	1.40	0	5	0	0	0	0	5	10	0	0	5	0	0	10	5	0
G8-4	20.1	21.1	17.4	23.7	1.58	0	15	0	0	0	0	5	10	0	0	0	0	0	5	10	0
G8-5	20.3	22.5	18.2	25.6	1.75	0	10	0	0	0	0	5	10	0	5	0	0	0	5	10	5
G8-6	18.0	20.0	15.4	23.0	1.40	0	10	0	0	0	0	5	5	0	0	5	0	0	5	5	5
G8-7	17.0	17.8	14.0	20.8	1.58	0	10	0	0	5	0	5	5	0	0	5	0	0	10	5	0
G8-8	19.1	21.0	16.8	24.1	1.75	0	10	0	0	0	0	5	10	0	5	5	0	0	5	5	5
G8-9	17.7	19.2	14.7	22.3	1.58	0	10	0	0	5	0	5	5	0	5	0	0	0	5	10	0
G8-10	19.2	20.0	16.2	22.5	1.58	5	10	0	0	0	0	5	10	0	0	5	0	0	5	5	0
G8-11	19.5	21.2	17.0	23.9	1.75	5	10	0	0	0	0	5	10	0	0	0	10	0	5	5	0
G8-12	4.5	-7.0	0.0	0.1	1.05	0	0	0	0	0	0	5	10	0	0	5	5	0	0	0	5
G8-13	20.2	22.3	18.1	25.3	1.58	0	10	0	0	0	0	5	10	0	0	5	0	0	5	5	5
G8-14	18.9	20.5	16.6	23.5	1.75	5	5	0	0	0	0	5	10	0	5	5	0	0	5	10	0
G8-15	19.6	20.8	17.0	24.0	1.58	0	10	0	0	0	0	5	10	0	0	0	0	0	5	10	5
G8-16	19.7	21.9	17.5	25.0	1.40	0	5	0	0	0	0	5	5	0	0	5	5	0	10	0	5
G8-17	19.8	22.1	17.4	25.0	1.40	5	5	0	0	0	0	0	5	0	0	5	5	0	10	0	5
G8-18	21.3	23.0	19.1	25.2	1.58	0	10	0	0	0	0	5	10	0	0	5	0	0	5	5	5
G8-19	21.9	22.9	19.9	25.2	1.58	0	5	0	0	5	0	5	10	0	0	5	5	0	5	5	0
G8-20	18.3	20.0	15.9	22.7	1.58	0	10	0	0	5	0	5	5	0	0	5	0	0	5	10	0
R1	43.4	26.8	35.7	18.2	3.50	0	0	0	0	0	0	0	100	0	0	0	0	0	0	0	0
R2	38.8	25.7	32.4	16.7	2.63	0	0	0	0	0	0	0	75.0	0	0	0	0	0	0	0	0
R3	37.1	25.7	32.3	18.3	1.75	0	0	0	0	0	0	0	50.0	0	0	0	0	0	0	0	0
R4	31.3	24.2	28.8	19.7	0.88	0	0	0	0	0	0	0	25.0	0	0	0	0	0	0	0	0
R5	41.6	26.7	34.1	21.3	3.50	0	0	0	0	0	0	50.0	50.0	0	0	0	0	0	0	0	0
R6	38.4	26.9	32.2	20.4	2.63	0	0	0	0	0	0	37.5	37.5	0	0	0	0	0	0	0	0
R7	34.8	25.5	30.6	19.8	1.75	0	0	0	0	0	0	25.0	25.0	0	0	0	0	0	0	0	0
R8	5.4	-5.3	0.0	0.0	0.88	0	0	0	0	0	0	12.5	12.5	0	0	0	0	0	0	0	0
R9	n.d.[b]	n.d.	n.d.	n.d.	3.50	0	0	0	0	0	50.0	50.0	0	0	0	0	0	0	0	0	0
R10	25.2	23.1	24.5	22.6	2.63	0	0	0	0	0	22.8	0	52.2	0	0	0	0	0	0	0	0
R11	5.4	-3.9	0.1	0.7	1.75	0	0	0	0	0	15.2	0	34.8	0	0	0	0	0	0	0	0
R12	23.0	23.9	22.2	24.0	0.88	0	0	0	0	0	7.6	0	17.4	0	0	0	0	0	0	0	0
R13	36.6	28.5	31.7	31.6	3.50	0	0	0	0	0	0	20.0	46.7	0	0	0	0	0	0	33.3	0
R14	32.5	26.4	29.1	21.2	2.63	0	0	0	0	0	0	15.0	35.0	0	0	0	0	0	0	25.0	0
R15	25.6	24.5	24.6	22.8	1.75	0	0	0	0	0	0	10.0	23.4	0	0	0	0	0	0	16.7	0
R16	5.4	-5.2	0.0	0.1	0.88	0	0	0	0	0	0	5.0	11.7	0	0	0	0	0	0	8.3	0

[a]G*x*-*y* refers to the y^{th} best catalyst in the x^{th} generation and R*x* refers to the x^{th} reference catalyst. [b]The performance of Ref. 9 (3.5 mmol/g-support, Fe_{50}-Ni_{50}/γ-Al_2O_3) could not be evaluated due to the catalyst clogging.

Table 3.3. 10 best performing catalysts at 500 ºC.

						Catalyst composition (%)														
Cat. code[a]	CH_4 conv.	CO_2 conv.	H_2 yield	CO yield	Total loading (mmol/g-support)	Mg	Al	Ca	V	Mn	Fe	Co	Ni	Cu	Zn	Sr	Zr	Mo	Pd	La	Ce
G2-11	20.7	24.4	20.3	26.8	1.58	0	0	5	0	0	0	0	5	0	0	5	10	0	5	10	5
G7-17	22.0	24.0	20.1	26.5	1.58	0	10	0	0	0	0	5	10	0	0	5	0	0	5	5	5
G2-16	20.7	23.8	20.0	26.5	1.05	0	0	0	0	5	0	0	10	0	0	5	5	0	0	0	5
G6-12	21.4	24.5	20.0	26.5	1.58	0	10	0	0	0	0	5	10	0	0	5	0	0	5	5	5
G8-19	21.9	22.9	19.9	25.2	1.58	0	5	0	0	5	0	5	10	0	0	5	5	0	5	5	0
G2-5	19.9	23.9	19.6	26.2	1.75	5	10	0	0	0	0	5	10	0	5	0	0	0	5	10	0
G4-11	21.1	23.7	19.6	26.4	1.40	0	5	0	0	0	0	5	5	0	0	5	5	0	10	0	5
G4-17	21.5	23.3	19.6	25.3	1.75	5	10	0	0	0	0	5	10	0	5	0	0	0	5	10	0
G1-1	20.2	23.8	19.5	26.4	2.10	0	5	5	0	0	0	5	5	0	0	5	10	0	10	10	5
G7-11	21.5	23.7	19.5	26.5	1.58	0	10	0	0	0	0	5	10	0	0	0	0	0	5	10	5

[a]G*x*-*y* refers to the y^{th} best catalyst in the x^{th} generation.

3.3.5. Selection of elements

The evolution process changes catalysts in a way to increase the performance, where elements that have a positive effect on the performance will be selected more, and vice versa. Figure 3.7 shows how element selection change over the course of evolution. G0, 1 are composed of the top 20 catalyst from 0^{th} and 1^{st} catalysts evaluated under the previous experimental conditions. The elements selected by evolution were Ni, Al > La > Pd > Co, and the eliminated elements were Ca, V, Fe, Cu, and Mo. Ni and Pd have been reported as highly active elements on their own. La plays a role in promoting CO_2 adsorption, and Co is a typical element that inhibits carbon deposition. Al may play a role in linking the support (γ-Al_2O_3) and the active elements, since this element is also contained in the support.

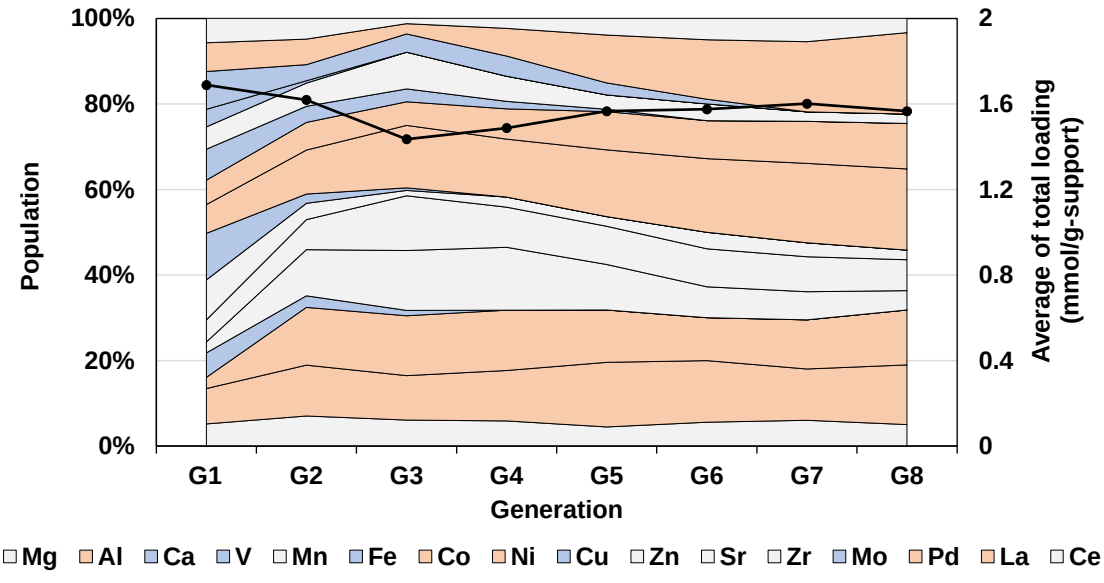

Figure 3.7. Percent stacked area chart for the selection of elements along with the generation.

3.3.6. Principal component analysis

The relationship between catalytic performance and each element was visualized by principal component analysis (Figure 3.8). The closer the direction between the arrows, the stronger the correlation between items, and the longer the arrows, the greater the variability of the data. From Figure 3.8, high CH_4 conversion and CO_2 conversion are necessary to obtain high H_2 yield. The weak correlation between loading amount suggests that selecting synergistic combinations is more important than increasing loading amount in the design of high performance catalysts.

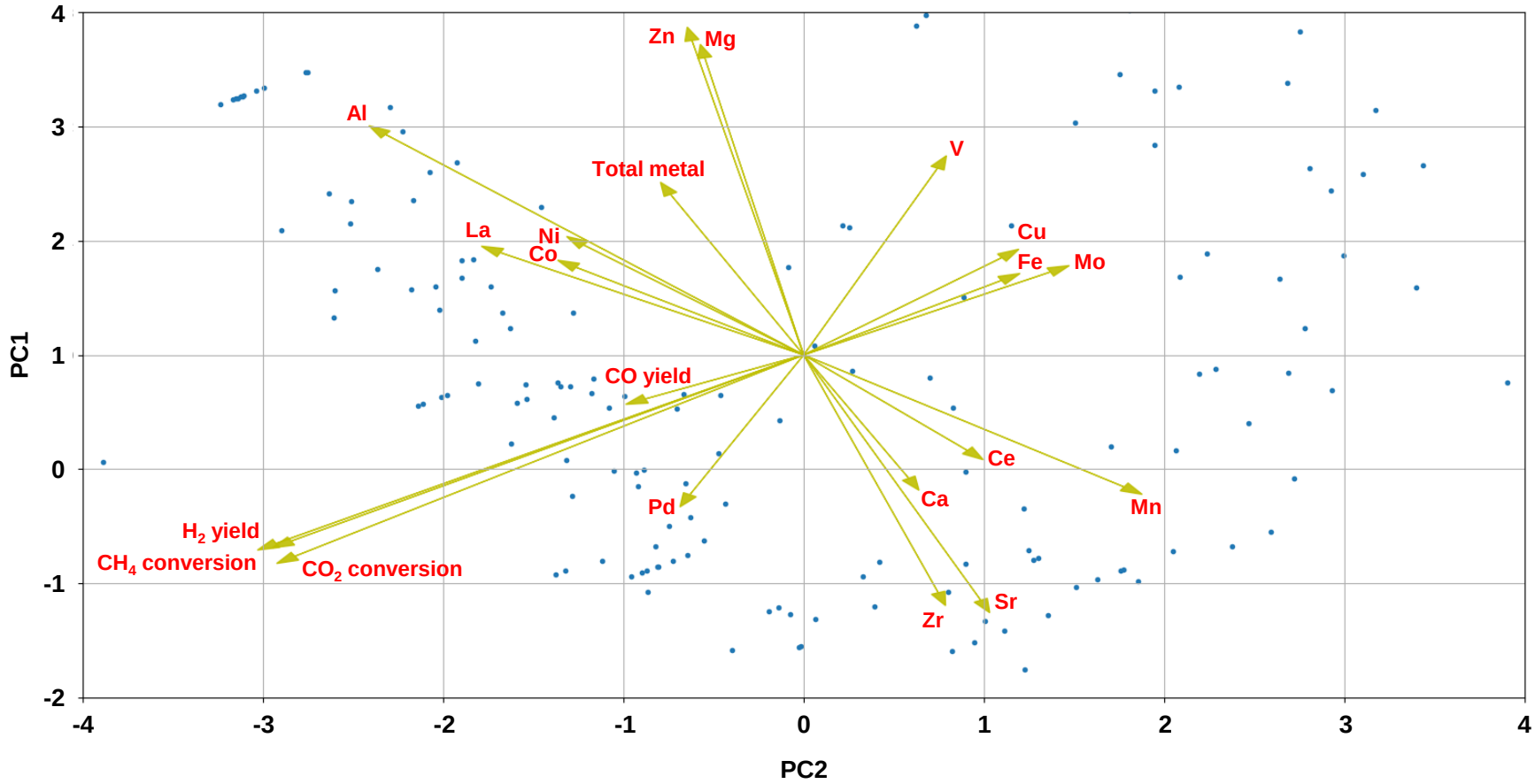

Figure 3.8. Visualize the correlation between elements and catalytic performance in 160 catalysts by principal component analysis.

3.3.7. Decision tree analysis

Decision tree classification was used to visualize catalyst design guidelines. 260 catalysts were classified as ≥15% H_2 yield and others. The percentage of element content was used as the features, and based on the Gini index, each leaf was divided until it was completely pure. For visible clarity, the obtained tree was pruned with a restriction of more than 10 samples to each split (Figure 3.9). The entire tree without pruning is shown in Figure 3.10. In Figure 3.9, of the 101 catalysts with H_2 yields greater than 15%, 59% contained no Mo, Fe, Mn, or Ca and contained Pd. Of these, 57% contained Al.

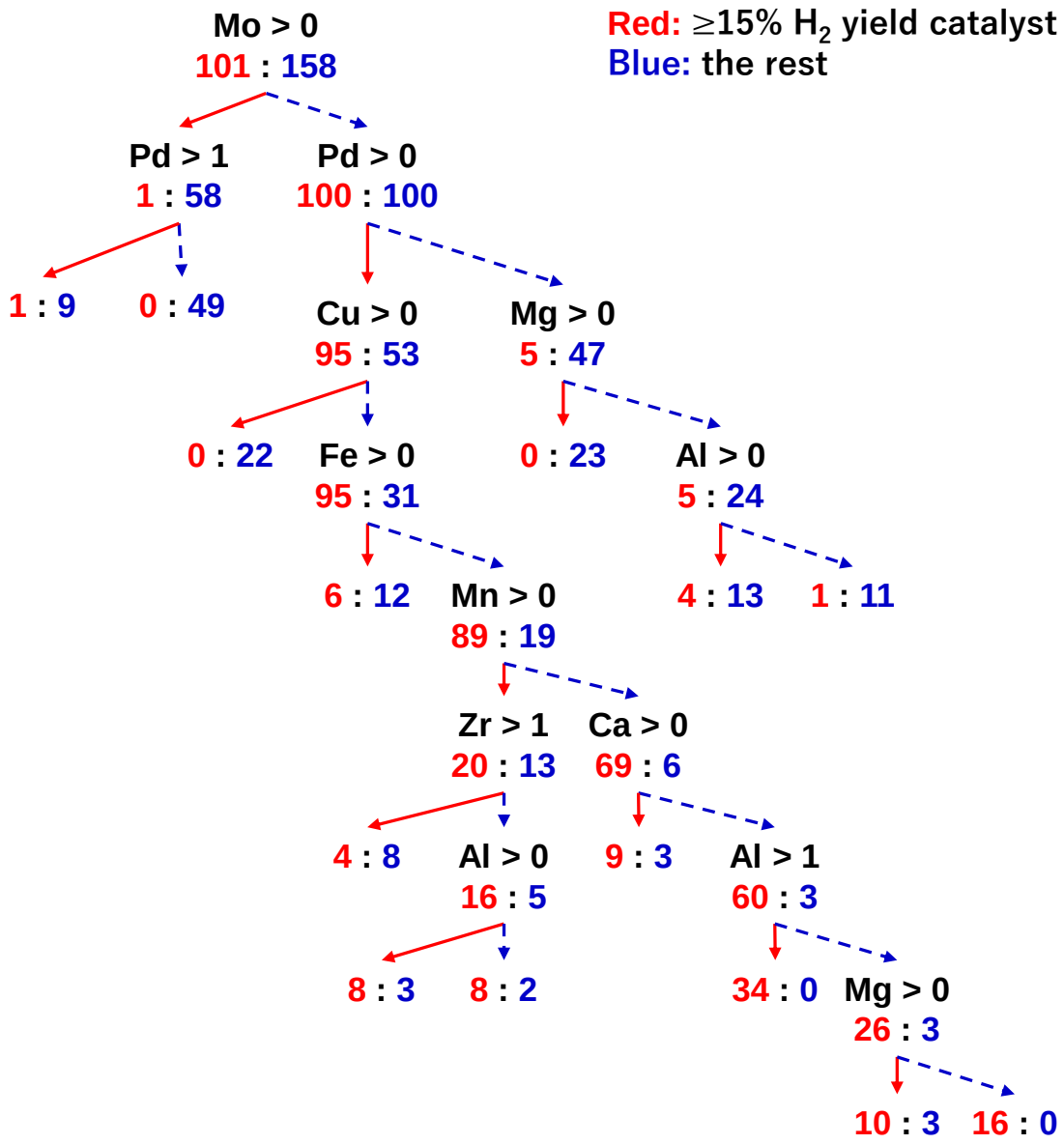

Figure 3.9. Catalyst design guideline visualized by decision tree classification. 260 catalysts are classified into the H_2 yield ≥15% (red) or other (blue) using the percentage of elements in the catalyst. The numbers in each split and leaf correspond to the numbers of catalysts for the two classes.

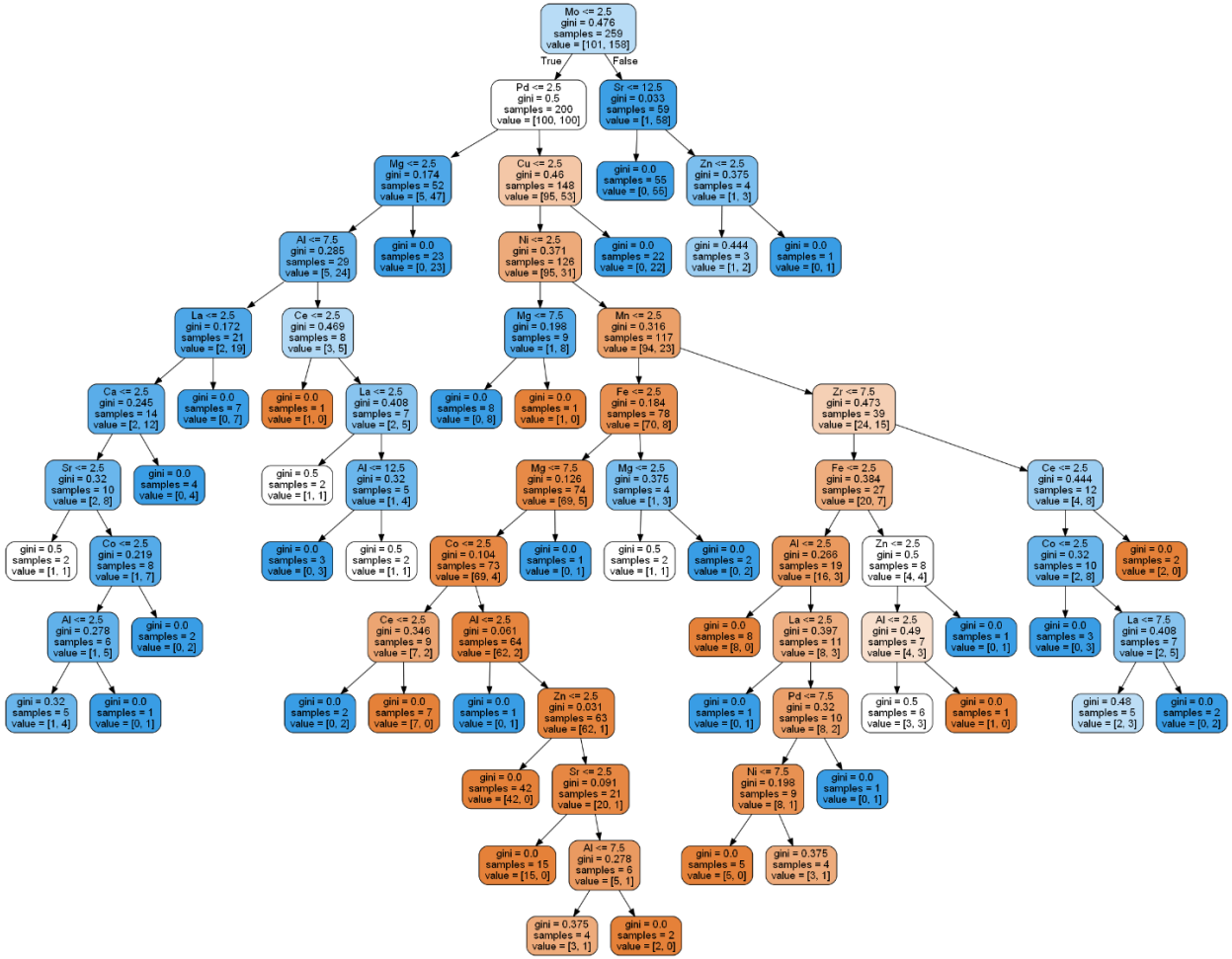

Figure 3.10. Entire decision tree. The 260 catalysts are classified into the H_2 yield ≥15% (red) or other (blue) using the percentage of elements in the catalyst.

3.3.8. Synergism and catalytic performance

In order to evaluate the interaction between elements, I introduced a synergy value as defined in Equation (3.7),

$$\text{Synergy}\ (\alpha, \beta) = \text{H}_2\ \text{yield}_{\alpha\cap\beta}/\text{H}_2\ \text{yield}_{\alpha\Delta\beta} \quad (3.7).$$

This is the ratio of the performance averaged across catalysts containing both elements α and β (α∩β) to the performance of the combination containing either α or β (αΔβ). If this value is greater than 1, the combination is considered synergistic, and vice versa. Figure 3.11 confirms that the synergistic effect and catalytic performance showed a quadratic increase. This suggests that catalyst performance may be determined by the synergistic combination of highly active elements.

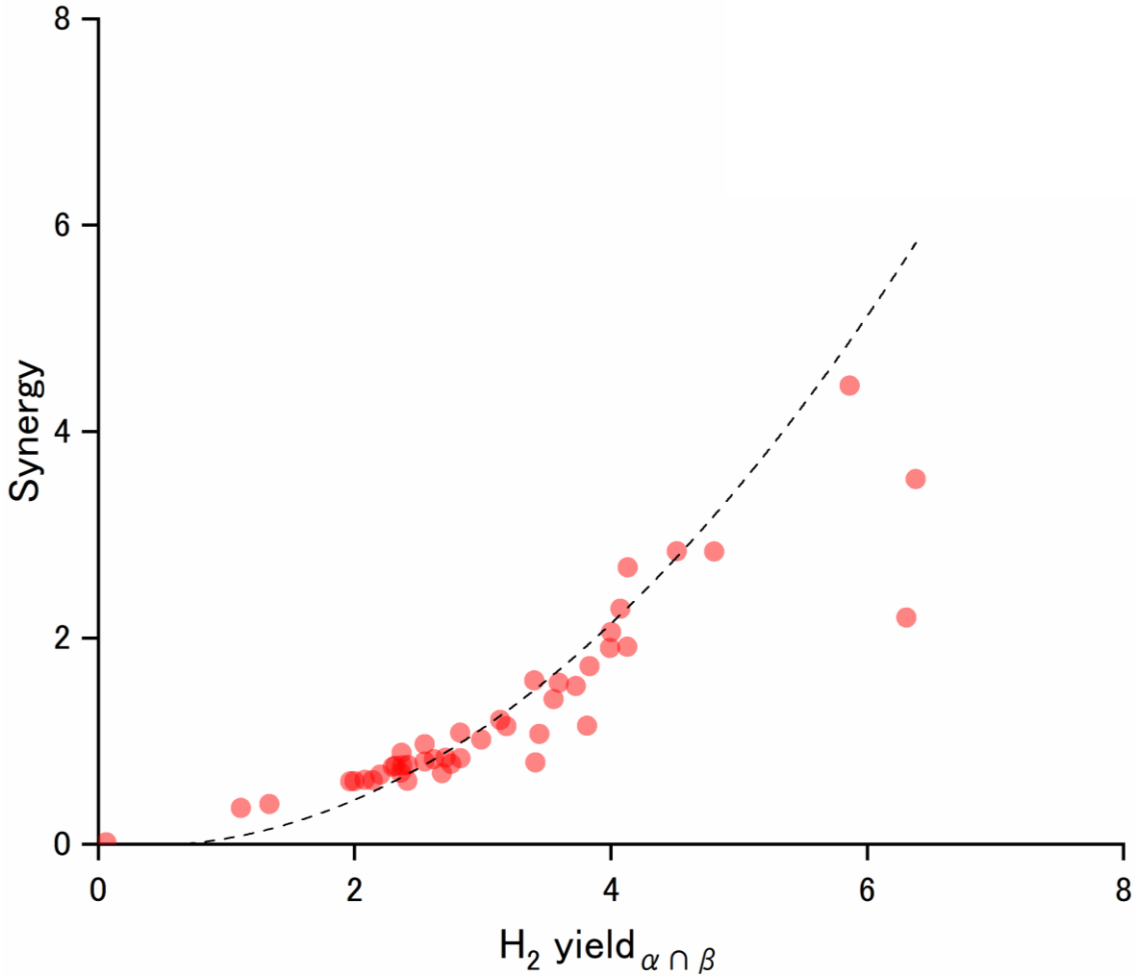

Figure 3.11. Impact of synergistic combinations on the performance of catalysts at 500 ºC. The synergy is evaluated based on Equation (3.7). It compares the average H_2 yield of catalysts between when both of element α and β are contained and when either of α and β is contained. H_2 $yield_{\alpha\cap\beta}$ corresponds to the former case, i.e., the average H_2 yield of catalysts having both of α and β.

3.3.9. Synergistic and antagonistic combinations

Table 3.4 shows the most synergistic and antagonistic combination. In the synergy

side, elements that frequently appeared are Ni > Pd, Sr > Co, Zr > Ca in this order. Focusing on the types of combinations, it can be seen that they consist of a single highly active element (Ni, Pd), a combination that inhibits coking (Co), a combination that promotes dispersion (Zr, Sr), and a combination that promotes CO_2 adsorption (Ca). This suggests that the combination of highly active elements, or elements that can assist them, work synergistically to improve catalytic performance. In the antagonist side, elements that frequently appeared are V >> Mn, Cu, Zn in this order.

Table 3.4. Synergistic and antagonistic combinations of elements[a]

Ranking	Synergistic combination				Antagonistic combination			
	α	β	Synergy	$\langle 1/\mathrm{Abs} \rangle_{\alpha \cap \beta}$	α	β	Synergy	$\langle 1/\mathrm{Abs} \rangle_{\alpha \cap \beta}$
1	Ni	Pd	13.28	5.91	V	Ni	0.02	0.06
2	Sr	Pd	4.44	5.86	V	Pd	0.02	0.07
3	Zr	Pd	3.54	6.38	V	Sr	0.02	0.06
4	Ni	Sr	2.84	4.52	V	Co	0.02	0.06
5	Co	Pd	2.84	4.81	V	Zr	0.02	0.07
6	Sr	Zr	2.68	4.13	V	Ce	0.03	0.06
7	Ni	Zr	2.28	4.08	Al	V	0.03	0.06
8	Ca	Pd	2.20	6.31	V	La	0.03	0.07
9	Co	Ni	2.06	4.00	Ca	V	0.04	0.07
10	Ca	Co	1.91	4.13	V	Mn	0.04	0.06
11	Al	La	1.43	4.03	V	Zn	0.05	0.06
12	Mg	Zn	1.43	2.52	V	Fe	0.05	0.06
13	Ca	Sr	1.43	4.49	V	Cu	0.05	0.06
14	Co	Ni	1.40	5.09	V	Mo	0.05	0.06
15	Ni	La	1.37	4.84	Mg	V	0.05	0.07
16	Al	Co	1.36	4.15	Zn	Sr	0.20	0.72
17	Ca	Pd	1.35	4.86	Mn	Zn	0.30	0.68
18	Ca	Co	1.35	3.96	Mn	Fe	0.31	0.75
19	Mn	Ce	1.34	3.73	Cu	Ce	0.32	0.99
20	Sr	Ce	1.34	4.45	Cu	La	0.33	1.04

[a]An impact of combining two elements, α and β, is evaluated based on Equation (3.7). The larger the synergy value, the more synergistic the combination, and vice versa. H_2 $\mathrm{yield}_{\alpha \cap \beta}$ indicates the average H_2 yield for catalysts which contain both of the elements (α and β).

2.3.8. Visualization by force-directed graph

In order to derive heuristics on the design of more complex catalysts, binary interactions between elements were visualized using a force-directed graph (Figure 3.12). Figure 3.12 shows a graph where node represents an element and edge reflects the synergy value of the corresponding element combination. The higher the synergy value, the more the corresponding nodes attract each other. Figure 3.12 shows that there are clusters of elements in close proximity to each other (Ca, Co, Ni, Sr, Zr, Pd). The fact that a cluster is formed indicates that the elements belonging to the cluster are synergistic with each other. The 10 best performing catalysts in Table 3.3 commonly include these elements, leading to the hypothesis that catalysts with more synergistic combinations will perform better. This trend was also observed in the design of stabilizer formulations in the photo-degradation of polystyrene discussed in chapter 2. Other elements are located far from clusters, some in isolation (Mg, V, Fe, Cu, Zn, Mo). Among these elements, V, Fe, Cu, and Mo correspond were eliminated during evolution (Figure 3.7), and the reason for elimination is that they are antagonistic to the others.

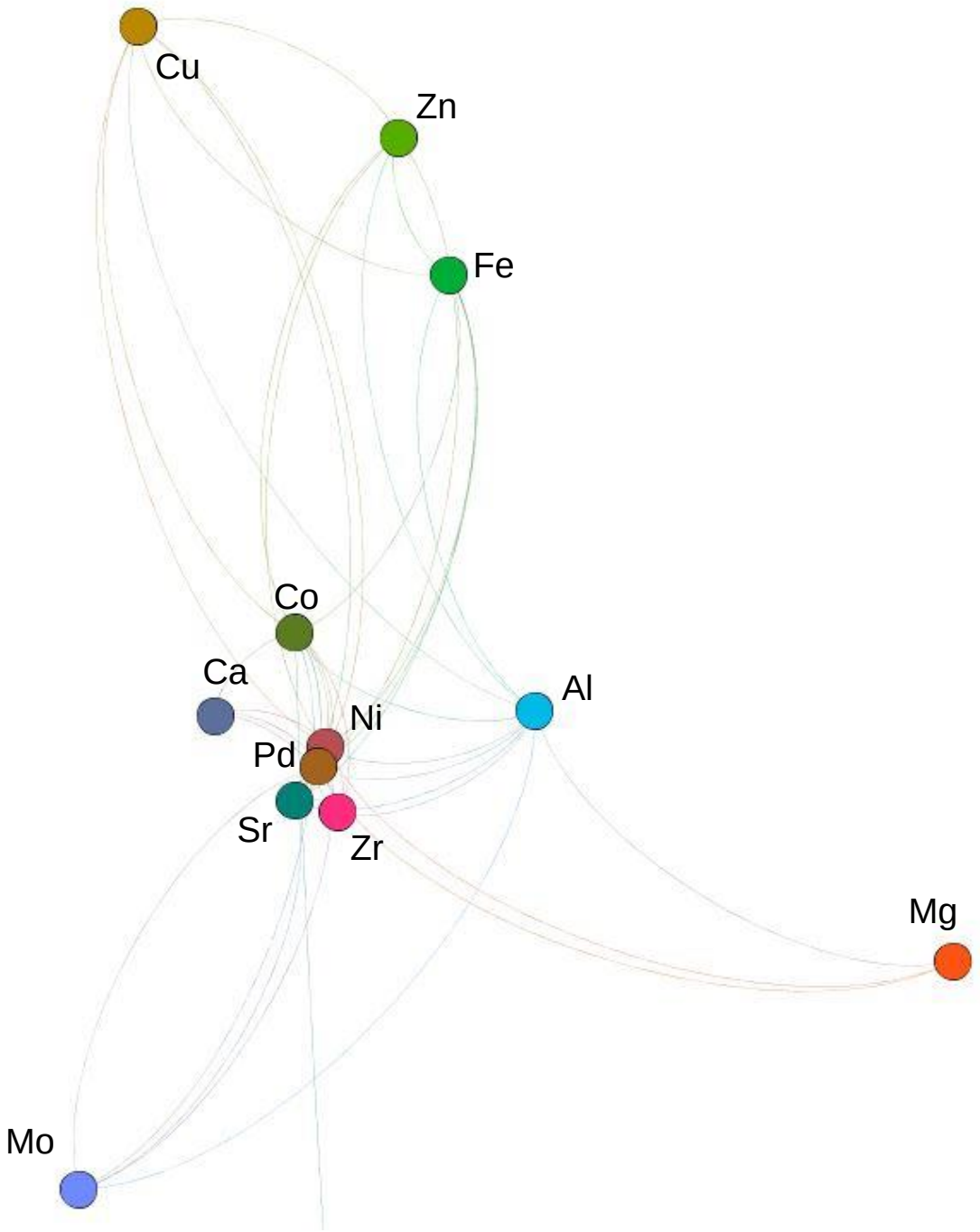

Figure 3.12. Visualization of binary interactions based on a force-directed graph. The nodes represent each element. An edge reflects the synergy value between the correspondent elements, where the closer the nodes are, the more synergistic the elements are. V showed a strong antagonistic effect, and drifted far away from the other elements.

3.4. Conclusions

In this chapter, a multidimensional exploration for DRM catalysts was performed combining the HTE instrument and GA, which can evaluate the performance of 20 catalysts at once. Catalyst clogging during the process of catalyst evolution made it difficult to evaluate 20 catalysts at once. To address this problem, experimental conditions were changed to a reaction temperature (500 ºC), total flow rate (Q = 20 mL/channel), and CH_4/CO_2 ratio (1.00), and the catalyst was evaluated for 20000 sec. The catalytic performance was defined as the H_2 yield averaged over 15000-20000 sec, where the performance is stable, and the catalyst exploration is continued. In addition, the obtained data set was analyzed to derive guidelines for catalyst design. Major findings are as follows.

- Most high-performance catalysts obtained through evolution are composed of elements that are highly active on their own and elements that assist those elements.
- The combination of highly active elements or elements that can assist them work synergistically to improve catalytic performance.
- To design a high-performance catalyst, it is important to use highly active elements and elements that can assist them as the main components.

Reference

[1] Palermo, A.; Holgado Vazquez, J. P.; Lambert, R. M. New Efficient Catalysts for the Oxidative Coupling of Methane. *Catal. Letters* **2000**, *68* (3–4), 191–196.

[2] Kobayashi, T.; Yamada, T.; Kayano, K. Effect of Basic Metal Additives on NOx Reduction Property of Pd-Based Three-Way Catalyst. *Appl. Catal. B Environ.* **2001**, *30* (3–4), 287–292.

[3] Carvalho, L. S.; Pieck, C. L.; Rangel, M. C.; Fígoli, N. S.; Grau, J. M.; Reyes, P.; Parera, J. M. Trimetallic Naphtha Reforming Catalysts. I. Properties of the Metal Function and Influence of the Order of Addition of the Metal Precursors on Pt-Re-Sn/γ-Al2O3-Cl. *Appl. Catal. A Gen.* **2004**, *269* (1–2), 91–103.

[4] Takahashi, K.; Takahashi, L.; Le, S. D.; Kinoshita, T.; Nishimura, S.; Ohyama, J. Synthesis of Heterogeneous Catalysts in Catalyst Informatics to Bridge Experiment and High-Throughput Calculation. *J. Am. Chem. Soc.* **2022**, *144* (34), 15735–15744.

[5] Wang, M.; Zhu, H. Machine Learning for Transition-Metal-Based Hydrogen Generation Electrocatalysts. *ACS Catal.* **2021**, *11* (7), 3930–3937.

[6] Troshin, K.; Hartwig, J. F. Snap Deconvolution: An Informatics Approach to High-Throughput Discovery of Catalytic Reactions. *Science (80).* **2017**, *357* (6347), 175–181.

[7] Aratani, N.; Katada, I.; Nakayama, K.; Terano, M.; Taniike, T. Development of

High-Throughput Chemiluminescence Imaging Instrument for Parallel Evaluation of Polymer Lifetime. *Polym. Degrad. Stab.* **2015**, *121*, 340–347.

[8] Chammingkwan, P.; Terano, M.; Taniike, T. High-Throughput Synthesis of Support Materials for Olefin Polymerization Catalyst. *ACS Comb. Sci.* **2017**, *19* (5), 331–342.

[9] Dao, A. T. N.; Shimokata, J.; Takeuchi, K.; Nakayama, K.; Taniike, T. Stabilization of Recombinant Spider Silk in Thermo-Oxidative Degradation: High-Throughput Screening for Antioxidants. *Polym. Degrad. Stab.* **2018**, *153*, 37–46.

[10] Nguyen, T. N.; Nhat, T. T. P.; Takimoto, K.; Thakur, A.; Nishimura, S.; Ohyama, J.; Miyazato, I.; Takahashi, L.; Fujima, J.; Takahashi, K.; Taniike, T. High-Throughput Experimentation and Catalyst Informatics for Oxidative Coupling of Methane. *ACS Catal.* **2020**, *10* (2), 921–932.

[11] Nakanowatari, S.; Nguyen, T. N.; Chikuma, H.; Fujiwara, A.; Seenivasan, K.; Thakur, A.; Takahashi, L.; Takahashi, K.; Taniike, T. Extraction of Catalyst Design Heuristics from Random Catalyst Dataset and Their Utilization in Catalyst Development for Oxidative Coupling of Methane. *ChemCatChem* **2021**, *13* (14), 3262–3269. https://doi.org/10.1002/cctc.202100460.

[12] Nguyen, T. N.; Seenivasan, K.; Nakanowatari, S.; Mohan, P.; Tran, T. P. N.; Nishimura, S.; Takahashi, K.; Taniike, T. Factors to Influence Low-Temperature Performance of Supported Mn–Na2WO4 in Oxidative Coupling of Methane. *Mol. Catal.* **2021**, *516* (November), 111976.

[13] Taniike, T.; Kitamura, T.; Nakayama, K.; Takimoto, K.; Aratani, N.; Wada, T.; Thakur, A.; Chammingkwan, P. Stabilizer Formulation Based on High-Throughput Chemiluminescence Imaging and Machine Learning. *ACS Appl. Polym. Mater.* **2020**, *2* (8), 3319–3326.

[14] Takimoto, K.; Takeuchi, K.; Ton, N. N. T.; Taniike, T. Exploring Stabilizer Formulations for Light-Induced Yellowing of Polystyrene by High-Throughput Experimentation and Machine Learning. *Polym. Degrad. Stab.* **2022**, *201*, 109967.

[15] Palmer, C.; Upham, D. C.; Smart, S.; Gordon, M. J.; Metiu, H.; McFarland, E. W. Dry Reforming of Methane Catalysed by Molten Metal Alloys. *Nat. Catal.* **2020**, *3* (1), 83–89.

[16] Jang, W. J.; Shim, J. O.; Kim, H. M.; Yoo, S. Y.; Roh, H. S. A Review on Dry Reforming of Methane in Aspect of Catalytic Properties. *Catal. Today* **2019**, *324* (July 2018), 15–26.

[17] Lavoie, J. M. Review on Dry Reforming of Methane, a Potentially More Environmentally-Friendly Approach to the Increasing Natural Gas Exploitation. *Front. Chem.* **2014**, *2* (NOV), 1–17.

[18] Singh, R.; Dhir, A.; Mohapatra, S. K.; Mahla, S. K. Dry Reforming of Methane Using Various Catalysts in the Process: Review. *Biomass Convers. Biorefinery* **2020**, *10* (2), 567–587.

[19] Arora, S.; Prasad, R. An Overview on Dry Reforming of Methane: Strategies to

Reduce Carbonaceous Deactivation of Catalysts. *RSC Adv.* **2016**, *6* (110), 108668–108688.

[20] Oki, M.; Ahmad, Galadima. A Review on Coke Management During Dry Reforming of Methane. *J. Energy Res.* **2015**; 39, 1196–1216

[21] Bradford, M. C. J.; Vannice, M. A. Catalytic Reforming of Methane with Carbon Dioxide over Nickel Catalysts I. Catalyst Characterization and Activity. *Appl. Catal. A Gen.* **1996**, *142* (1), 73–96.

[22] Cheng, D. guo; Zhu, X.; Ben, Y.; He, F.; Cui, L.; Liu, C. jun. Carbon Dioxide Reforming of Methane over Ni/Al2O3 Treated with Glow Discharge Plasma. *Catal. Today* **2006**, *115* (1–4), 205–210.

[23] Dębek, R.; Zubek, K.; Motak, M.; Galvez, M. E.; Da Costa, P.; Grzybek, T. Ni-Al Hydrotalcite-like Material as the Catalyst Precursors for the Dry Reforming of Methane at Low Temperature. *Comptes Rendus Chim.* **2015**, *18* (11), 1205–1210.

[24] Abdullah, B.; Abd Ghani, N. A.; Vo, D. V. N. Recent Advances in Dry Reforming of Methane over Ni-Based Catalysts. *J. Clean. Prod.* **2017**, *162*, 170–185.

[25] Sharifianjazi, F.; Esmaeilkhanian, A.; Bazli, L.; Eskandarinezhad, S.; Khaksar, S.; Shafiee, P.; Yusuf, M.; Abdullah, B.; Salahshour, P.; Sadeghi, F. A Review on Recent Advances in Dry Reforming of Methane over Ni- and Co-Based Nanocatalysts. *Int. J. Hydrogen Energy* **2021**, (Article in press).

[26] Ballarini, A.; Basile, F.; Benito, P.; Bersani, I.; Fornasari, G.; De Miguel, S.; Maina, S. C. P.; Vilella, J.; Vaccari, A.; Scelza, O. A. Platinum Supported on

Alkaline and Alkaline Earth Metal-Doped Alumina as Catalysts for Dry Reforming and Partial Oxidation of Methane. *Appl. Catal. A Gen.* **2012**, *433–434*, 1–11.

[27] Inui, T.; Saigo, K.; Fujii, Y.; Fujioka, K. Catalytic Combustion of Natural Gas as the Role of On-Site Heat Supply in Rapid Catalytic CO2H2O Reforming of Methane. *Catal. Today* **1995**, *26* (3–4), 295–302.

[28] A. Álvarez, M.; Bobadilla, L. F.; Garcilaso, V.; Centeno, M. A.; Odriozola, J. A. CO2 Reforming of Methane over Ni-Ru Supported Catalysts: On the Nature of Active Sites by Operando DRIFTS Study. *J. CO2 Util.* **2018**, *24* (November 2017), 509–515.

[29] Rostrup-Nielsen, J. R.; Bak Hansen, J. H. CO2-Reforming of Methane over Transition Metals. *Journal of Catalysis*. 1993, pp 38–49.

[30] Claridge, J. B.; Green, M. L. H.; Tsang, S. C.; York, A. P. E.; Ashcroft, A. T.; Battle, P. D. A Study of Carbon Deposition on Catalysts during the Partial Oxidation of Methane to Synthesis Gas. *Catal. Letters* **1993**, *22* (4), 299–305.

[31] Torrez-Herrera, J. J.; Korili, S. A.; Gil, A. Recent Progress in the Application of Ni-Based Catalysts for the Dry Reforming of Methane. *Catal. Rev. - Sci. Eng.* **2021**, *00* (00), 1–58.

[32] Jang, W. J.; Jeong, D. W.; Shim, J. O.; Kim, H. M.; Han, W. B.; Bae, J. W.; Roh, H. S. Metal Oxide (MgO, CaO, and La2O3) Promoted Ni-Ce0.8Zr0.2O2 Catalysts for H2 and CO Production from Two Major Greenhouse Gases. *Renew. Energy* **2015**, *79* (1), 91–95.

[33] Jang, W. J.; Jeong, D. W.; Shim, J. O.; Roh, H. S.; Son, I. H.; Lee, S. J. H2 and CO Production over a Stable Ni-MgO-Ce 0.8Zr0.2O2 Catalyst from CO2 Reforming of CH4. *Int. J. Hydrogen Energy* **2013**, *38* (11), 4508–4512.

[34] Xu, G.; Shi, K.; Gao, Y.; Xu, H.; Wei, Y. Studies of Reforming Natural Gas with Carbon Dioxide to Produce Synthesis Gas. X. The Role of CeO2 and MgO Promoters. *J. Mol. Catal. A Chem.* **1999**, *147* (1–2), 47–54.

[35] Song, J. H.; Han, S. J.; Song, I. K. Hydrogen Production by Steam Reforming of Ethanol Over Mesoporous Ni–Al2O3–ZrO2 Catalysts. *Catal. Surv. from Asia* **2017**, *21* (3), 114–129.

[36] Marinho, A. L. A.; Toniolo, F. S.; Noronha, F. B.; Epron, F.; Duprez, D.; Bion, N. Highly Active and Stable Ni Dispersed on Mesoporous CeO2-Al2O3 Catalysts for Production of Syngas by Dry Reforming of Methane. *Appl. Catal. B Environ.* **2021**, *281* (May 2020), 119459.

[37] Adesina, A. A. The Role of CO2 in Hydrocarbon Reforming Catalysis: Friend or Foe? *Curr. Opin. Chem. Eng.* **2012**, *1* (3), 272–280.

[38] Akiki, E.; Akiki, D.; Italiano, C.; Vita, A.; Abbas-Ghaleb, R.; Chlala, D.; Drago Ferrante, G.; Laganà, M.; Pino, L.; Specchia, S. Production of Hydrogen by Methane Dry Reforming: A Study on the Effect of Cerium and Lanthanum on Ni/MgAl2O4 Catalyst Performance. *Int. J. Hydrogen Energy* **2020**, *45* (41), 21392–21408.

[39] Tomishige, K.; Li, D.; Tamura, M.; Nakagawa, Y. Nickel-Iron Alloy Catalysts for

Reforming of Hydrocarbons: Preparation, Structure, and Catalytic Properties. *Catal. Sci. Technol.* **2017**, *7* (18), 3952–3979.

[40] Jović, A.; Brkić, K.; Bogunović, N. An Overview of Free Software Tools for General Data Mining. *2014 37th Int. Conv. Inf. Commun. Technol. Electron. Microelectron. MIPRO 2014 - Proc.* **2014**, No. May, 1112–1117.

[41] Pedregosa, F.; Varoquaux, G.; Gramfort, A.; et al. Scikit-learn: Machine learning in Python. *J. Mach. Learn. Res.* **2011**, *12*, 2825− 2830.

[42] Bastian, M.; Heymann, S.; Jacomy, M. Gephi: An Open Source Software for Exploring and Manipulating Networks. *Proceedings of the International AAAI Conference on Web and Social Media* **2009**, *3*, 361–362.

[43] An, M.; Chang, D.; Hong, D.; Fan, H.; Wang, K. Metabolic Regulation in Soil Microbial Succession and Niche Differentiation by the Polymer Amendment under Cadmium Stress. *J. Hazard. Mater.* **2021**, *416*, 126094.

[44] Arman, A.; Hagos, F. Y.; Abdullah, A. A.; Mamat, R.; Aziz, A. R. A.; Cheng, C. K. Syngas Production through Steam and CO2 Reforming of Methane over Ni-Based Catalyst-A Review. *IOP Conf. Ser. Mater. Sci. Eng.* **2020**, *736* (4).

[45] Osazuwa, O. U.; Abidin, S. Z. An Overview on the Role of Lanthanide Series (Rare Earth Metals) in H2 and Syngas Production from CH4 Reforming Processes. *Chem. Eng. Sci.* **2020**, *227*, 115863.

Chapter 4

General Conclusion

Chapter 4

In general, the composition and structure of the materials to be designed are multifaceted because improving the performance of a material requires controlling multiple factors. However, because the interactions between elements in multidimensional material design are extremely complex, material development to date has mainly been a trial-and-error approach, in which materials synthesis and evaluation are repeated based on intuition and experience. In this thesis, we aim to control chemical reactions through multidimensional material exploration by combining materials informatics and high-throughput experiments. The versatility of the methodology proposed in this thesis will be demonstrated by exploring different material systems in different fields, such as stabilizer formulations for the prevention of yellowing of polymers and low-temperature dry reforming of methane as a catalyst. The main conclusions are as follows:

In chapter 2, I established an HTE protocol for the inhibition of yellowing of polystyrene by solution film casting on microplates and UV-visible spectroscopy using a microplate reader, and combined this with genetic algorithms (GA) to achieve stabilization. This was combined with a genetic algorithm (GA) to achieve a large-scale exploration for stabilizing agent formulations. Furthermore, the obtained experimental data were analyzed from a data science perspective. The analysis revealed that the durability of polymers can be improved by synergistic combination of stabilizers that play complementary roles in inhibiting degradation, or by synergistic combination of stabilizers of the same type with different reactivity and stability. The hypothesis that it is

important to combine as many stabilizers as possible that are synergistic with each other in order to design high performance formulations was derived, and this was substantiated by additional experiments.

In chapter 3, a multidimensional design of catalysts for the low-temperature dry reforming (DRM) of methane was investigated using a combination of HTE instrument and GA. Analysis of the data sets obtained for various catalysts and experimental conditions showed that increasing temperature and CO_2 flow rate contributed significantly to the decrease in H_2 yield due to the reverse water gas shift, a side reaction of DRM, while catalyst loading contributed little to H_2 yield, CO yield, while Pd, which was abundant in the high-performance catalysts found in GA, was found to have a hydrogen spillover effect, which is a combination of Pd, which improves Ni dispersion and reduction, and La and Ce, which promote metal dispersion and CO_2 adsorption on γ-Al_2O_3. lanthanides were confirmed to be present. As in chapter 2, I also found that the inclusion of as many synergistic elements as possible is important for the design of high-performance catalysts.

In summary, the two verifications achieved a large-scale combinatorial search. In addition, it was found that it is very important to select and coexist elements that establish synergistic effects with each other in the multidimensional material design for chemical reaction control. In conclusion, this study has demonstrated a new methodology for multidisciplinary material design through “Realization of multidimensional exploration”, ”Discovery of new combinations” and “Derivation of design guidelines”.

Achievements

Main Publication

1. Takimoto, K.; Takeuchi, K.; Ton, N. N. T.; Taniike, T. Exploring Stabilizer Formulations for Light-Induced Yellowing of Polystyrene by High-Throughput Experimentation and Machine Learning. *Polym. Degrad. Stab.* **2022**, *201*, 109967.

Other Publications

1. Nguyen, T. N.; Nhat, T. T. P.; Takimoto, K.; Thakur, A.; Nishimura, S.; Ohyama, J.; Miyazato, I.; Takahashi, L.; Fujima, J.; Takahashi, K.; Taniike, T. High-Throughput Experimentation and Catalyst Informatics for Oxidative Coupling of Methane. *ACS Catal.* **2020**, *10* (2), 921–932.

2. Taniike, T.; Kitamura, T.; Nakayama, K.; Takimoto, K.; Aratani, N.; Wada, T.; Thakur, A.; Chammingkwan, P. Stabilizer Formulation Based on High-Throughput Chemiluminescence Imaging and Machine Learning. *ACS Appl. Polym. Mater.* **2020**, *2* (8), 3319–3326.

International Conference

Poster

1. Takimoto, K., Kaneda, S., Taniike, T., Development of dry reforming catalyst using high-throughput experiment and genetic algorithm, First international symposium on High-Throughput Catalyst Design, online, June 14-15, 2021.

Domestic conferences

Oral

1. Takimoto, K., Taniike, T., Exploring stabilizer formulations for light-induced yellowing of polystyrene by high-throughput experimentation and machine learning, 日本化学会 第 102 春季年会, online, March 23-26, 2022.
2. Takimoto, K., Taniike, T., ポリスチレンの黄変抑制における添加剤の組み合わせ効果に関する研究, 第 69 回高分子討論会, online, September 16-18, 2020.
3. Takimoto, K., Nakayama, K., Takeuchi, K., Taniike, T., マイクロプレート法と遺伝的アルゴリズムを用いたポリスチレンの光劣化, マテリアルライフ学会 第 24 回春季研究発表会, Yokohama, February 21, 2020.
4. Takimoto, K., Takeuchi, K., Taniike, T., マイクロプレートを用いた高分子材料の安定化に関する耐光性評価, マテリアルライフ学会 第 30 回研究発表会, Nagoya, July 4-5, 2019.

Awards

1. Takimoto, K., マテリアルライフ学会研究奨励賞, マイクロプレート法と遺伝的アルゴリズムを用いたポリスチレンの光安定化, マテリアルライフ学会 第 24 回春季研究発表会, Yokohama, February, 2020.
2. Takimoto, K., マテリアルライフ学会研究奨励賞, マイクロプレートを用いた高分子材料の安定化に関する耐光性評価, マテリアルライフ学会 第 30 回研究発表会, Nagoya, July, 2019.

Grant

1. 科学技術振興機構 次世代研究者挑戦的研究プログラム, October 2021–March 2023